

DEVELOPMENT OF AN ALUMINIUM CORELESS IRONLESS
GENERATOR FOR EV APPLICATIONS

AKHTAR RAZUL RAZALI

UMP

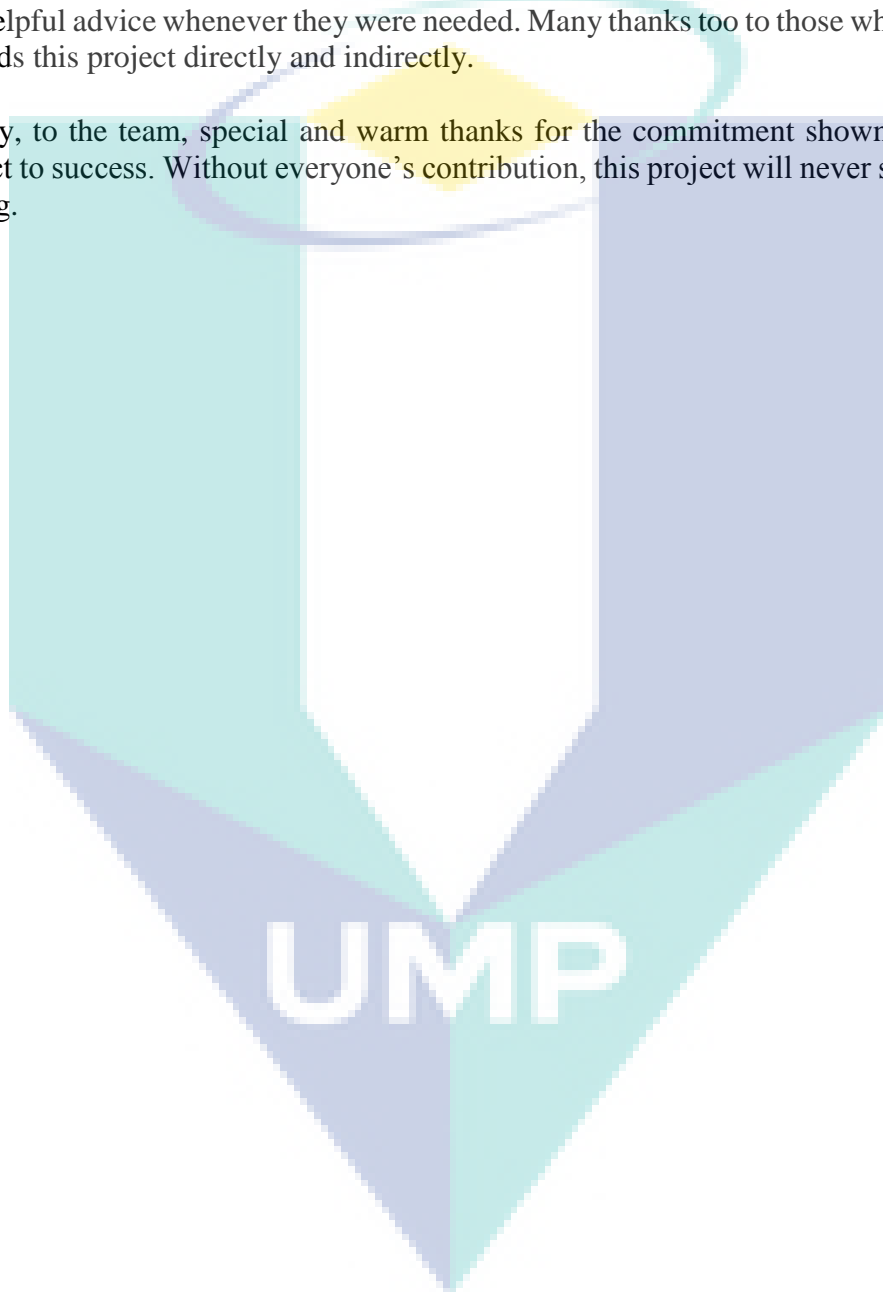
FINAL REPORT

RDU 150365

ACKNOWLEDGEMENTS

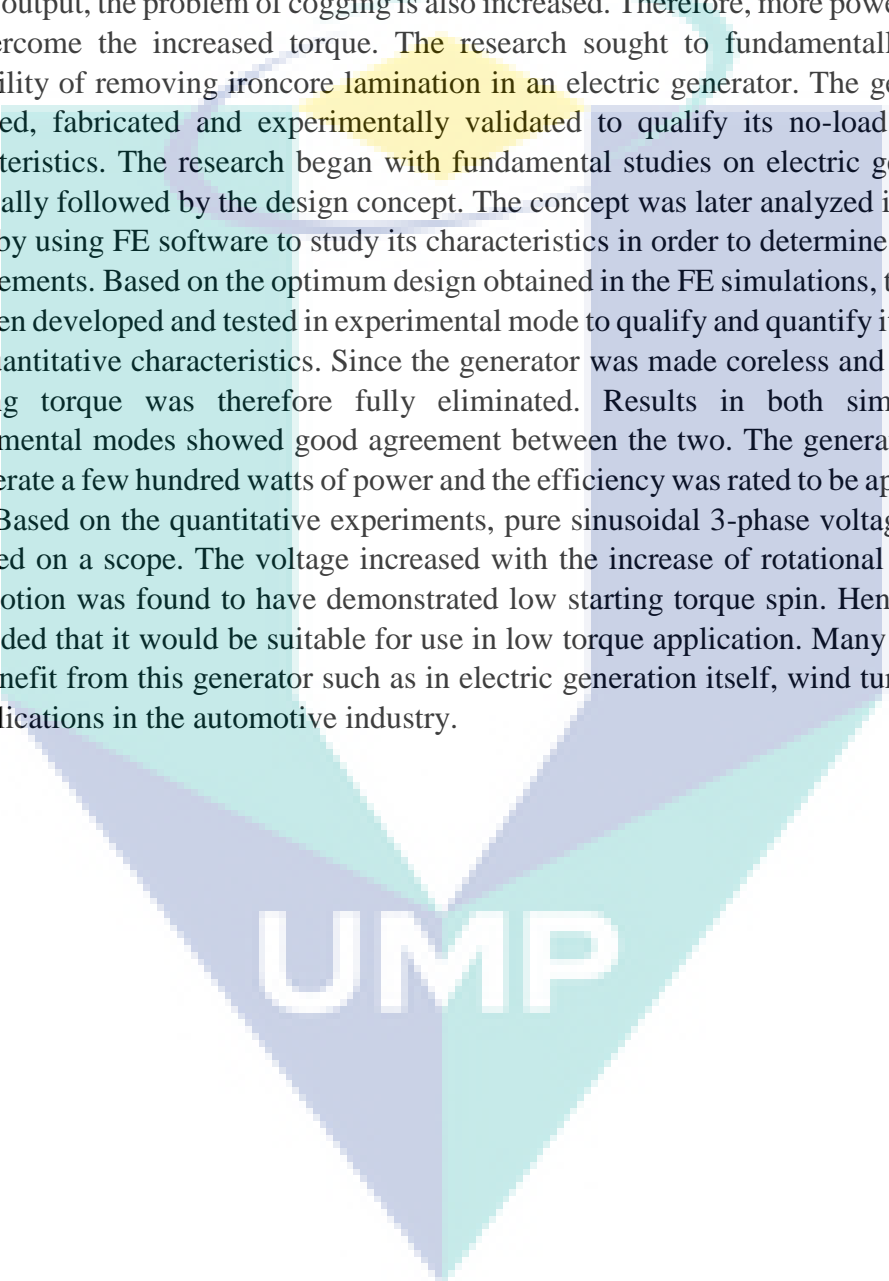
The researchers would like to address their gratitude to the Universiti Malaysia Pahang for the financial assistance through RDU 150365. Special thanks also go to Mr. Yap Wee Leong, who is very dedicated to keep this project running and successfully graduated his Master Degree. Not to forget, to those helpful teaching engineers, Mr. Aziha, Mr. Asmizam, Mr. Rozikin and Mr. Hafietz for their trust (for the machineries usage), support and helpful advice whenever they were needed. Many thanks too to those who contributed towards this project directly and indirectly.

Finally, to the team, special and warm thanks for the commitment shown to drive this project to success. Without everyone's contribution, this project will never see this happy ending.



ABSTRACT

The presence of cog in ironcore generator is seen somehow restricting the application of the generator where low rotational torque is required. Cogging creates an attraction force between magnets and ironcore lamination in a generator. More power is required to overcome cogging before the generator can be spun continuously. With the increase of power output, the problem of cogging is also increased. Therefore, more power is required to overcome the increased torque. The research sought to fundamentally study the possibility of removing ironcore lamination in an electric generator. The generator was designed, fabricated and experimentally validated to qualify its no-load and loaded characteristics. The research began with fundamental studies on electric generator and eventually followed by the design concept. The concept was later analyzed in simulation mode by using FE software to study its characteristics in order to determine its optimum arrangements. Based on the optimum design obtained in the FE simulations, the generator was then developed and tested in experimental mode to qualify and quantify its qualitative and quantitative characteristics. Since the generator was made coreless and ironless, the cogging torque was therefore fully eliminated. Results in both simulation and experimental modes showed good agreement between the two. The generator managed to generate a few hundred watts of power and the efficiency was rated to be approximately 75%. Based on the quantitative experiments, pure sinusoidal 3-phase voltage wave was captured on a scope. The voltage increased with the increase of rotational speed. Cog-free motion was found to have demonstrated low starting torque spin. Hence, it can be concluded that it would be suitable for use in low torque application. Many applications can benefit from this generator such as in electric generation itself, wind turbine as well as applications in the automotive industry.

The logo for UMP (Universiti Malaysia Perlis) is a large, stylized letter 'M' composed of four overlapping triangles. The top-left triangle is light blue, the top-right is light green, the bottom-left is light purple, and the bottom-right is light teal. The letters 'UMP' are printed in white, bold, sans-serif font across the center of the 'M' shape.

UMP

ABSTRAK

Kewujudan gigi roda atau tugal dalam penjana elektrik berteraskan besi kelihatan menghadkan aplikasi penjana elektrik dalam keadaan yang memerlukan putaran kilas atau tork yang rendah. Penugalan menghasilkan satu daya tarikan di antara magnet-magnet dengan teras besi berlamina di dalam penjana elektrik. Kuasa yang lebih diperlukan untuk mengatasi masalah gigi roda sebelum penjana elektrik boleh diputar secara berterusan. Dengan meningkatnya output kuasa, masalah penugalan juga meningkat. Oleh itu, lebih kuasa diperlukan untuk mengatasi peningkatan kilasan. Penyelidikan ini bertujuan mengkaji asas-asas kemungkinan penggunaan penjana elektrik tanpa teras besi berlamina. Penjana elektrik direka, dibina dan diuji untuk disahkan ciri-ciri penjana elektrik tanpa beban dan dengan beban secara uji kaji. Penyelidikan ini bermula dengan kajian asas terhadap penjana elektrik dan seterusnya konsep reka bentuk. Konsep ini kemudiannya dianalisis secara simulasi dengan menggunakan perisian FE untuk mengkaji ciri-cirinya dan menentukan perkiraan optimumnya. Berdasarkan reka bentuk optimum yang diperolehi secara simulasi menggunakan FE, penjana elektrik ini kemudian dibina dan diuji secara uji kaji untuk mengukur ciri-ciri kualitatif dan kuantitatif. Oleh kerana penjana ini dibuat dengan tanpa teras dan juga tanpa menggunakan besi, penugalan kilas dapat dihapuskan sepenuhnya. Keputusan dalam kedua-dua simulasi dan eksperimen telah menunjukkan keserasian antara kedua-duanya. Penjana elektrik ini berjaya menjana beberapa ratus watt kuasa dan dengan anggaran keberkesanan 75%. Berdasarkan eksperimen kuantitatif, gelombang bentuk sinus tulen bervoltan 3 fasa telah dikesan pada skop. Voltan didapati meningkat dengan peningkatan kelajuan putaran. Gerakan tanpa gigi roda didapati menghasilkan putaran kilas permulaan yang rendah. Oleh itu, dapatlah disimpulkan bahawa ia sesuai untuk kegunaan dalam aplikasi yang memerlukan kilas yang rendah. Banyak aplikasi dapat memanfaatkan penjana ini seperti dalam penjana elektrik sendiri, turbin angin dan juga dalam aplikasi lain dalam industri automotif.

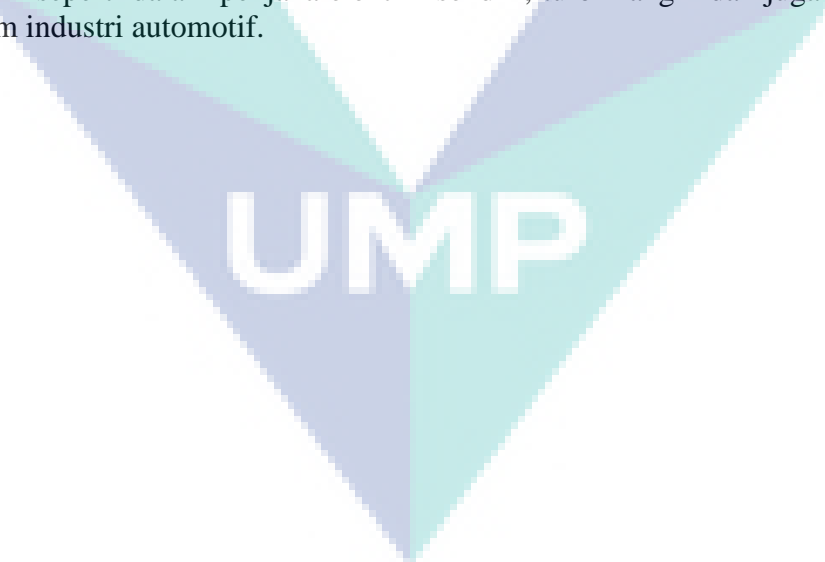
The logo of Universiti Malaysia Perlis (UMP) is a large, stylized letter 'V' shape. The left side of the 'V' is light blue, and the right side is light green. The letters 'UMP' are written in white, bold, sans-serif font across the center of the 'V'.

TABLE OF CONTENTS

		Page
ACKNOWLEDGEMENTS		ii
ABSTRACT		iii
ABSTRAK		iv
TABLE OF CONTENTS		v
LIST OF TABLES		viii
LIST OF FIGURES		ix
LIST OF SYMBOLS		xii
LIST OF ABBREVIATIONS		xiii
CHAPTER 1 INTRODUCTION		
1.1	Research Background	1
1.2	Objectives	3
1.3	Research Scopes	3
CHAPTER 2 LITERATURE REVIEW		
2.1	Electricity Generation and Its Technology	4
	2.1.1 Concept Regarding to Magnetic Field	4
	2.1.2 Concept Regarding to Magnetic Field Cutting	8
	2.1.3 Concept Regarding to Connection Used	9
2.2	Ironcore Electricity Generator	11
	2.2.1 Element and Working Principle	11
	2.2.2 Application of An Ironcore Generator	14
2.3	Losses In An Ironcore Generator	16
	2.3.1 Hysteresis Losses	17
	2.3.2 Eddy Currents	19
2.4	Issues Related to Iron Core Lamination	20
	2.4.1 Attraction between Ironcore Lamination and Permanent Magnets	20
	2.4.2 Cogging Torque in An Ironcore Generator	20

2.5	Ironless/Coreless Generator Design and Principle	21
2.6	Coreless Generator	23
	2.6.1 Application of Coreless Generator	23
	2.6.2 Arrangement/Configuration of Coreless Generator	27
2.7	Design Consideration of An Ironless Coreless Generator	34
	2.7.1 Magnet Used on the Ironless Coreless Generator	34
	2.7.2 Coil Design for the Ironless Coreless Generator	35
	2.7.3 Gap Distance between the Magnets	37
	2.7.4 Number of Poles and Coils for the Ironless Coreless Generator	39
2.8	Finite Element Tool For Electromagnetism Analysis	39
2.9	Summary	41
CHAPTER 3 PRELIMINARY STUDIES: FINITE ELEMENT ANALYSIS		
3.1	Introduction	42
3.2	Procedure	43
3.3	Results for The Finite Element Analysis	45
	3.3.1 Number of Coil Turns per Phase	45
	3.3.2 Gap Distance between the Magnet Pairs	50
	3.3.3 Magnet Grade Used on Magnet Pairs	56
	3.3.4 Discussion on The Simulation Results	62
3.4	Optimum Parameter for The Ironless Coreless Electricity Generator	63
3.5	Conclusion	70
CHAPTER 4 DEVELOPMENT WORKS FOR IRONLESS CORELESS ELECTRICITY GENERATOR		
4.1	Introduction	71
4.2	Structural Analysis on Ironless Coreless Electricity Generator	72
4.3	Fabrication for The Ironless Coreless Electricity Generator	75
4.4	Test Bed Assembly	84
CHAPTER 5 OPEN CIRCUIT TEST ON IRONLESS CORELESS ELECTRICITY GENERATOR		
5.1	Introduction	86

5.2	Material and Equipment	87
5.3	Experimental Setup and Procedures	89
5.4	Result of The Open Circuit Test	90
5.5	Discussions	96
5.6	Summary	97

CHAPTER 6 CLOSED CIRCUIT TEST ON IRONLESS CORELESS ELECTRICITY GENERATOR

6.1	Introduction	98
6.2	Material and Equipment	99
6.3	Experiment Setup and Procedure	101
6.4	Results for The Closed Circuit Test	104
	6.4.1 Various Rotational Speed Constant Load Test	105
	6.4.2 Maximum Power Point Tracking Test	111
6.5	Discussion	117
6.6	Summary	120

CHAPTER 7 CONCLUSION AND RECOMMENDATION

7.1	Conclusion	122
7.2	Recommendation	123

REFERENCES		124
-------------------	--	-----

UMP

LIST OF TABLES

Table No.	Title	Page
2.1	Efficiency result	26
2.2	Energy yield result	26
2.3	Result of power output in 3 different numbers of poles	30
3.1	Summary of the finite element analysis on the number of coil turns per phase	49
3.2	Summary of the finite element analysis on the gap distance between magnet pairs	55
3.3	Summary of the finite element analysis on magnet grade used on magnet pairs	61
5.1	The result for the experiment with different rotational speed	95
6.1	Result for power output for various rotational speed constant load test	107
6.2	The result for power input, power after inverter and power after motor for various rotational speed constant load test	108
6.3	Result of torque and efficiency for various rotational speed constant load test	108
6.4	Result for power output for maximum power point tracking test	114
6.5	Result for power input, power after inverter and power after motor for maximum power point tracking test	114
6.6	Result for torque and efficiency for maximum power point tracking test	115
7.1	Summary of the Objectives and Achievements on Research for The Ironless Coreless Electricity Generator	124

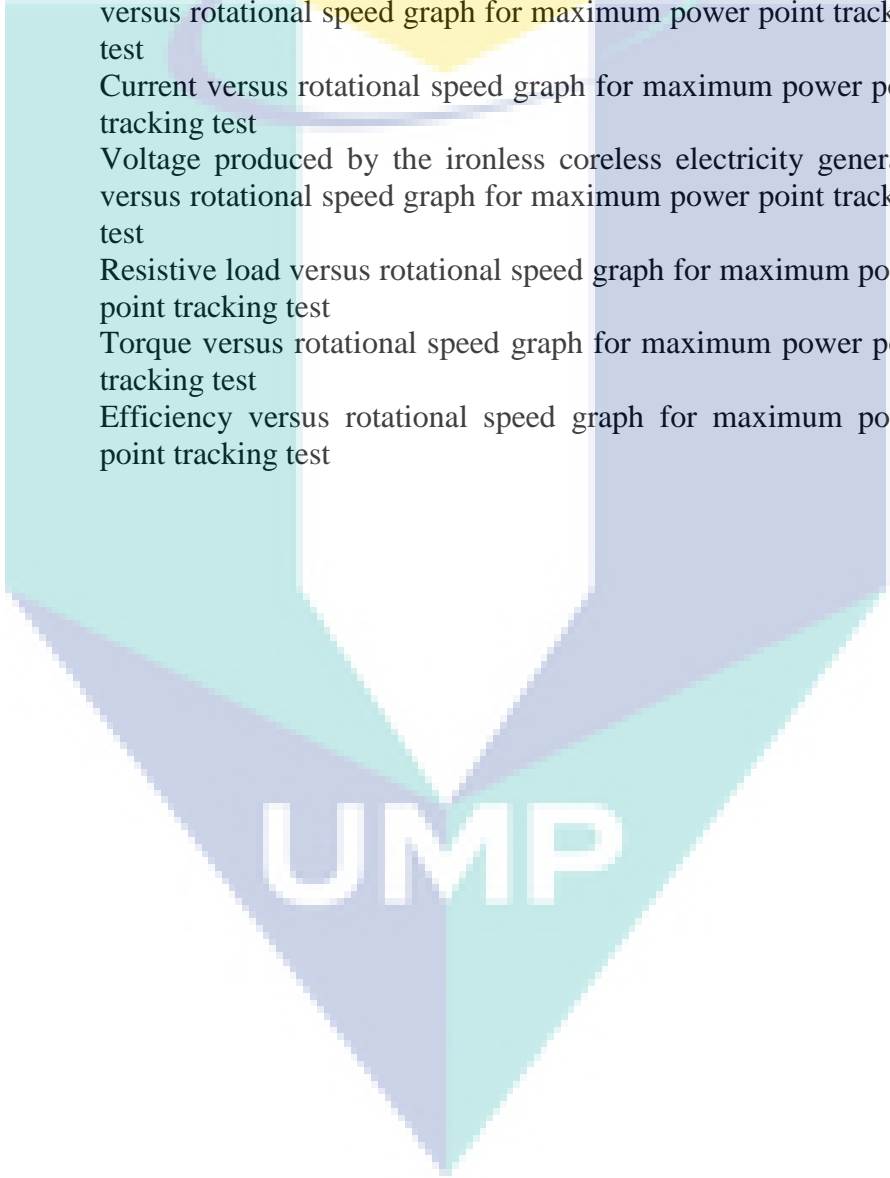
UMP

LIST OF FIGURES

Figure No.	Title	Page
2.1	Figure shows the different line density in weaker and stronger magnetic field	5
2.2	Illustration shows the magnetic flux line in the vicinity of coil	7
2.3	Illustration shows the tightly wound circular coil and the toroid coil	7
2.4	Fleming's left-hand rule on magnetic field	8
2.5	Fleming's right-hand rule on magnetic field	9
2.6	Example of wye configuration connection	10
2.7	Example of Delta connection	11
2.8	Illustration shows construction of the core-type transformer	12
2.9	Illustration shows the core-type transformer	12
2.10	Illustration shows the various position of armature as well as generator terminal voltage in various position of armature	14
2.11	Example of conventional generator	15
2.12	Example of alternator for the vehicles	16
2.13	Hysteresis loop	18
2.14	Slotless single-stator double-rotor APFM configuration	22
2.15	Slotted double-stator single-rotor AFPM configuration	23
2.16	Wind turbine generating system model using AFPM generator	24
2.17	Illustration shows the structure of the stacked magnetic circuit	27
2.18	Illustration shows the arrangement of poles of 3 different numbers of poles	29
2.19	Illustration shows the averaged magnetic field with respect to the gap distance between the rotors of 3 different numbers of poles	29
2.20	Proposed machine structure of high-speed coreless surface mounted APFM generator	31
2.21	Illustration shows the proposed machine structure of Javadi S. and Mirsalim M.	32
2.22	Illustration shows the flux path of proposed machine structure of Javadi S. and Mirsalim M.	32
2.23	Illustration shows the machine structure of Javadi S. and Mirsalim M.'s research	33
2.24	Illustration shows the machine structure of Dr. Zikowski Łukasz and Koczara Włodzimierz's research	34
2.25	Coil dimension for the axial-flux permanent magnet generator.	36
2.26	Approximated power of the generator via the different relative thickness of coil (c/τ)	37
2.27	Approximated power of the generator varies on air-gap distance	38
2.28	Magnetic flux density distribution for the three-phase small scale PMSG	40
3.1	Magnetic Flux Density Contour Plot for 500 Coil Turns per Phase Analysis	46
3.2	Magnetic Flux of FEM Coil for 500 Coil Turns per Phase Analysis	47
3.3	Circuit Voltage for 500 Coil Turns per Phase Analysis	47
3.4	Torque for 500 Coil Turns per Phase Analysis	48
3.5	Magnetic Flux Density Contour Plot for 14mm Gap Distance	51

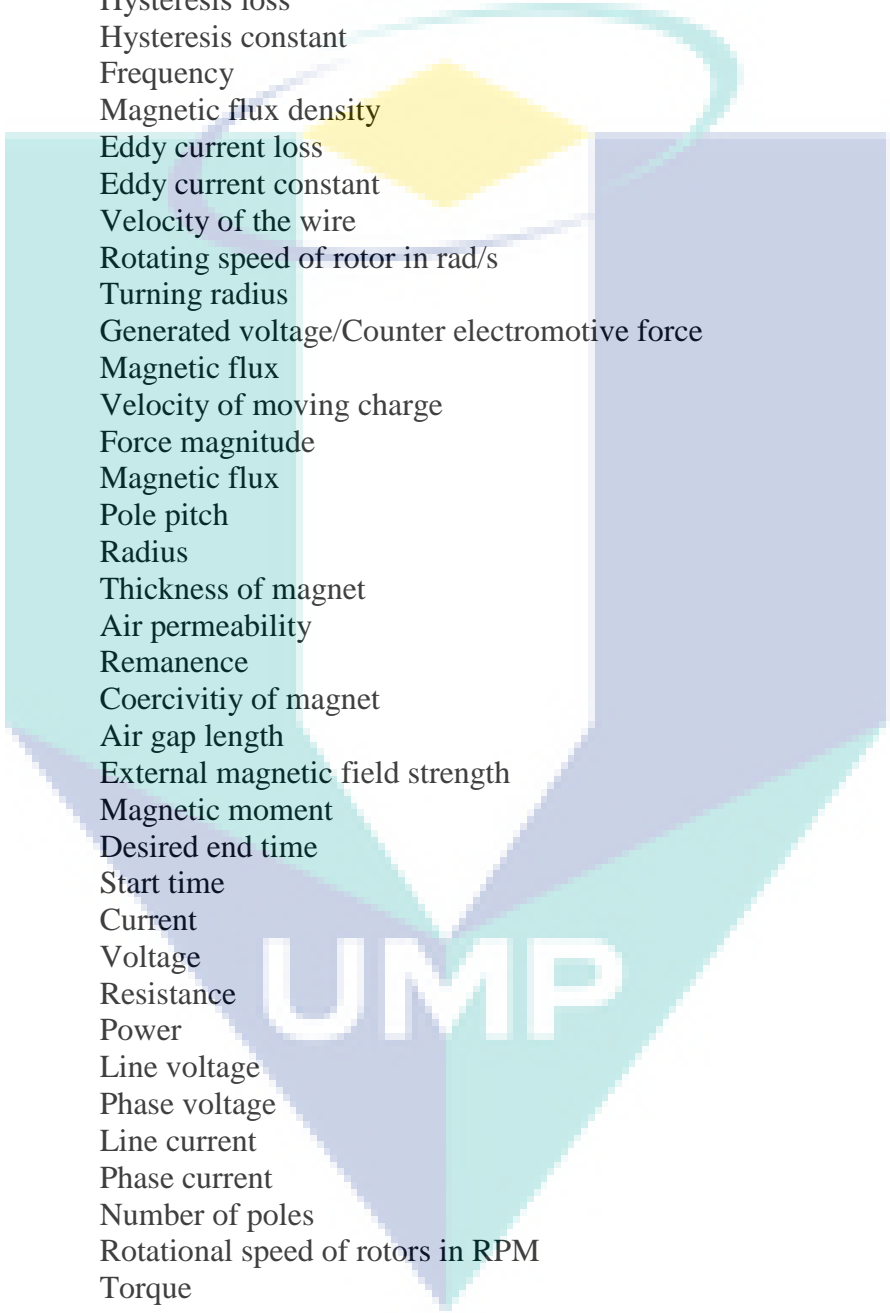
	Analysis	
3.6	Magnetic Flux of FEM Coil for 14mm Gap Distance Analysis	52
3.7	Circuit Voltage for 14mm Gap Distance Analysis	52
3.8	Torque for 14mm Gap Distance Analysis	53
3.9	Magnetic Flux Density Contour Plot for N42 Neodymium Magnet Analysis	57
3.10	Magnetic Flux of FEM Coil for N42 Neodymium Magnet Analysis	58
3.11	Circuit Voltage for N42 Neodymium Magnet Analysis	58
3.12	Torque for N42 Neodymium Magnet Analysis	59
3.13	Magnetic Flux Density Contour Plot for Optimum Parameter Design Analysis	65
3.14	Magnetic Flux of FEM Coil for Optimum Parameter Design Analysis	65
3.15	Circuit Voltage for Optimum Parameter Design Analysis	66
3.16	Rotor Torque for Optimum Parameter Design Analysis	66
3.17	Current for Optimum Parameter Design Analysis	67
3.18	Electric Power for Optimum Parameter Design Analysis	67
3.19	Joule Loss for Optimum Parameter Design Analysis	68
4.1	Result of von Mises stress test on the ironless coreless electricity generator	73
4.2	Result of displacement test on the ironless coreless electricity generator	74
4.3	Result for strain test on the ironless coreless electricity generator	74
4.4	Fabrication using CNC machine	77
4.5	Fabricated rotor	77
4.6	Fabricated stator	78
4.7	Fabricated support plate	78
4.8	Jig used to do the coiling	79
4.9	Top view for the coil with core	80
4.10	Side view for the completed coil with core	80
4.11	Coil is assembled on the stator	81
4.12	Jig used to disassemble magnet from bulk	82
4.13	North pole is assemble into rotor	83
4.14	Assembled ironless coreless electricity generator	84
4.15	Test bed used to test the ironless coreless electricity generator	85
5.1	Specification of the three phase induction motor	87
5.2	Tachometer used to measure rotational speed of rotors	88
5.3	Inverter used on the open circuit test	89
5.4	Phase voltages and characteristics for rotational speed of a) 113.4 RPM, b) 171.8 RPM. c) 233.5 RPM, d) 293.6 RPM and e) 352.8 RPM	92
5.5	Voltage output versus rotational speed of the rotor for ironless coreless electricity generator	95
6.1	DC electronic load used in the close circuit test	100
6.2	Rectifier used in the closed circuit test	100
6.3	Method to connect ironless coreless generator, DC electronic load unit and oscilloscope	102
6.4	Flow chart for the closed circuit experiment and setup	103
6.5	The voltage output before and after the rectifier	104

6.6	Power generated by ironless coreless electricity generator versus rotational speed graph	109
6.7	Current generated by the ironless coreless electricity generator versus rotational speed graph	110
6.8	Voltage produced by the ironless coreless electricity generator versus rotational speed graph	110
6.9	Torque of the ironless coreless electricity generator versus rotational speed graph	111
6.10	Efficiency of the ironless coreless electricity generator versus rotational speed graph	111
6.11	Power generated by the ironless coreless electricity generator versus rotational speed graph for maximum power point tracking test	116
6.12	Current versus rotational speed graph for maximum power point tracking test	117
6.13	Voltage produced by the ironless coreless electricity generator versus rotational speed graph for maximum power point tracking test	117
6.14	Resistive load versus rotational speed graph for maximum power point tracking test	118
6.15	Torque versus rotational speed graph for maximum power point tracking test	118
6.16	Efficiency versus rotational speed graph for maximum power point tracking test	119

The logo for UIMP (University of Management and Applied Sciences) is a large, stylized shield shape. It is composed of several overlapping geometric shapes in shades of teal, light blue, and yellow. The letters 'UIMP' are written in a bold, white, sans-serif font across the center of the shield.

UIMP

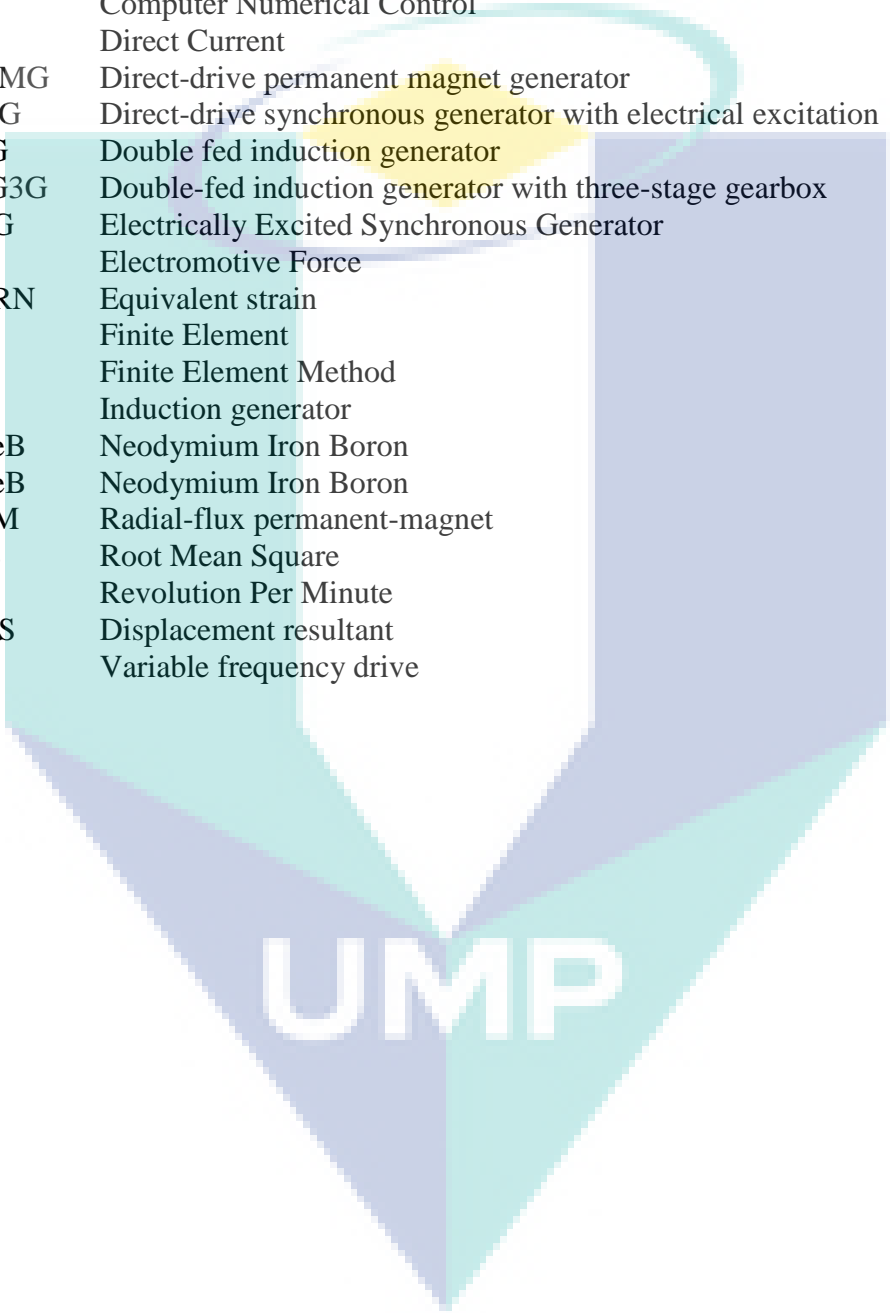
LIST OF SYMBOLS



η	efficiency
P_{out}	Power output
P_{in}	Power input
P_{loss}	Power losses
W_h	Hysteresis loss
K_h	Hysteresis constant
f	Frequency
B_m	Magnetic flux density
W_e	Eddy current loss
K_e	Eddy current constant
v	Velocity of the wire
ω	Rotating speed of rotor in rad/s
R	Turning radius
e	Generated voltage/Counter electromotive force
B	Magnetic flux
u	Velocity of moving charge
f	Force magnitude
ϕ	Magnetic flux
τ	Pole pitch
r	Radius
g	Thickness of magnet
μ_0	Air permeability
B_r	Remanence
H_c	Coercivity of magnet
δ	Air gap length
H_c	External magnetic field strength
m	Magnetic moment
t_1	Desired end time
t_0	Start time
I	Current
V	Voltage
R	Resistance
P	Power
V_L	Line voltage
V_ϕ	Phase voltage
I_L	Line current
I_ϕ	Phase current
p	Number of poles
N	Rotational speed of rotors in RPM
τ	Torque

LIST OF ABBREVIATIONS

AC	Alternating Current
AFPM	Axial-flux permanent-magnet
CAD	Computer Aided Design
CEMF	Counter Electromotive Force
CNC	Computer Numerical Control
DC	Direct Current
DDPMG	Direct-drive permanent magnet generator
DDSG	Direct-drive synchronous generator with electrical excitation
DFIG	Double fed induction generator
DFIG3G	Double-fed induction generator with three-stage gearbox
EESG	Electrically Excited Synchronous Generator
emf	Electromotive Force
ESTRN	Equivalent strain
FE	Finite Element
FEM	Finite Element Method
IG	Induction generator
NdFeB	Neodymium Iron Boron
NdFeB	Neodymium Iron Boron
RFPM	Radial-flux permanent-magnet
RMS	Root Mean Square
<i>rpm</i>	Revolution Per Minute
URES	Displacement resultant
VFD	Variable frequency drive



UMP



CHAPTER 1

INTRODUCTION

1.1 RESEARCH BACKGROUND

Ironcore lamination in a generator is used to confine and guide magnetic flux as to boost its efficiency to the maximum. Ironcore, as the name implies, consists of lamination of highly permeable core material which can increase the density of the magnetic flux in over several thousand times. The advantage of confining and guiding the flux, however, gives a major drawback to the generator. When the ironcore lamination is exposed to the magnetic field, magnetic particles in the core tend to line up with the magnetic field of the permanent magnets. When the magnets are rotated, their magnetic fields change direction. This induces continuous movement of the ironcore's magnetic particles in order for them to align with the change of magnetic field direction and coincidentally produces molecular friction. This in turn produces heat and is then transmitted/ distributed to the ironcore lamination and windings. Heat causes increase in winding resistance and at the same time retains electromagnetism in the windings and ironcore laminations.

Electromagnetism in the ironcore lamination acts as a magnet and reacts (attracts and repels) with the magnetic field of a permanent magnet. The more power is generated from the generator, the more power is required to maintain its rotation as the

input torque increased proportionally to the power output. Therefore, the more heat is generated, the stronger the electromagnetism exists in the core, causing unwanted attraction force with the magnetic field of a permanent magnet. The attraction force between permanent magnets and ironcore lamination in a generator, or also known as 'cog', is seen as one of the major inefficiencies in the generator (Zhang et al., 2013; Ting & Yeh, 2014).

Cog increases spinning torque, which indirectly increases the amount of work/ energy used to spin the generator. The energy to overcome cog is basically proportional to the output power produced. The larger the output power is produced, the larger the amount of torque is required to spin (or to maintain the rotation speed). The presence of cog in the system, however, has made this conventional generator far from being usable in low torque application (Ahmed & Ahmad, 2013; Kobayashi et al., 2009). Continuous and consistent power is required to overcome cog, and the power varies when rotational speed varies.

There have been many attempts to reduce cog in order to increase the application boundary of a generator (Kurt, Gör & Demirtaş, 2014). Most of the efforts focus on the ironcore optimization in design to minimize the effect of cog; however, the presence of cog is still inevitable (Gor & Kurt, 2016). An effort made to remove iron core material from an electric motor was demonstrated with great success more than a decade ago. The success story of this ironless motor has been widely shared by both the researchers and players in the industries. The idea behind this achievement is removing the iron core lamination and replacing it with non-ferrous material. The ironless motor works flawlessly and one of the major advantages comes from its outstanding positional accuracy and repeatability due to no cogging affecting the positioning.

A similar idea may be applied to demonstrate coreless generator design. Effort made on this subject, however, is still lacking (Mahmoudi et al., 2013; Virtic & Avsec, 2011). The idea of removing ironcore lamination material may cause non-concentrated flux and lead to deterioration in output power efficiency (Ahmed & Ahmad, 2013). However, there is a method which may be used to concentrate and focus magnetic flux to create denser magnetic field. An additional permanent magnet arrangement added to the generator may be a solution to address this issue. The absence of ironcore lamination

in the system also represents cog-free rotation. This provides advantage in terms of very low starting torque and less counter electromotive force is produced.

1.2 RESEARCH OBJECTIVES

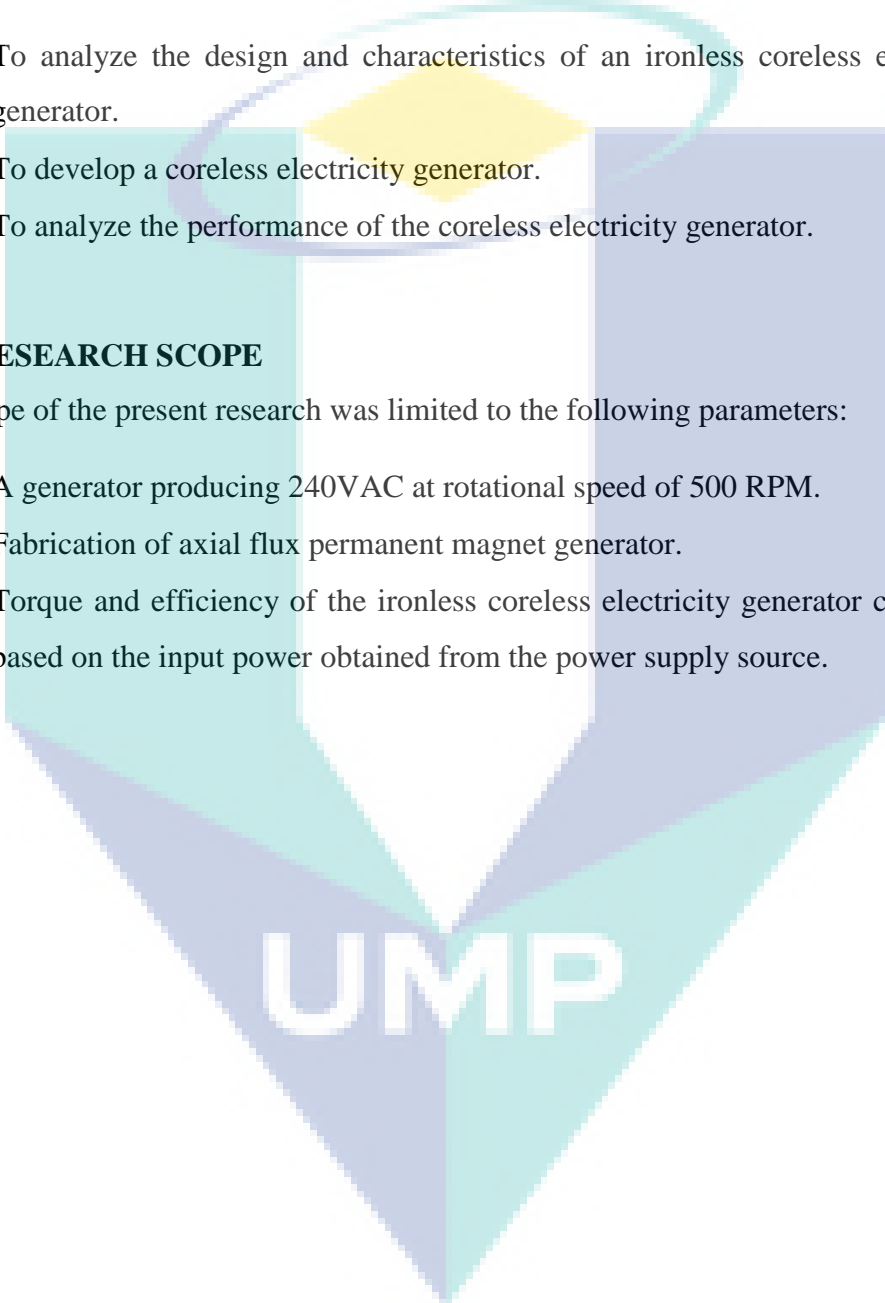
The present study sought to achieve the following objectives:

- To analyze the design and characteristics of an ironless coreless electricity generator.
- To develop a coreless electricity generator.
- To analyze the performance of the coreless electricity generator.

1.3 RESEARCH SCOPE

The scope of the present research was limited to the following parameters:

- A generator producing 240VAC at rotational speed of 500 RPM.
- Fabrication of axial flux permanent magnet generator.
- Torque and efficiency of the ironless coreless electricity generator calculated based on the input power obtained from the power supply source.



UMP

CHAPTER 2

LITERATURE REVIEW

2.1 ELECTRICITY GENERATION AND ITS TECHNOLOGY

2.1.1 Concept Regarding to Magnetic Field

In the early 1800s, H. C. Oersted, a Danish physicist proposed that the electricity and magnetism were interconnected by showing that the electric current produced magnetic effects. After that, the French scientist, Andre Marie Ampère showed this interconnected phenomenon by using the formula, known as Ampère's law. A few years after the Ampère's law had been introduced, the English scientist Faraday agreed with the statement that magnetic field could generate electric field. In addition, he stated that the changing of magnetic field would give a voltage output. This statement became known as the Faraday's law.

Magnetic field can be represented by lines of force, which is a concept connected to Faraday's law. The strength of magnetic field can be visualised by observing the density of these lines. Figure 2.1 shows the comparison of the density of lines between weaker and stronger magnetic fields. The magnetic field is stronger if the magnetic strength of the magnet is stronger.

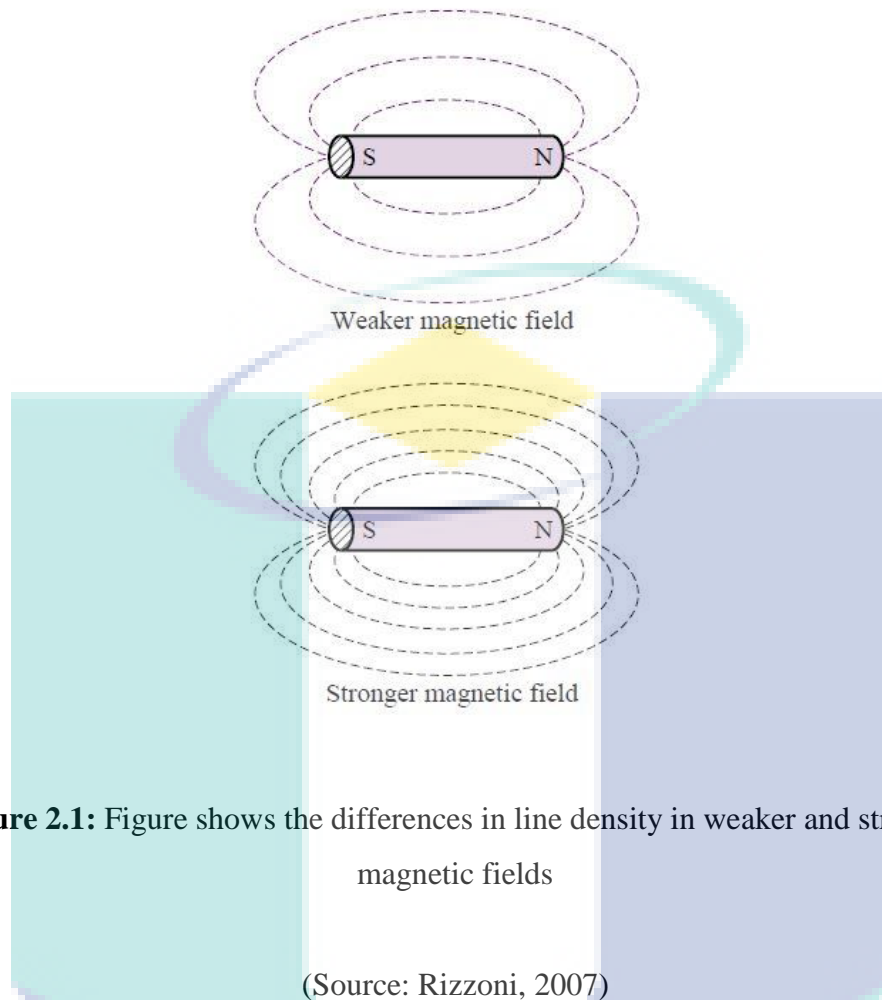


Figure 2.1: Figure shows the differences in line density in weaker and stronger magnetic fields

(Source: Rizzoni, 2007)

Magnetic fields are generated by the motion of electric charge, and this effect is measured by the force that is exerted on a moving charge. If the charge is moving at velocity, u , in a direction of the magnetic field with an angle, θ , the magnitude of the force is given by the following equation:

$$f = quB \sin \theta \quad (2.1)$$

The magnetic flux, ϕ , is defined as the integral of the density of flux over the surface area. For simplicity, assuming the magnetic flux line is perpendicular to cross-sectional area, A , the magnetic flux can be defined as:

$$\phi = \int_A B dA \quad (2.2)$$

Faraday's law states that if an imaginary surface, A , is bounded with a conductor, and then the changing of magnetic field would induce a voltage and a current in the conductor.

Figure 2.2 below shows the flux line of the magnetic field in the vicinity of a coil. If the coil encloses a magnetic material, a greater flux density can be generated from the generated magnetic field by the coil. Usually the core is made of ferromagnetic materials such as steel and iron. Some alloy and oxides of iron that exhibit magnetic properties are also used to produce the core. Winding a coil around a ferromagnetic material can be considered beneficial because it is able to complete two tasks at one time: it forces the magnetic flux to concentrate around the coil, and if the shape of the magnetic material is appropriate, it will force the closed path for the flux lines to be almost entirely enclosed within the ferromagnetic material. The typical arrangements of the inductor are shown in Figure 2.3. A conventional generator uses the winding as in Figure 2.3. The flux densities for tightly wound circular coil are expressed as:

$$B = \frac{\mu Ni}{l} \quad (2.3)$$

As for the flux density for toroid coil, the expression is given as follows:

$$B = \frac{\mu Ni}{2\pi r_2} \quad (2.4)$$

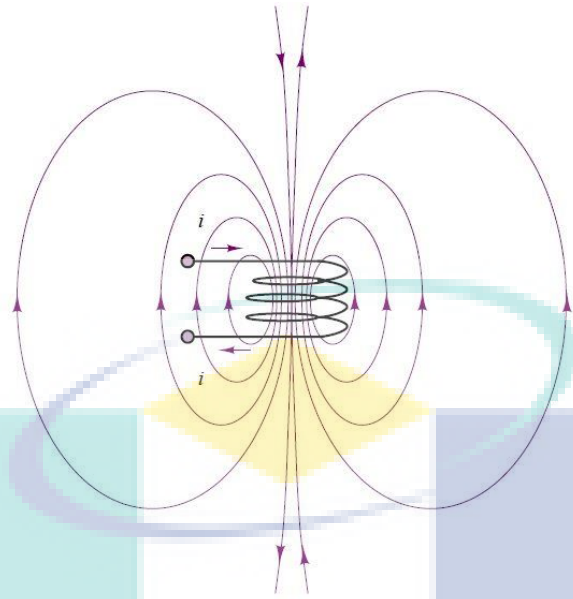


Figure 2.2: Illustration shows the magnetic flux line in the vicinity of coil

(Source: Rizzoni, 2007)

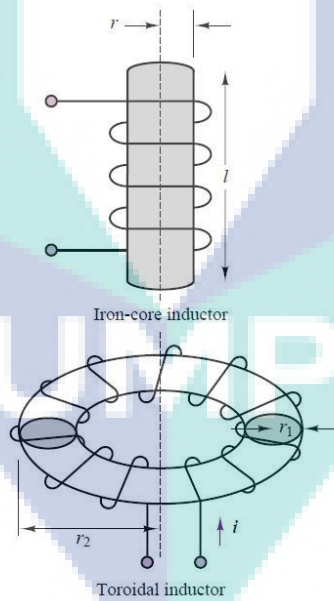


Figure 2.3: Illustration shows the tightly wound circular coil and the toroid coil

(Source: Rizzoni, 2007)

2.1.2 Concept Regarding Magnetic Field Cutting

Based on Fleming's right-hand rule, when a wire moves through a magnetic field at a velocity, a certain amount of voltage can be generated. The generated voltage is opposite with the current generated based on Fleming's left-hand rule. Figure 2.4 shows the usage of Fleming's left-hand rule on the magnetic field where F is the force acting on the wire, B is the flux density and I is the current produced while Figure 2.5 shows the usage of Fleming's right-hand rule on the magnetic field where e is the generated voltage or also called counter electromotive force, B is the magnetic flux while v is the velocity of wire.

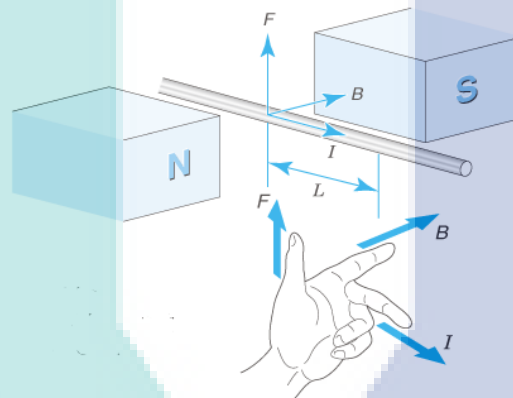


Figure 2.4: Fleming's left-hand rule on magnetic field

(Source: Nidec Corporation)

UMP

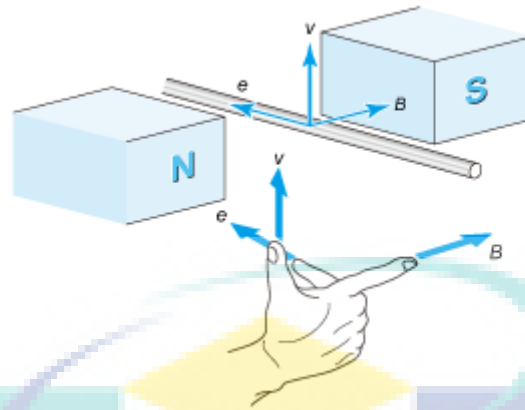


Figure 2.5: Fleming's right-hand rule on magnetic field

(Source: Nidec Corporation)

Since the generated voltage function is to reduce the current, it is also called the counter electromotive force. The velocity, v , can be expressed as in Eq. 2.5. The counter electromotive force that has been generated in the wire is expressed in Eq. 2.6.:

$$v = \omega R \quad (2.5)$$

$$e = BLR\omega \quad (2.6)$$

where v is the velocity of the wire, ω is the rotating speed of rotor in radian per second, and R is the turning radius in metre. From equation 2.6, the counter electromotive force is proportional to the rotating speed ω .

2.1.3 Concept Regarding to Connection Used

Most of the power we use today is generated and distributed using three-phase power connection, which is the arrangement in three sinusoidal voltages generated out of phase with each other. The reason for doing this is to increase the efficiency of power generated and distributed since it does lower the weight of conductors and other components. In contrast to the power produced by single-phase system which has a pulsating nature, a three-phase system can deliver a steady and constant supply of power.

Another important advantage of three-phase power is that a three-phase motor has non-zero starting torque, unlike the single-phase counterpart.

There are two types of three-phase power connections, namely, wye (Y) configuration or sometimes also called star configuration, and delta (Δ) configuration. Figure 2.6 shows an example of wye configuration circuit.

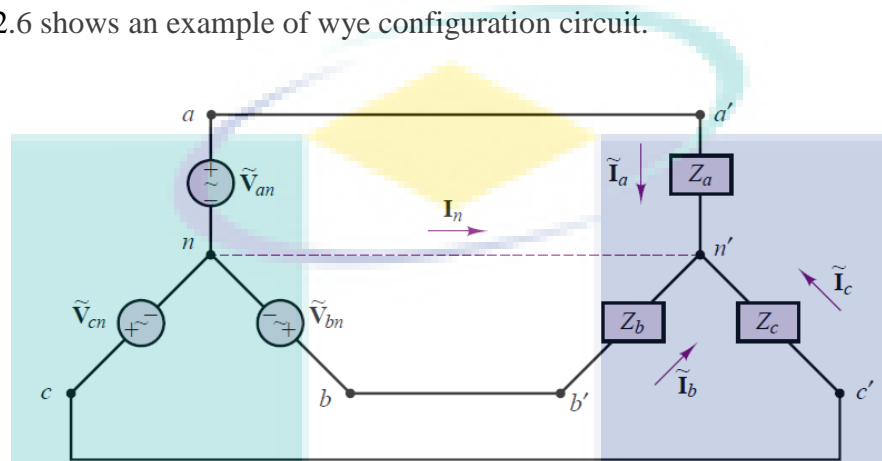


Figure 2.6: Example of wye configuration connection

(Source: Rizzoni, 2007)

Based on Figure 2.6, for wye configuration, each of the three voltages is 120 degrees out of phase with the others. In the circuit shown in Figure 2.6, the resistive loads are balanced. These three AC sources are all connected together at a node called the neutral node, n . It is also possible to connect the three AC sources into a three-phase power connection in delta (Δ) connection, although in practice this configuration is rarely used. Figure 2.7 shows the example of delta connection in circuit.

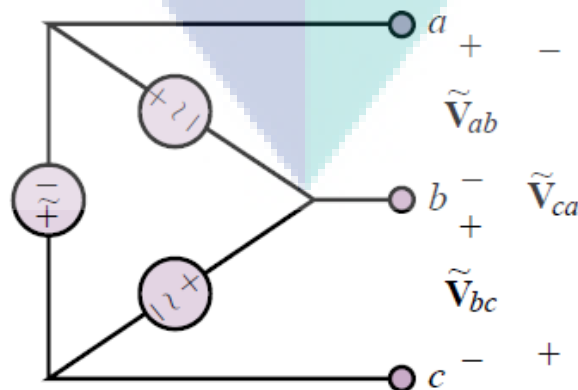


Figure 2.7: Example of Delta connection

(Source: Rizzoni, 2007)

2.2 IRONCORE ELECTRICITY GENERATOR

2.2.1 Element and Working Principle

There are two types of generators: alternating current generator (AC) and direct current generator (DC). Both of them have the same function, which is converting mechanical power into electricity based on the fundamental principle of Faraday's law of electromagnetic induction. For the cored type generator, it is normally found as function of electric amplifier, or so called transformer. The cored type generator is made of several rounding of coils around the iron-core itself. Basically, the name associated with the construction of transformer depends on how the primary and secondary windings are done around the central laminated core. There are two most commonly used designs of transformer construction, namely, the Closed-core Transformer and the Shell-core Transformer. In the closed-core type or core form type transformer, the primary and secondary windings are wound outside and surround the core ring, while for the shell-type or shell form transformer, the primary and secondary windings pass inside the steel magnetic circuit and form a shell around the winding. Figure 2.8 and Figure 2.9 show the construction of the core-type transformer.

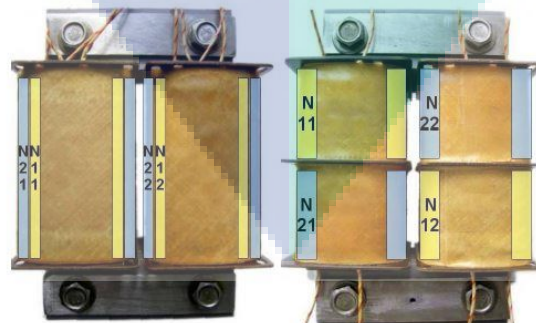


Figure 2.8: Illustration shows construction of the core-type transformer

(Source: Doebbelin et al., 2008)

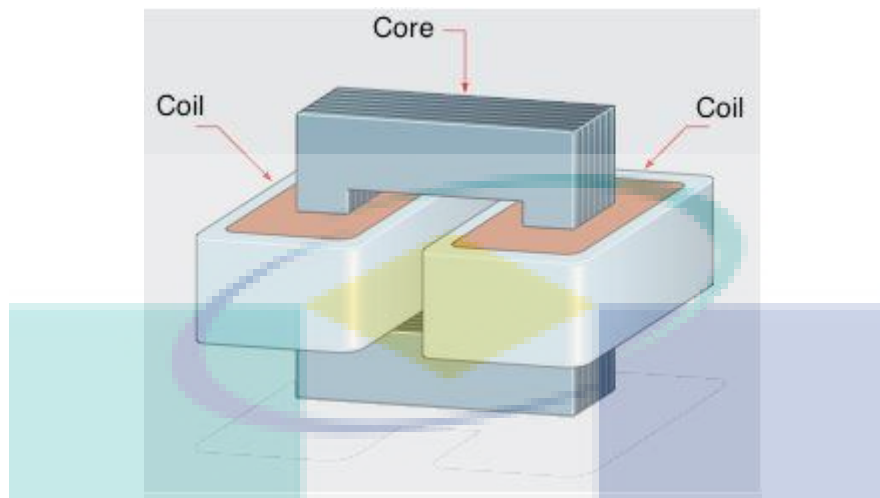


Figure 2.9: Illustration shows the core-type transformer

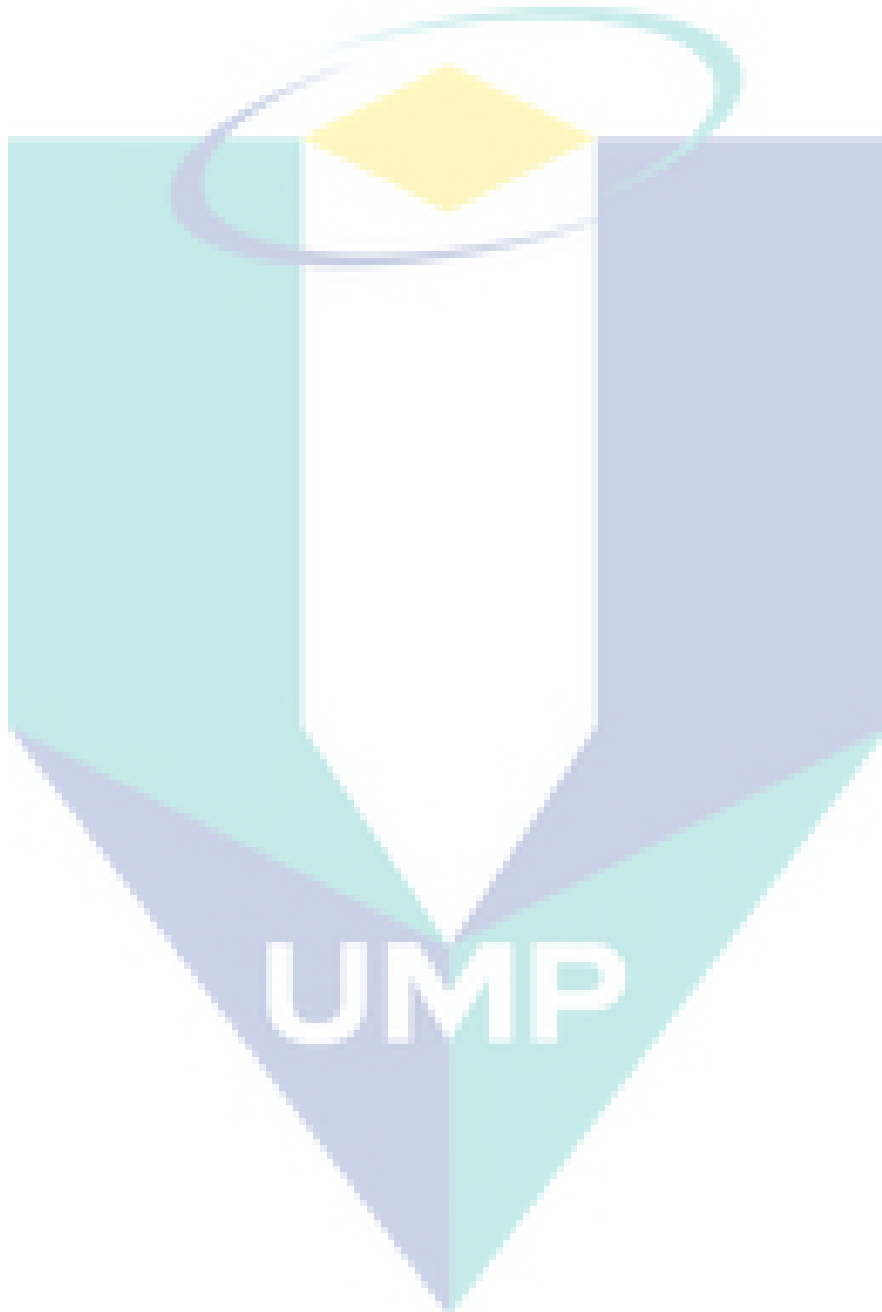
(Source: electrical-info.com)

An electricity generator consists of a wire loop that can be rotated in a stationary magnetic field and thus, induced emf is produced in the loop. The induced emf will be picked up or used by the sliding contact or brushes by connecting the loop to an external circuit.

The pole pieces provide the magnetic field to the wire loop. The loop that rotates through the field is called armature. The two ends of armature loop are connected to slip rings which rotate along the armature. The brushes ride against the ring and the generated voltage will appear across the brushes.

The armature loop rotates in clockwise direction. The starting point is shown as position A in Figure 2.10. The armature loop is perpendicular to the magnetic field at this point. The black and white conductors are moving to become parallel with the field. In this instance, it does not cut any lines of the flux in the magnetic field and thus, no emf is induced in the conductors. This position is called neutral plane. As armature loop rotates from position A to position B, the conductors cut through more flux until they reach position B, which is the maximum of the flux cutting. The emf at position B is maximum. When the armature loop rotates from position B to position C, the number

of flux cutting decreases until it reaches the position C, where there are no flux cuttings because it is parallel with the magnetic field again. This process repeats from position A to position B, followed by position C and the position D and finally back to the original point which is position A.



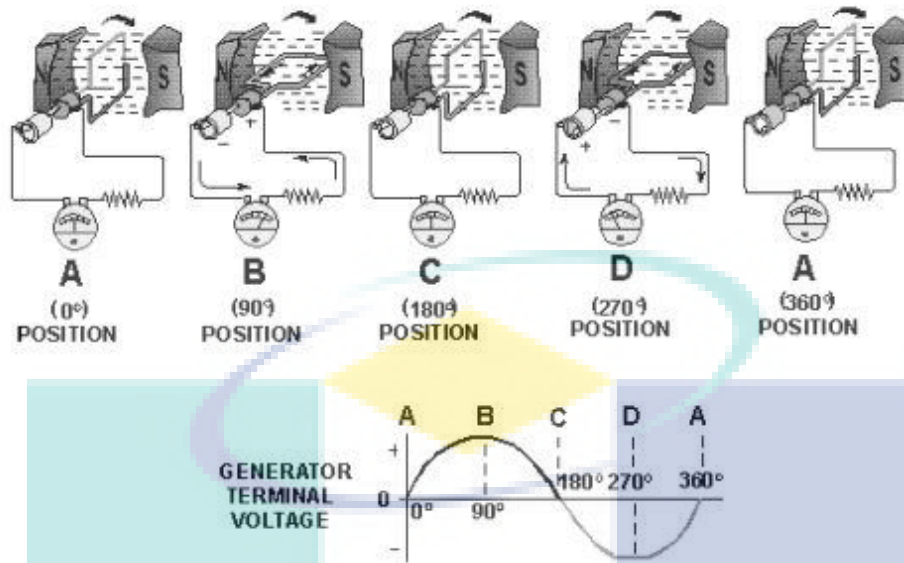


Figure 2.10: Illustration shows the various position of armature as well as generator terminal voltage in various position of armature

(Source: NEETS Module 1, Chapter 5 2013)

Spinning a wire loop within a uniform magnetic field induces a voltage between the loop terminals. If the loop terminals are connected with an electrical load, a current will be produced in the circuit. The current generated by a basic electrical generator is alternating current. If the generator is intended to supply direct current, it must have a collector, which is a device working as a mechanical rectifier (Portela, Sepúlveda, & Esteves, 2008).

2.2.2 Application of An Ironcore Generator

Several applications of such electricity generator are used in our daily life. As we walk around the night market, we realise that the electrical power is provided by the stall owner themselves. They use conventional electricity generator to provide the electricity to power up electrical appliances such as light bulbs. Some house owners also use such generators to power up their houses. This type of generator uses diesel, gasoline or propane to make the motor rotate. When the motor rotates, the alternator

produces electricity to the users. Normally the motor of the generator runs at a constant speed around 3600 rpm.



Figure 2.11: Example of a conventional generator

(Source: Portable Generator Review, 2014)

Alternator, the electricity generator for vehicles, is used to generate electric power for the electrical systems of the vehicles. It is also a major component for the vehicles since it is used to charge battery and prolong the battery life of the vehicles. The alternator is connected to the engine using drive belt or serpentine belt. When the engine is started, the rotational force of the engine drives the serpentine belt, and the serpentine belt transfers the rotational force to the alternator and thus, electric power is generated.

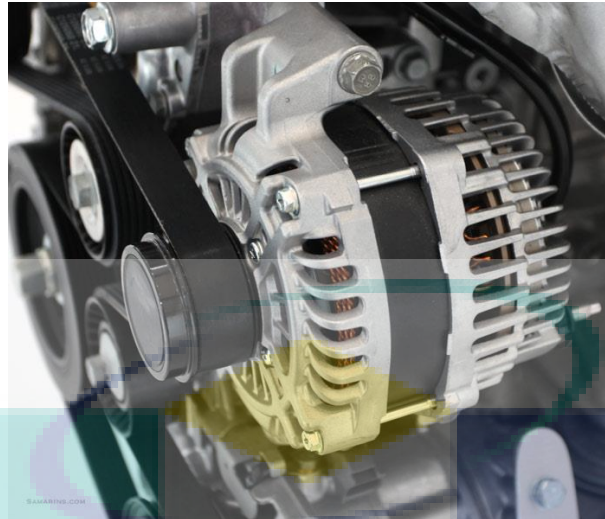


Figure 2.12: Example of an alternator for vehicles

(Source: Samarins.com)

2.3 LOSSES IN AN IRONCORE GENERATOR

The efficiency of the iron core generator is relatively low, typically less than 50%. Recent development of generator which employs the same type of magnet used in the Muller Dynamo has increased the generator efficiency up to 70%. In other words, 50% to 70% of the mechanical energy used to turn the rotor is converted into electricity that can be used by other electrical appliances. It should be noted that 30% to 50% of the energy is wasted due to various losses. For the iron core electricity generator, it requires more work to overcome the counter electromotive force because when the coil is electrified, the magnetic force will be produced within itself and the CEMF will occur between the coil and the magnet. In terms of output power, the cored electricity generator will face losses because of the eddy current losses and hysteresis losses caused by the usage of the ferromagnetic material used in the cored electricity generator. Eq. 2.7 shows the calculation for the efficiency, η , for the generator.

$$\eta = \left(\frac{P_{out}}{P_{in}} \right) 100\% \quad (2.7)$$

To calculate the power output, P_{out} in order to calculate the efficiency, η , Eq. 2.8 is used for this purpose.

$$P_{out} = P_{in} - P_{loss} \quad (2.8)$$

In terms of mechanical power, it can be calculated by using Eq. 2.9 while the electrical power is calculated using Eq. 2.10 where τ is torque, ω is rotational speed in rad/s, I is the current and V is the voltage.

$$P_{mechanical} = \tau\omega \quad (2.9)$$

$$P_{electrical} = IV \quad (2.10)$$

2.3.1 Hysteresis Losses

The hysteresis losses are caused by the tiny magnetic motion when a changing magnetic field is applied. Every time hysteresis loop is traversed, energy generated is lost. This loss is directly proportional to the size of the hysteresis loop of the material. The loop is generated by measuring the magnetic flux of a ferromagnetic material while the magnetizing force is changed. A ferromagnetic material that has never been previously magnetized or has been thoroughly demagnetized will follow the dashed line. As the line demonstrates, the greater the amount of current applied, the stronger the magnetic field in the component. At point "a", almost all of the magnetic domains are aligned and an additional increase in the magnetizing force will produce very little increase in magnetic flux. At this stage, the material has reached the point of magnetic saturation. When magnetizing force is reduced to zero, the curve will move from point "a" to point "b." At this point, it can be seen that some magnetic flux remains in the material even though the magnetizing force is zero. This is referred to as the point of retentivity on the graph and indicates the remanence or level of residual magnetism in the material. As the magnetizing force is reversed, the curve moves to point "c", where the flux has been reduced to zero. This is called the point of coercivity on the curve. The force required to remove the residual magnetism from the material is called the

coercive force or coercivity of the material. As the magnetizing force is increased in the negative direction, the material will again become magnetically saturated but in the opposite direction (point "d"). Reducing magnetizing force to zero brings the curve to point "e." It will have a level of residual magnetism equal to that achieved in the other direction. Increasing magnetizing back in the positive direction will return flux density to zero. It should be noted that the curve does not return to the origin of the graph because some force is required to remove the residual magnetism. The curve will take a different path from point "f" back to the saturation point where it will complete the loop.

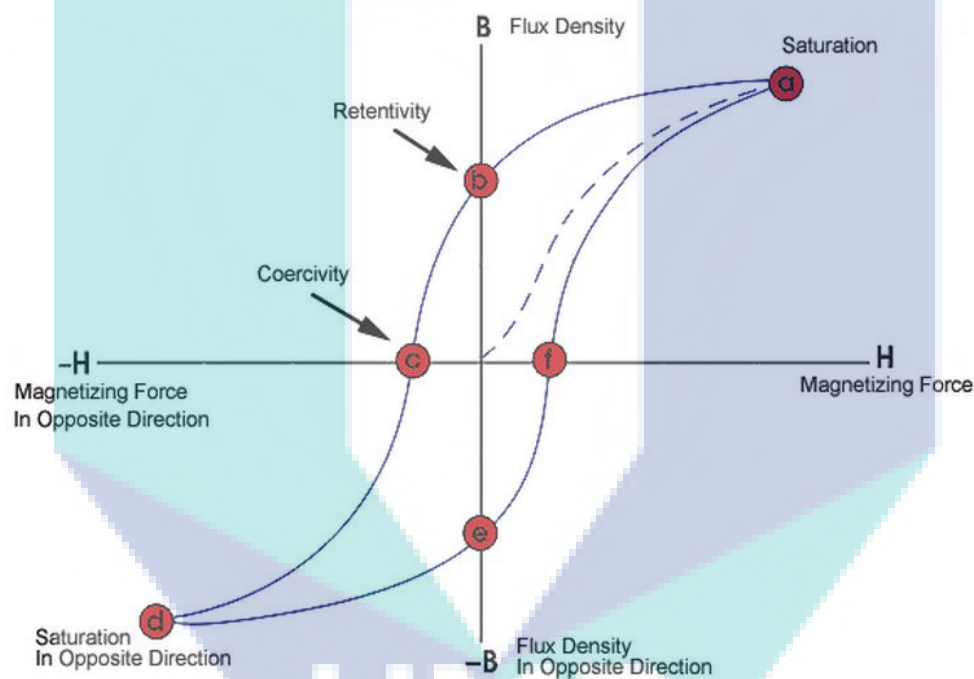


Figure 2.13: Hysteresis loop

(Source: NDT Resource Center)

Eq. 2.11 shows the calculation for the hysteresis loss, W_h where K_h represents hysteresis constant, f represents frequency, B_m represents flux density and n represents Steinmetz exponent, which ranges from 1.5 to 2.5. Since the iron is used, the value will be 1.6.

$$W_h = K_h f (B_m)^n \quad (2.11)$$

2.3.2 Eddy Currents

The armature of the iron core generator is made from soft iron, which is a material that has conductor characteristics and also magnetic characteristics. When a conductive material rotates in a magnetic field, there will be currents induced within it. These induced currents are called eddy currents. The power dissipated from the iron core generator in the form of heat, as a result of the eddy current, is considered a loss of the generator. The resistance of any mentioned material is inversely proportional to its cross sectional area. Eq. 2.12 is used to calculate the eddy current loss, W_e , where K_e represents eddy current constant.

$$W_e = K_e f^2 K_f^2 B_m^2 \quad (2.12)$$

The total power loss, P_{loss} , with consideration of the hysteresis losses and the eddy current losses, can be calculated using Eq. 2.13.

$$P_{loss} = K_h f B_m^n + K_e f^2 B_m^2 \quad (2.13)$$

UMP

2.4 ISSUES RELATED TO IRON CORE LAMINATION

2.4.1 Attraction between Ironcore Lamination and Permanent Magnets

The iron core as well as the permanent magnets used in the iron core generator carries important roles in making the iron core electricity generator functional. Because of the attraction between the iron core lamination and the permanent magnets, it makes the iron core electricity generator become less efficient. Based on the design of the iron core electricity generator, the cogging effect is always present within the generator itself. It is because the force between the permanent magnets and the iron core lamination stack of the iron core electricity generator causes not only the attraction force between themselves, but also a force in the direction of motion as well. This type of force depends on the relative position of the laminated teeth with regards to the magnetic poles for the iron core electricity generator (Stampfi, 2003).

2.4.2 Cogging Torque in An Ironcore Generator

The cogging torque may also be referred to as reluctance torque due to the reluctance variation that exists in the tooth and slot of the magnet current source (Mosincat, Lu & Pedersen, 2011). Cogging torque as high as 25% of the rated torque can result due to the improper design of the machines (Krishnan, 2009).

Choosing the right angle of clearance at the both ends will help to reduce the cogging effects within the iron core generator. Nevertheless, ironless configuration will be the right solution for high smoothness of motion. This is because the ironless configuration has no cogging effect since it has no iron moving parts at all (Stampfi, 2003). Other techniques such as varying the magnet strength used on the generator, varying the magnet arc length, the slot width, and the radial shoe depth as well as using fractional slots per pole, can be used to minimize the cogging torque of the generator (Krishnan, 2009; Bianchi & Bolognani, 2002). Almost all techniques that are used to reduce the cogging torque also reduce the counter-electromotive force and thus, reduce the resultant running torque (Mosincat, Lu & Pedersen, 2011).

2.5 IRONLESS/ CORELESS GENERATOR DESIGN AND PRINCIPLE

Other than iron core generator, recently the researcher had introduced coreless electricity generator towards the global. The principle of electricity generation for the coreless electricity generator is based on the concept of Fleming's left hand rule and Fleming's right hand rule stated in Section 2.1 of this chapter. When the rotor spins, the magnetic flux is cut by the coil on the stator, and thus, electric current is produced.

The coreless configuration for the generator eliminates the usage of ferromagnetic material within the generator, thus eliminating the eddy current as well as hysteresis losses which are caused by the ferromagnetic materials. This type of generator can be stacked axially, allowing the users to simplify the mechanical construction (Gieras, Wang & Kamper, 2008). The coreless configuration of the axial flux permanent magnet generator machine can operate at higher efficiency compared to the conventional generator as it does eliminate the core losses within the generator itself (Lombard & Kamper, 1999; Wang et al., 2005; Madawala & Boys, 2005).

Due to the compactness and lightness as well as the high efficiency of the axial-flux coreless machine, it is among the most suitable candidate for many automotive applications (Mirzaei, Mirsalim & Abdollahi, 2007). Because of the absence of core loss that is caused by the iron core itself, the coreless stator axial-flux permanent-magnet (AFPM) machine can operate with higher efficiency compared to the conventional iron core machines (Del Ferraro et al., 2006). Due to the result of power loss reduction of the coreless electricity generator, it helps to improve the machine efficiency (Oh & Emadi 2004; Huang et al., 1999; Parviainen, Niemelä & Pyrhönen, 2004). The coreless configuration of AFPM generator is able to operate at higher efficiency than conventional generator regardless of the rotational speed, because of the elimination of core losses (Di Napoli et al., 1991; Spooner & Chalmers, 1992).

For the coreless type generator, it normally acts as a converter, which converts kinetic energy into electrical energy that is normally found as a part of wind turbine. In this coreless type generator, it is made up of two different parts, namely, rotor and stator. There are five different types of combination for coreless type generator: a double-stator slotted type; a double-rotor slotted type; a single-sided axial flux permanent magnet

with stator balance; a single-sided axial flux permanent magnet with rotor balance; and, a slotless single-stator double-rotor type. It has been claimed that the two-sided axial flux permanent magnet type is better than the one-sided axial flux permanent magnet (Li & Chen, 2008). Figure 2.14 and Figure 2.15 show the configuration of slotless single-stator double-rotor AFPM and slotted double-stator single-rotor AFPM configuration, respectively.

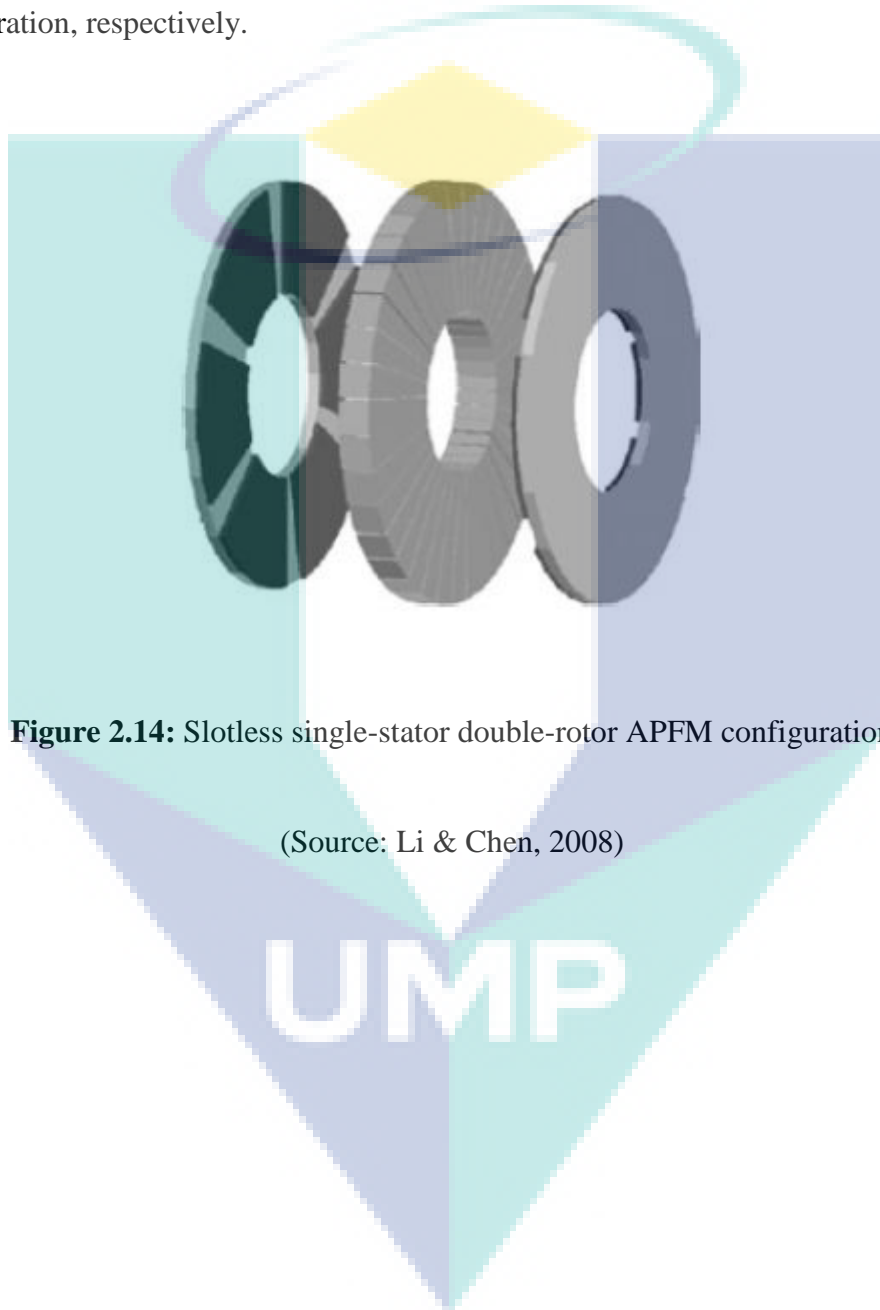


Figure 2.14: Slotless single-stator double-rotor APFM configuration

(Source: Li & Chen, 2008)



Figure 2.15: Slotted double-stator single-rotor AFPM configuration

(Source: Li & Chen, 2008)

2.6 CORELESS GENERATOR

2.6.1 Application of Coreless Generator

In the near future, it is anticipated that wind energy generation system can be another potential source of alternative energy (Abdullah et al., 2012; Saidur et al., 2010) to replace the usage of non-renewable energy. The key factor of harvesting wind power from the wind is the conversion efficiency of power generator of the wind power generation system (Gieras, Wang & Kamper, 2008; Muljadi, Butterfield & Wan, 1999). Since the coreless electricity generator has no cogging torque as well as starting torque, it is suitable to be applied in the wind turbine. This is because there is no iron being used in the stator, which avoids direct magnetic attraction between rotor and stator (Gieras, Wang and Kamper, 2008). Moreover, APFM machine has thin magnets, means that smaller than radial-flux counterparts. (Mahmoudi, Rahim & Hew, 2011). Its compactness and disk-shaped profile make it very suitable for pairing it for the usage of wind turbine electricity generation (Chalmers & Spooner, 1999). For instance, based on their research, Ahmed and Ahmad (year) have proposed the usage of axial flux permanent magnet (AFPM) as a part of the wind turbine. Figure 2.16 shows the construction of wind turbine using axial flux permanent magnet (APFM) generator.

The comparison results demonstrate that the proposed model for the wind power generator exhibits improved efficiency with variable speed operation, higher energy yield and better wind power utilization. Moreover, the maximum efficiency of the proposed generator at the rated operating conditions is 96.6%, compared to 95.7% in the AFPM generator model proposed. The proposed design has also reduced the weight of the nacelle since it uses non-ferromagnetic cores that are lighter in weight compared to the ferromagnetic material and provides a gearless turbine system (Ahmed & Ahmad, 2013). Compared to Radial Flux Permanent Magnet (RFPM), AFPM has smaller volume and lower mass with the same power rating (Gieras, Wang & Kamper, 2008).

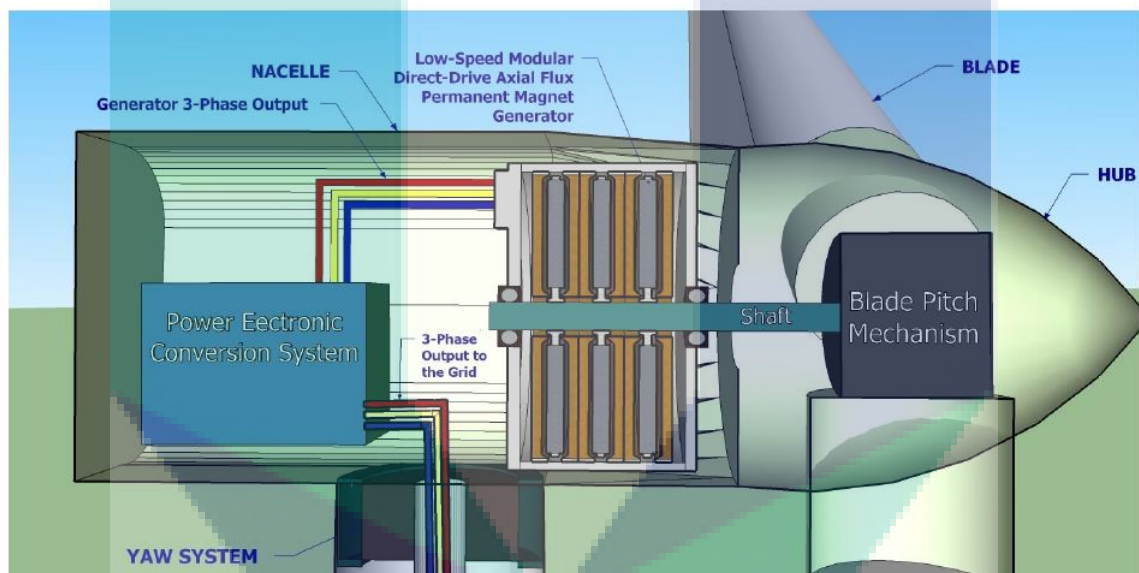


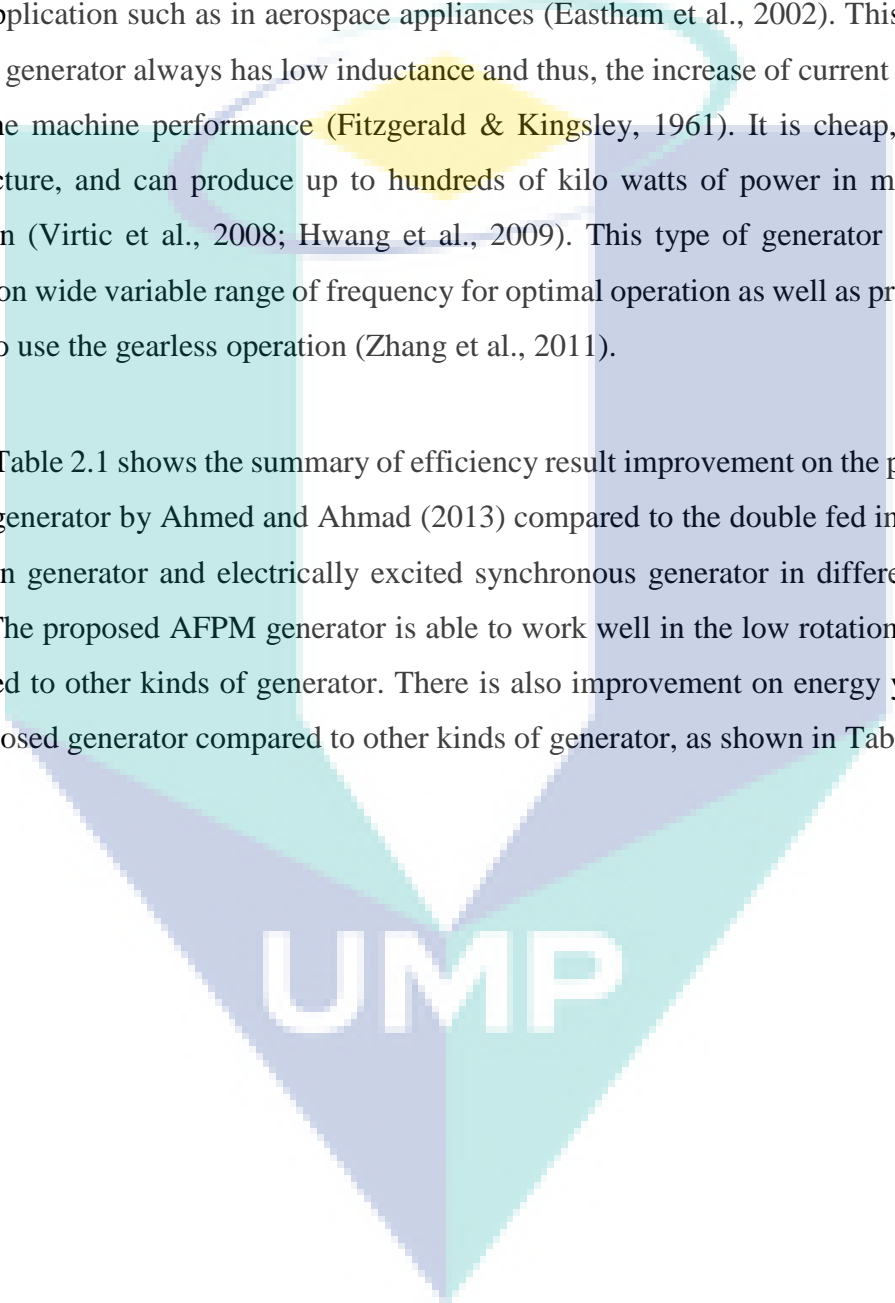
Figure 2.16: Wind turbine generating system model using AFPM generator

(Source: Ahmed & Ahmad, 2013)

Compared to other types of generator, the permanent magnet synchronous generator is more preferred as it has higher efficiency, reliability, power density, construction without the usage of gears and is light-weight. (Molina, dos Santos & Pacas, 2010; Li, Haskew, & Xu, 2010; Lopez, 2007; Muyeen et al., 2010; Qiu, Zhou & Li, 2011). The permanent-magnet motors are gaining reputation amongst the researchers because of their high-power density, high torque-to-inertia ratio, and high efficiency (Lombard & Kamper, 1999; Breton et al., 2000) as well as their robustness

(Chen & Liu, 2012). The high compactness and disk-shaped profile make the model suitable for integration with mechanical components such as wind turbine and internal combustion engine (Wang et al., 2005) as well as additional generator for hybrid vehicles. The AFPM generator has been investigated for medium-speed application such as automotive generators (Caricchi, Crescimbinì & Santini, 1995) as well as high-speed application such as in aerospace appliances (Eastham et al., 2002). This kind of coreless generator always has low inductance and thus, the increase of current does not affect the machine performance (Fitzgerald & Kingsley, 1961). It is cheap, easy to manufacture, and can produce up to hundreds of kilo watts of power in multi disk operation (Virtic et al., 2008; Hwang et al., 2009). This type of generator can also operate on wide variable range of frequency for optimal operation as well as provide an option to use the gearless operation (Zhang et al., 2011).

Table 2.1 shows the summary of efficiency result improvement on the proposed AFPM generator by Ahmed and Ahmad (2013) compared to the double fed induction, induction generator and electrically excited synchronous generator in different wind speed. The proposed AFPM generator is able to work well in the low rotational speed compared to other kinds of generator. There is also improvement on energy yields of the proposed generator compared to other kinds of generator, as shown in Table 2.2.

The logo for UMP (Universiti Malaysia Perlis) is a large, stylized letter 'U' composed of four overlapping triangles in shades of teal and blue. The letters 'UMP' are printed in white, bold, sans-serif font across the center of the 'U' shape.

UMP

Table 2.1: Efficiency result

Wind Speed (m/s)	Percentage improvement in efficiency of the Proposed AFPM Generator compared to:		
	DFIG	IG	EESG
12	26.69%	36.36%	24.73%
9	31.06%	IG stalled	34.62%
6	46.68%	IG stalled	42.62%
3	DFIG stalled	IG stalled	66.33%

(Source: Ahmed & Ahmad, 2013)

Table 2.2: Energy yield result

Percentage improvement in Energy Yield of the Proposed Generator compared to:		
DFIG	IG	EESG
32.41%	50.80%	24.75%

(Source: Ahmed & Ahmad, 2013)

Axial Flux Permanent Magnet (AFPM) generators are usually driven at low speeds, and hence, to increase the output power, a higher number of pole pairs are used. The special characteristic of the axial-flux coreless permanent-magnet generator is the usage of non-ferromagnetic holder to counteract the centrifugal forces acting on the magnet during the rotation of the rotor disks (Hosseini, Agha-Mirsalim & Mirzaei, 2008).

2.6.2 Arrangement/ Configuration of Coreless Generator

To confirm the performance of this kind of generator, they manufacture a small model of coreless generator using stacked magnetic circuit (Kobayashi et al., 2009).

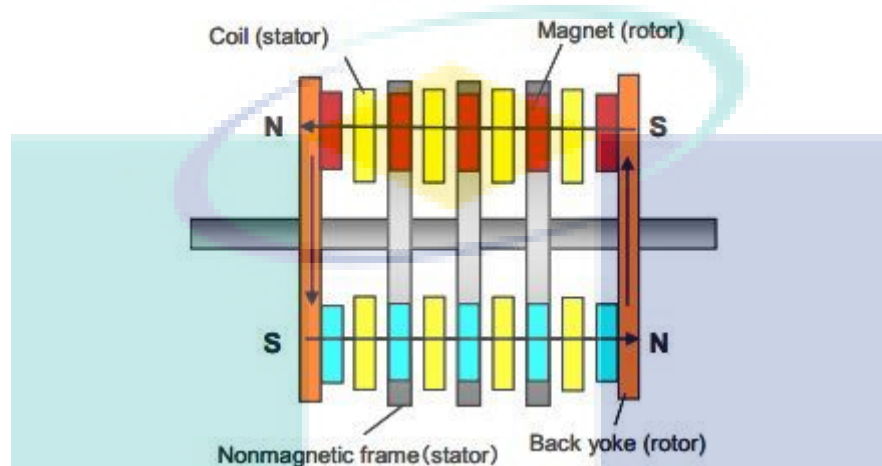


Figure 2.17: Illustration shows the structure of the stacked magnetic circuit

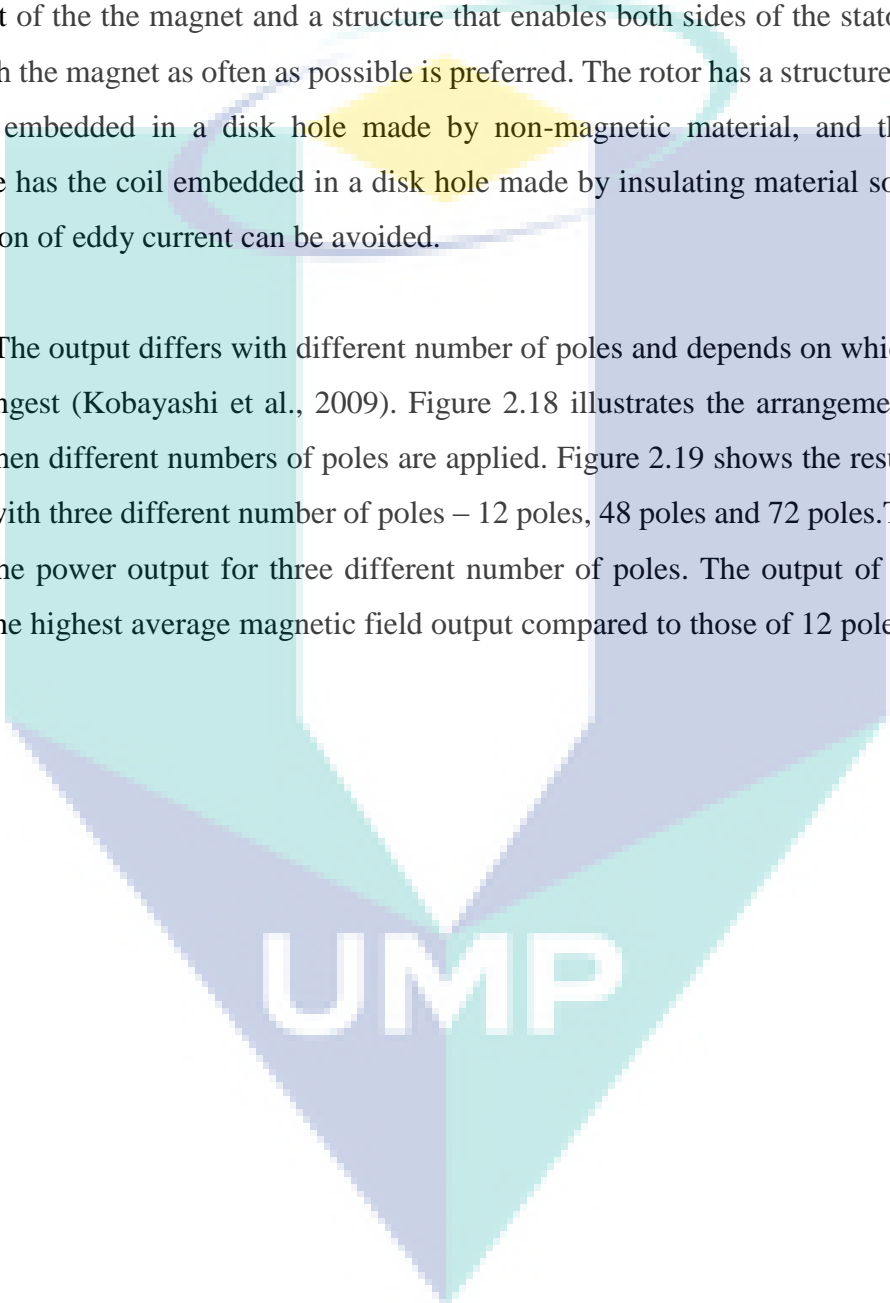
(Source: Kobayashi et al., 2009)

This structure involves the axial gap coreless generator stacked in the axial direction. The rotor is coupled on the rotational shaft and the stator is arranged accordingly to the case. The permanent magnet is fixed to rotors in the ring shape and the magnetization direction is aligned with the neighbouring rotor, and magnetic field is generated between the gaps and the rotors. The magnet is attached with ferromagnetic material at the edge of axial direction in order to suppress the magnetic flux external leakage of the magnet. The flux is recycling to increase the magnetic field in the gap. It is structured to increase the magnetic field in the gap of the rotors by forming the closed magnetic circuit on the magnet of stacked rotor as well as the edge back yoke of the stacked magnetic circuit.

The stator is positioned in the gap of the rotor; the coreless coil is placed in a ring shaped in the stator so that it is able to generate the electromotive force by receiving the alternating magnetic field. The generated voltage can be directly proportional to the stator number as each stator receives the alternating magnetic field in the same phase.

It can be done by connecting the coil in series at the same position of each stator. The increase of the voltage generation is directly proportional with the increase of the power output, and the generated voltage is also proportional to the strength of magnetic field. It is advised that the gap between rotors be made as small as possible so that it can increase the magnetic field. Moreover, the thickness of the rotor should not be more than that of the the magnet and a structure that enables both sides of the stator coil to approach the magnet as often as possible is preferred. The rotor has a structure with the magnet embedded in a disk hole made by non-magnetic material, and the stator structure has the coil embedded in a disk hole made by insulating material so that the generation of eddy current can be avoided.

The output differs with different number of poles and depends on which one is the strongest (Kobayashi et al., 2009). Figure 2.18 illustrates the arrangement of the poles when different numbers of poles are applied. Figure 2.19 shows the result of the output with three different number of poles – 12 poles, 48 poles and 72 poles. Table 2.3 shows the power output for three different number of poles. The output of 48 poles shows the highest average magnetic field output compared to those of 12 poles and 72 poles.

The logo for UIMP (Universiti Malaysia Perlis) is a large, stylized letter 'V' shape. The left side of the 'V' is light blue, the right side is light green, and the bottom point is a darker blue. The letters 'UIMP' are written in white, bold, sans-serif font across the bottom of the 'V' shape.

UIMP

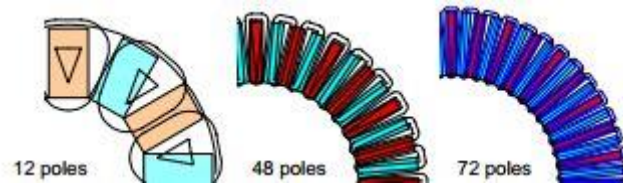


Figure 2.18: Illustration shows the arrangement of poles of three different numbers of poles

(Source: Kobayashi et al., 2009)

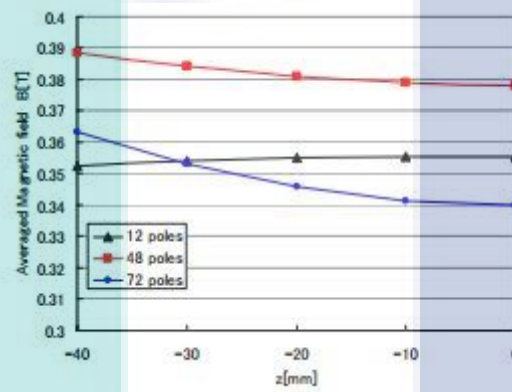


Figure 2.19: Illustration shows the average magnetic field with respect to the gap distance between the rotors of three different numbers of poles

(Source: Kobayashi et al., 2009)

UMP

Table 2.3: Results of power outputs in three different numbers of poles

Pole number	12	48	72
Rated power [MW]	7.8	6.5	5.4
Magnet weight [ton]	52	47	46
Coil weight [ton]	42	22	18
Efficiency	0.96	0.97	0.97
Drive type	Direct drive		
Rated rotation speed [rpm]	13		
Diameter of rotor [m]	9.6		
Cooling	Natural		

(Source: Kobayashi et al., 2009)

The generator proposed by Ahmed and Ahmad (2013) consists of a multi-disc structure with three modules and each module comprises the same two stator discs and a rotor disc. The stator is serially connected and these three modules are connected in parallel so that the net output power of the generator can be increased. The stator and rotors are coreless, which will minimize the attraction force between stator and rotor as well as minimize the cogging effect, a force that resists the rotor to spin smoothly.

High-speed three phase 1kW coreless surface mounted with axial flux permanent magnet (APFM) generator with circular magnets and coils has been studied (Fei et al., 2010). Figure 2.20 illustrates the proposed machine structure of high-speed coreless surface mounted AFPM generator. The proposed design consists of two rotor discs and one stator disc in between the two rotor discs. There is sufficient clearance between the rotor and stator discs. The magnets on each rotor disc are aligned and faced with the opposite polarity during the assembly process.

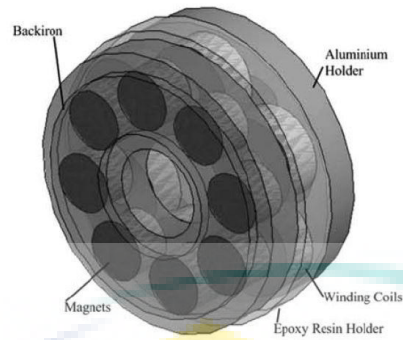


Figure 2.20: Proposed machine structure of high-speed coreless surface mounted APFM generator

(Source: Fei et al., 2010)

Coreless configuration of axial-flux machine eliminates ferromagnetic material, thus, it eliminates the eddy current and hysteresis losses in the generator and it can be axially stacked so that the mechanical construction of the coreless axial-flux machine can be simplified, reducing the weight of the stator so that small size actuator is able to be employed for winding shift (Javadi & Mirsalim, 2010). Figure 2.21 shows the proposed machine structure as used by Javadi and Mirsalim (2010) in their research, while Figure 2.22 and Figure 2.23 show its flux path and its machine part arrangement, respectively.

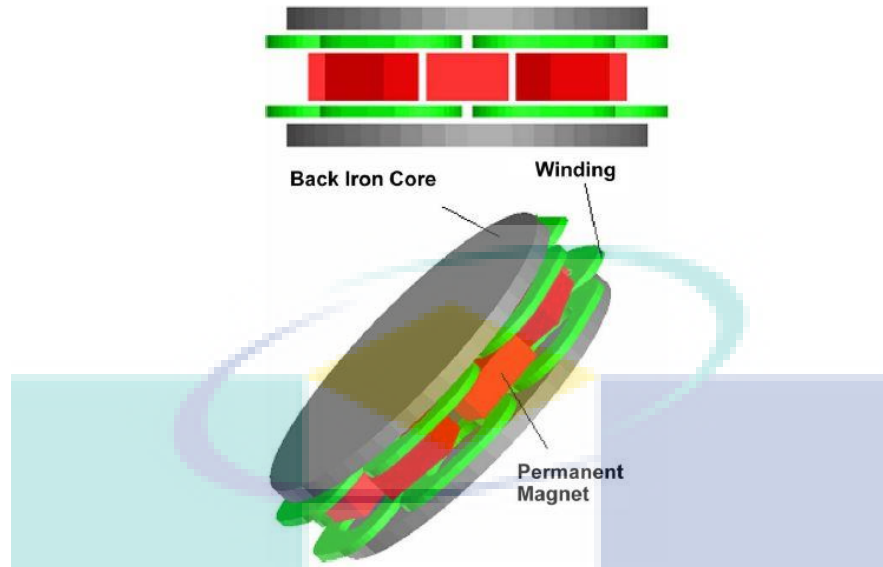


Figure 2.21: Illustration shows the proposed machine structure used by Javadi and Mirsalim (2010)

(Source: Javadi & Mirsalim, 2010)

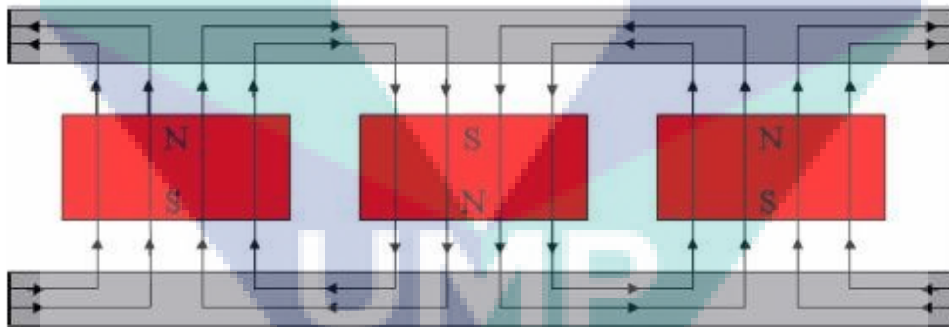


Figure 2.22: Illustration shows the flux path of proposed machine structure used by Javadi and Mirsalim (2010)

(Source: Javadi & Mirsalim, 2010)

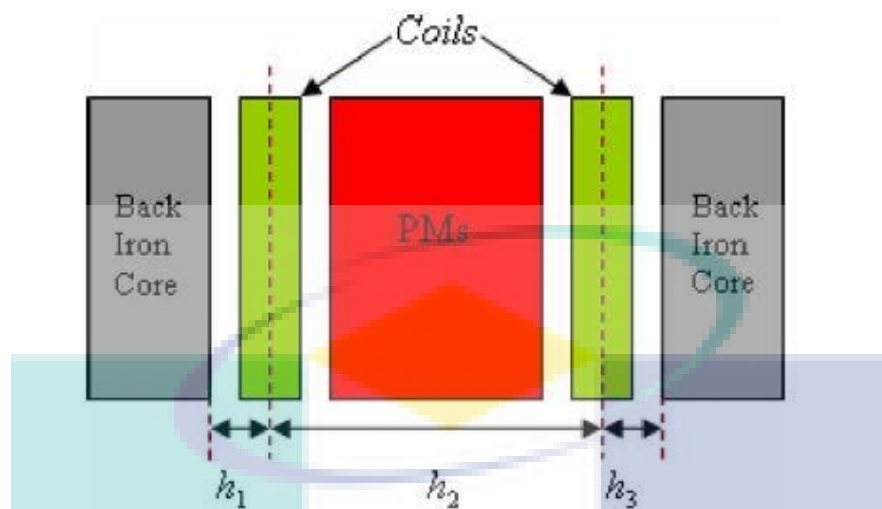


Figure 2.23: Illustration shows the machine parts arrangement used by Javadi and Mirsalim (2010) in their research

(Source: Javadi & Mirsalim, 2010)

Figure 2.24 shows the Drazikowski and Włodzimierz's (2011) research model which contains 12 pair poles synchronous machine and a double rotor equipped with 24 magnets per disk. Between the magnets, there are air-core three phase windings within them. This design has various advantages, for example, no starting and cogging torque, cheap and easy to manufacture. The biggest drawback for this design is that it requires the use of stronger magnets to obtain the same power like in iron-cored machine, which is the reason of higher reluctance of magnetic circuit (Drazikowski & Włodzimierz, 2011).

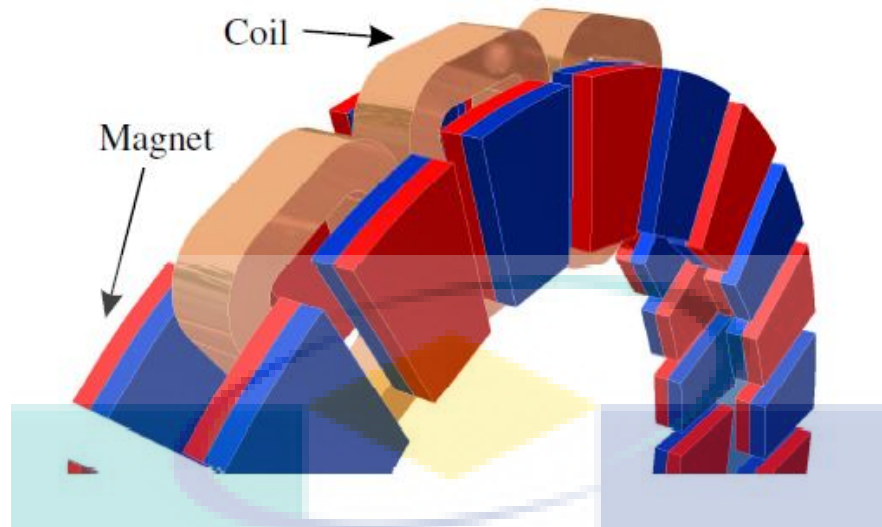


Figure 2.24: Illustration shows the machine structure in Drazikowski and Włodzimierz's research

(Source: Drazikowski & Włodzimierz, 2011)

2.7 DESIGNING IRONLESS CORELESS GENERATOR

2.7.1 Magnet Used in Ironless Coreless Generator

Since the magnet plays an important role in making the generator an efficient one, the process of choosing the magnet needs to be considered well. Neodymium Iron Boron (NdFeB) magnets are well known as the best magnet to be used. The continuous progress in the new high magnetic field rare-earth permanent magnets such as Neodymium Iron Boron (NdFeB) magnet, has given the automotive sector a great opportunity on novel topologies for electric machine (Mo et al., 2008). Greater availability and decreasing cost of high-energy permanent-magnet materials, which is Neodymium Iron Boron (NdFeB) magnet, has resulted in rapid permanent magnet generator development (Chan & Lai, 2007). This modern magnetic material can easily be obtained in the market with different shapes and grades, thus the design of the usage for these magnets can be done easily. It can provide power even during electrical network failure as a result of the built-in permanent self-excitation (Drazikowski & Włodzimierz, 2011).

For large-pole number, the diameter of the magnets and coils are fixed and limit the radial length of the active area, which makes the generator have large radius but small active length. As for the small-pole number, low-power turbines tend to spin relatively fast, but as power increases and a reduction in speed is required, the number of poles should increase, which can make the radial length of the active area become small compared to the radius of the stator. This kind of problem can be reduced by using trapezoidal or rectangular magnets whereby this helps the pole pitch and active length can be decoupled from each other (Bumby & Martin, 2005).

2.7.2 Coil Design for the Ironless Coreless Generator

The arrangement of the copper winding should be designed well so that maximum magnetic flux cutting can be done which maximises the efficiency of the generator itself. For the coreless electricity generator, coils of wire are used instead of multiple interconnected wires where the magnet rotates over them to produce the electricity. For instance, when the north pole of a magnet passes through a coil, the current flows in one direction, and when the south pole passes over the coil, current flows through in the opposite direction. Based on the theories, the most electricity is generated while the magnetic field is at 90 degrees to the coil winding and no electricity is generated when the magnetic field is parallel to the coil.

The magnet at the north pole pushes upward on the left radial leg of the coil and at the same time, the magnet at the south pole is pushing downward on the right radial leg. These two clockwise motions cause the electricity being generated. Notice that if both radial legs are pushing in the same direction, for example, the left and right radial leg are pushing upward together at the same time, the motion cancels out each other and thus, no electricity is generated. That is the reason which shows that it is essential to arrange the magnet poles alternatively so that the motion will not cancel out each other.

The size of the copper winding is also an important criterion for the efficiency of coreless electricity generator. Figure 2.25 shows the coil dimension for the axial-flux permanent magnet generator where c represents the thickness of the coil and $d(r)$ is the diameter of the coil.

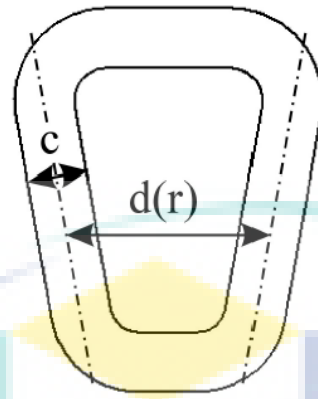


Figure 2.25: Coil dimension for the axial-flux permanent magnet generator

(Source: Drazikowski & Włodzimierz, 2011)

The pole pitch and diameter of coil can be calculated via Eq. 2.14 and Eq. 2.15 respectively where τ is pole pitch, r is radius, k is the number of coils per phase, n is the rotor rotation speed in rpm, l is the length of conducting wire, z is the number of turns, c is the coil thickness, d is the coil diameter as shown in Figure 2.25, while x is the actual position in mm and E is the electromotive force. In order to make pole pitch equal to diameter of coil, the thickness of the coil cannot be increased more than 33% of pole pitch because of geometrical relation. In other words, the distance between the coils must be equal to 133% of the pole pitch (Drazikowski & Włodzimierz, 2011). Figure 2.26 shows the approximated power of the generator via the different relative thickness of coil (c/τ) in Drazikowski and Włodzimierz's (2011) research.

$$\tau = 2r \sin(7.5^\circ) \quad (2.14)$$

$$E(x) = k \frac{2\pi r \cdot n}{60} l z \frac{1}{c} \left[\int_{x-\frac{1}{2c}}^{x+\frac{1}{2c}} B_m \sin\left(\frac{\pi}{\tau} x\right) dx - \int_{x-\frac{1}{2c}}^{x+\frac{1}{2c}} B_m \sin\left(\frac{\pi}{\tau} (x+d)\right) dx \right] \quad (2.15)$$

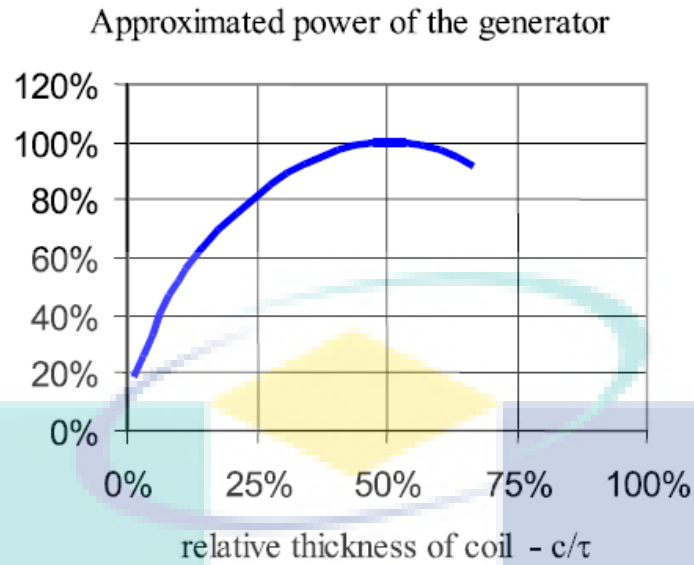


Figure 2.26: Approximated power of the generator via the different relative thickness of coil (c/τ)

(Source: Drazikowski & Włodzimierz, 2011)

2.7.3 Gap Distance between Magnets

The gap between magnets is also a point needed to be taken care of during the design of the coreless generator itself. If the gaps between the magnets are too far away, the efficiency of the generator cannot reach its full potential. However, if the gaps between the magnets are too close to each other, there will be no room or space left to place the stator (copper coil winding) between them.

The optimum air-gap size is calculated using Eq. 2.17, where B_m represents maximum flux density in the air-gap, g represents the thickness of magnet, μ_0 represents air permeability that can be calculated using Eq. 2.16, B_r is for remanence, H_c is for coercivity of magnet, δ represents air-gap length, H is for external magnetic field strength and m represents magnetic moment (Drazikowski & Włodzimierz, 2011).

$$\mu_0 = 4\pi \cdot 10^{-7} \frac{H}{m} \quad (2.16)$$

$$B_m = \frac{2g\mu_0 B_r H_c}{B_r \delta + 2g\mu_0 H_c} \quad (2.17)$$

In Drazikowski and Włodzimierz's (2011) research model, their machine optimum air-gap size was approximately 35mm. For economic reasons, 33mm was chosen as the preferred air-gap because increasing air-gap between 33mm to 38mm was found to have had no significant influence on the total output power.

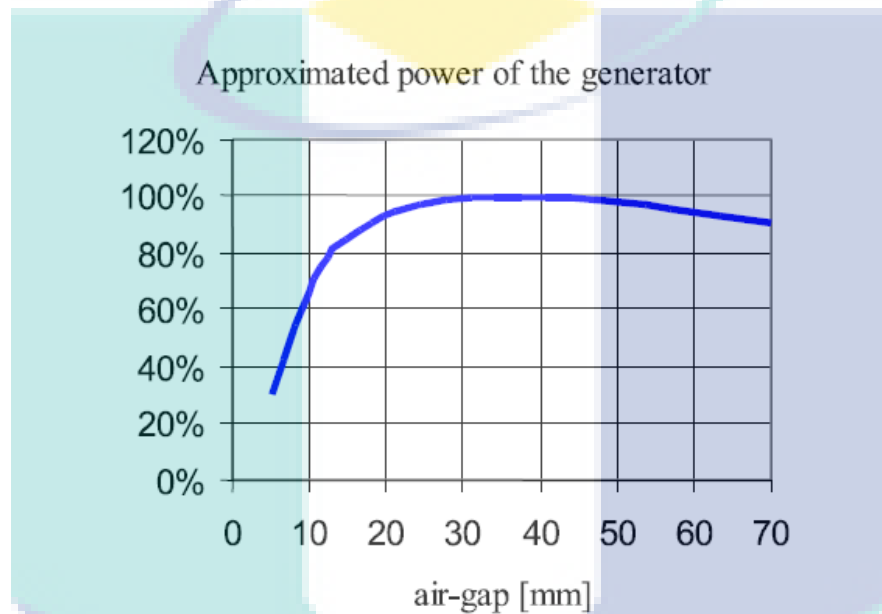


Figure 2.27: Approximated power of the generator varies on air-gap distance

(Source: Drazikowski & Włodzimierz, 2011)

UMP

2.7.4 Number of Poles and Coils for the Ironless Coreless Generator

There are a few sets of rules for the pole and slot combinations that make non-overlap windings valid as suggested by Gieras, Wang and Kamper (2008). The rules are:

- The number of poles must be even;
- The number of slots must be a multiple of the number of phases and must be even in the case of single layer windings;
- The number of coils and slots are equal in double layer windings; in single layer windings the number of coils is equal to half the number of slots;
- The number of coils in a coil group must be an integer;
- The number of slots cannot be equal to the number of poles.

To verify the number of poles, Eq. 2.16 is used to perform such function, as N represents rotational speeds of the rotors in RPM, f represents frequency of the rotors and p represents number of poles on each rotor (Rizzoni, 2007).

$$N = \frac{120f}{p} \quad (2.16)$$

2.8 FINITE ELEMENT TOOL FOR ELECTROMAGNETISM ANALYSIS

There are a lot of finite element tools in the market to solve and analyse the design based on the user needs, for example, ANSYS and Autodesk Multiphysics. As for the electromagnetism analysis, JMAG, Simulation Technology for Electromechanical Design is suitable in carrying out such task. JMAG, a software which specializes in conducting electromagnetic analysis, is used in this study because of its prominence in the electromagnetic field. This software is capable of analysing the electromechanical design such as Three-Phase Synchronous Generator (Jenal et al., 2013). In the research conducted by Pop et al. (2013) on the Axial-flux versus radial-flux permanent-magnet synchronous generators for micro-wind turbine application, JMAG-Designer 12.0 was used to analyse the performance of their small-scale three-phase axial-flux permanent magnet synchronous machine.

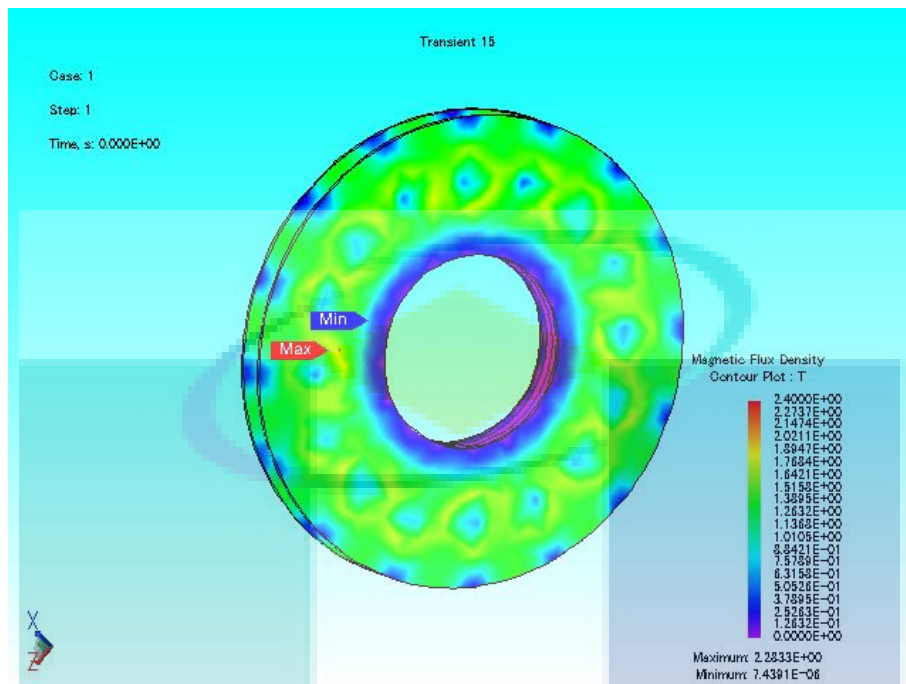


Figure 2.28: Magnetic flux density distribution for the three-phase small scale PMSG

(Source: Pop et al., 2013)

JMAG-Designer is the high-speed, high-precision Finite Element Analysis software tool at the core of JMAG. It has intuitive interface and precise modelling technology with a wide variety of result displays. Multifaceted evaluation of various design ideas is made possible by manipulating geometry, material properties and drive conditions. Hence, many parameters such as the number of turns of coil per phase and the type of magnet used can be specified and optimization on the ironless electricity generator can be done once the software is mastered.

2.9 SUMMARY OF THE CHAPTER

Studies have found that there are fundamental weaknesses of the iron core generator, for example, hysteresis losses and cogging torque which are caused by the iron core lamination. Both increase proportionally with the increase of power output. An increase in cogging torque has led the increment of shaft power input, hence reduces the efficiency of the system. An ironless motor works in the same principle as the conventional iron-cored motor does. However, the motor has no soft iron core lamination, hence, no cogging would be present. Therefore, high precision motion can be achieved because there is no attraction force, or in other words, cog does not exist. Similar technique may be used to adapt this idea to develop an ironless coreless generator. It is anticipated that with a similar design concept, the developed ironless coreless generator can benefit from what ironless motor has to offer. With the ironless and coreless design, the generator is expected to be cog-free, and thus requires lesser torque to spin if compared to the conventional generator. However, the efficiency of the ironless coreless generator still relies on the similar aspects of conventional generator, such as air gap distance, number of coils and turns, magnet grades, number of poles and type of connection. Based on the studies reviewed in this chapter, the air gap distance has to be kept closer in order to confine the most of the magnetic flux. The number of coils and turns have to be larger in order to produce high voltage electricity. In addition, magnet grades have to be the highest quality and of neodymium type to guarantee high density magnetic flux on the magnetic poles area. The number of poles has to be many with a view to increase the voltage output and stability. Studies which have been reviewed in this chapter were used to guide the present research in the development work of the ironless coreless generator.

CHAPTER 3

PRELIMINARY FINDINGS: FINITE ELEMENT ANALYSIS

3.1 INTRODUCTION

Prior to the fabrication works, finite element analysis was carried out to study the characteristics and behaviour of the designed ironless electricity generator. The generator concept design was done using Solidworks, a computer-aided design (CAD) tool. Concept design was then exported to a finite element analysis software dedicated for electromechanical analysis. JMAG Designer was the finite element analysis software used to perform electromagnetism analysis throughout this research because its ability to predict behavioural studies of new generator and electromechanical machine concepts has been widely proven (Jenal et al., 2013; Pop et al., 2013).

There were several parameters analysed using the JMAG Designer. Transient response analysis was used in the JMAG Designer because this research had to analyse the moving rotor. The parameters analysed were the number of coil turns per phase, gap distance between the magnet pairs as well as the magnet grade used. These few parameters were analysed under the open circuit condition, or there was no load on the ironless generator. It was because with this condition, the best result for each parameter could be obtained with minimum amount of analysis run time. After all results of parametric studies had been obtained, the model was redesigned based on the best result for each parameter. The redesigned model was then analysed using the finite element analysis again using closed circuit method to qualify its performance under some load.

3.2 PROCEDURE

In this research, electromechanical analysis was emphasized since the design involved the usage of magnet. Because of the magnet, electromechanical analysis could help gain the result of magnetic flux exerted by the magnet from the magnetic flux density distribution of the electricity generator design and the magnetic flux on the coil.

The ironless electricity generator was designed using CAD software, Solidworks, based on the knowledge from literature review. The proposed design for the ironless coreless electricity generator in this research was double-rotor single-stator configuration. Within the stator, there were 12 coils which were joined using three-phase star connection. As for the rotors, 16 magnets were embedded on each rotor. The ironless coreless electricity generator model was then exported to the JMAG designer software when design was done. The ironless coreless electricity generator model was analysed by using JMAG designer analysis software. Transient analysis was used to examine the model because it was able to simulate real life situation in which the ironless coreless electricity generator would be operating.

After choosing the type of magnets to be used in the analysis, the direction of the magnetic force was defined. Since the connection for the ironless coreless electricity generator model has to be in star three-phase connection, the circuit connection for the analysis on the model was set accordingly. The voltage probe was attached on the end of star three-phase connection so that the voltage for each phase could be shown. As for the open-loaded test, there was no load applied on the circuit. Meanwhile, for the closed-loaded test, the load was applied on the end of the star connection. After the connection for the analysis was defined, the rotation motion which needed to be applied on the rotors of the model was defined. It was set to 500 rotational per minute as the rotational speed would be the constant variable for this experiment. The U-phase, V-phase and W-phase FEM coils were defined accordingly and set to clockwise direction to avoid directional error on the circuit. All these coils were then synchronised with the circuit.

As for the meshing type in this analysis, the standard meshing with auto meshing method was chosen as the software set the appropriate meshing size by default for the ironless coreless electricity generator model. The step control for the analysis on the model for this research was set based on Eq. 3.1 where t_1 is desired end time of the analysis and t_0 is start time of analysis. For the case on this research, the regular intervals step control was chosen. It is because by using this type of step control, the regularity of the simulated situation for the model could be shown. The number of steps used was defined as 37 steps and the number of division was set to 36 divisions. The reason for the setting to be made in such a way was because the first steps of the simulation were not so significant since the generator just started to operate. Another reason was the simulation had to run in full cycle, as 36 divisions of analysis were able to finish it with 37 steps. The reason that the simulation just ran in one full cycle was because to save the time on running the analysis on the model since the outcome of the simulation would be the same. After all the setting was done, the analysis on the ironless coreless electricity generator model was started.

$$\text{Time Interval (s)} = \frac{t_1 - t_0}{\text{Division}} \quad (3.1)$$

Consequently, the analysis on the ironless coreless electricity generator was completed. Results such as the magnetic flux density contour plot, circuit voltage and magnetic flux of FEM coil were obtained in the open-loaded circuit test as there was no load applied on the analysis on the model. As for the closed-loaded circuit, the joule loss, current and electric power could be obtained since there was load applied on the analysis on the model and the current generated was flowing through the applied load.

Several parameters were tested on the generator. These parameters were the magnet grade used on the model, number of coil turns per phase and gap distance between the magnets. The reason to test the parameter was to gain knowledge on how these parameters would affect the output of the model. It would also help to get the optimized parameter which could be used on the fabrication works of the ironless coreless electricity generator.

3.3 RESULTS OF THE FINITE ELEMENT ANALYSIS

3.3.1 Number of Coil Turns per Phase

There were four sets of number of coil turns per phase done in this section: 500 coil turns per phase; 1000 coil turns per phase; 1500 coil turns per phase; and, 2000 coil turns per phase. Other parameters such as magnet grade used, material used on rotor and stator and gap distance between the magnet pairs remained constant so that the best results for the number of coil turns per phase could be obtained. The magnet grade used in this analysis was N48 Neodymium magnet, while the gap distance between the magnet pairs was set to 12mm and the material used on the rotor and stator was aluminium.

Figure 3.1 shows the magnetic flux density contour plot on the ironless electricity generator. It should be noted that in the Figure 3.1, there are three colours shown in the figure, namely, purple, blue and light blue. The purple colours signifies that there was no magnetic flux distribution within the area as the value of the magnetic flux density was 0T, while the lighter the blue colour signifies the more magnetic flux distribution happened within the area as the magnetic flux density value fluctuated between $4.4737 \times 10^{-2} \text{T}$ and $3.5789 \times 10^{-1} \text{T}$.

Figure 3.2 shows the magnetic flux of FEM coil. In this illustration, there are three different colours of wave. Black coloured wave represents magnetic flux within U-phase coil, red coloured wave is for the magnetic flux within V-phase coil and the magnetic flux within W-phase coil is shown by the green coloured wave. It can be seen that the circuit voltage for each phase had amplitudes of 0.5Wb/phase. The root mean square (RMS) value for the magnetic flux within the coil is shown as the dotted line. Each colour of the dotted line represents the RMS value for each phase. As shown in Figure 3.2, the RMS value for the magnetic flux within the coil is around 0.33Wb/phase. Figure 3.3 shows the circuit voltage for the ironless electricity generator with 500 coil turns per phase. For this, black coloured wave represents circuit voltage for U-phase coil and the black coloured dotted line indicates the RMS value for the circuit voltage for U-phase coil, while red colour represents V-phase coil and the W-phase coil is

shown as the green colour. The illustration indicates that the circuit voltage had an amplitude of approximately 180V/phase and the RMS value for the circuit voltage was around 132V/phase. Figure 3.4 indicates that the torque for the ironless coreless electricity generator with 500 coil turns per phase. The black colour wave in this figure represents the torque of the rotors of the generator and the black dotted line shows the RMS value for the torque of the rotors of the generator. As shown in Figure 3.4, the torque of the rotors of generator fluctuated within 1Nm and -4Nm and the RMS value of the torque of the rotors of the generator was around 2.39Nm.

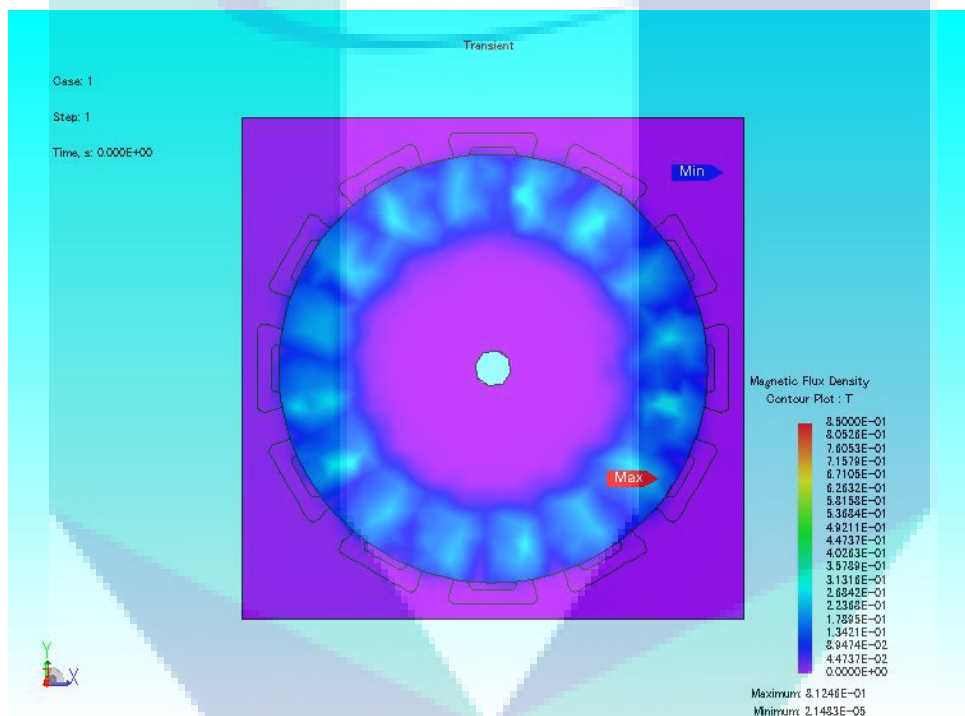


Figure 3.1: Magnetic Flux Density Contour Plot for 500 Coil Turns per Phase Analysis

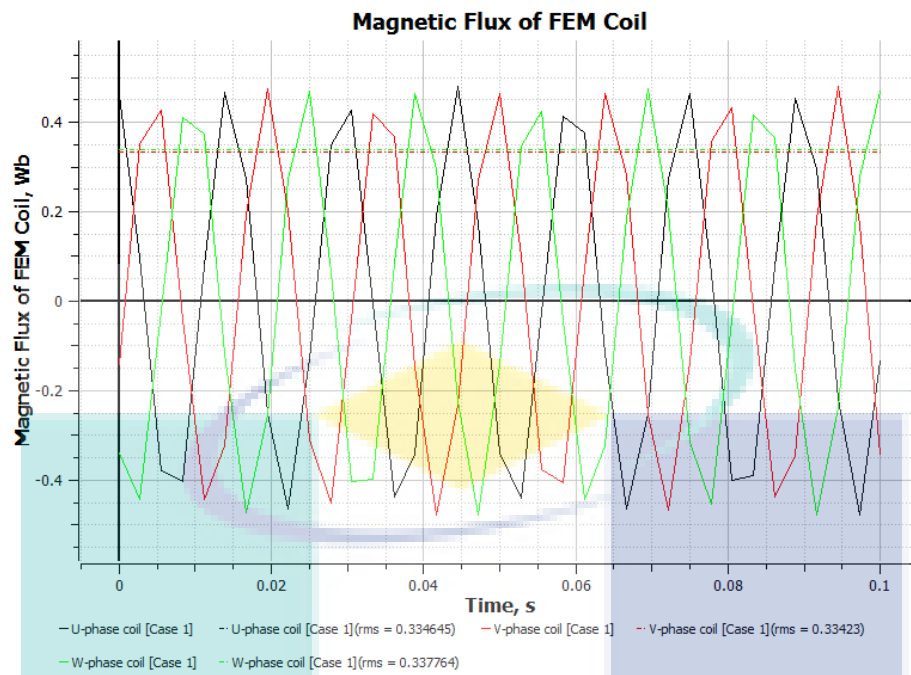


Figure 3.2: Magnetic Flux of FEM Coil for 500 Coil Turns per Phase Analysis

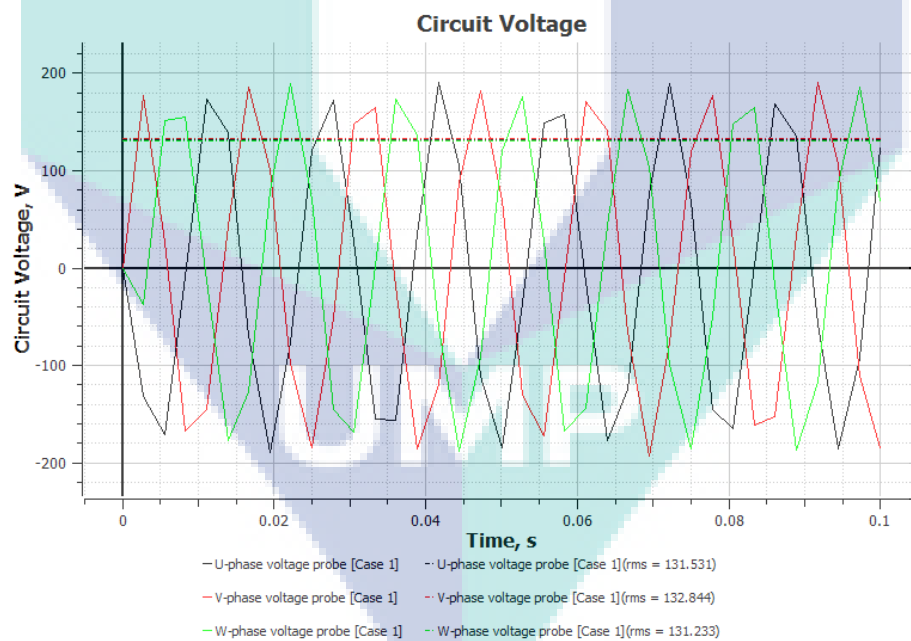


Figure 3.3: Circuit Voltage for 500 Coil Turns per Phase Analysis

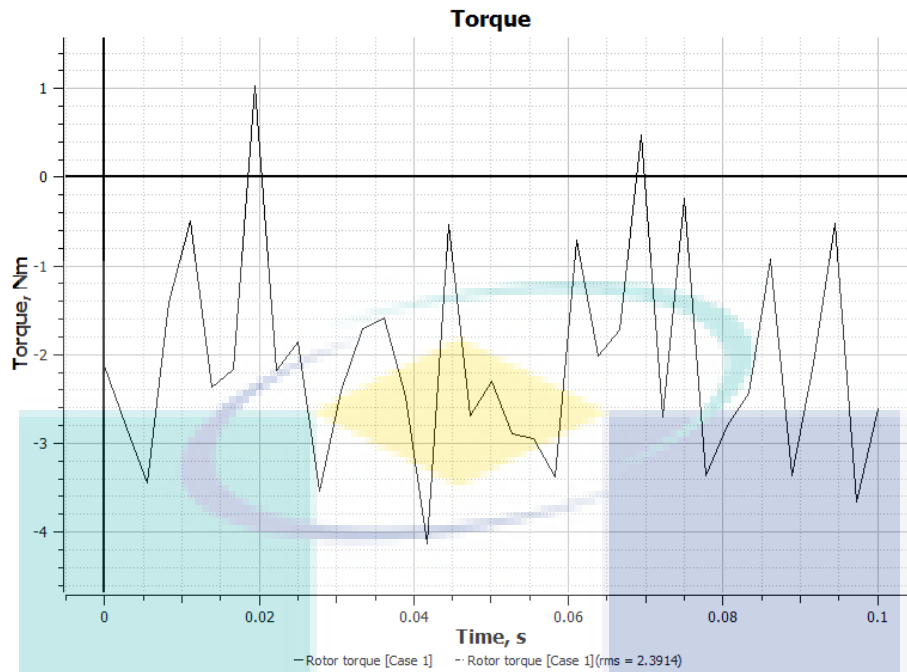


Figure 3.4: Torque for 500 Coil Turns per Phase Analysis

Table 3.1 shows the summary of the finite element analysis on the number of coil turns per phase. From the data in Table 3.1, it is apparent that the torque of the rotors of the ironless coreless electricity generator remained constant when the coil turns per phase increased. The value of the rotor torque in RMS was around 2.391Nm. The magnetic flux within U-phase coil, V-phase coil and W-phase coil as well as circuit voltage for U-phase coil, V-phase coil and W-phase coil showed an upward trend as the number of coil turns per phase increased. By comparing the results for 500 coil turns per phase and 1000 coil turns per phase, the output precisely increased one fold as observed in the 500 coil turns per phase analysis. As can be seen in Table 3.1, the RMS value for the magnetic flux per phase in the 500 coil turns per phase was approximately 0.336Wb/phase and this increased to 0.668Wb/phase for the magnetic flux per phase in the 1000 coil turns per phase. The magnetic flux value per phase further increased to approximately 1.003Wb/phase and 1.337Wb.phase in the 1500 coil turns per phase and in the 2000 coil turns per phase, respectively.

As for the value of circuit voltage, an upward trend was also observed when the coil turns per phase increased. In the 500 coil turns per phase, the RMS value was approximately 132V/phase and later increased to 264V/phase in the 1000 coil turns per

phase. The value of the circuit voltage further increased to approximately 396V/phase and 528V/phase in the 1500 coil turns per phase and in the 2000 coil turns per phase, respectively.

Table 3.1: Summary of the finite element analysis on the number of coil turns per phase

	500 coil turns per phase	1000 coil turns per phase	1500 coil turns per phase	2000 coil turns per phase
Gap distance between the magnet			12mm	
Magnet grade used			N48 Neodymium Magnet	
Material used on rotor and stator			Plastic	
Rotational speed of rotor			500RPM	
Rotor Torque (Nm_{rms})	2.391	2.391	2.391	2.391
Magnetic flux for U-phase coil (Wb_{rms})	0.335	0.669	1.004	1.339
Magnetic flux for V-phase coil (Wb_{rms})	0.336	0.668	1.003	1.337
Magnetic flux for W-phase coil (Wb_{rms})	0.338	0.676	1.013	1.351
Circuit voltage for U-phase coil (V_{rms})	131.531	263.061	394.592	526.123
Circuit voltage for V-phase coil (V_{rms})	132.844	265.687	398.531	531.374
Circuit voltage for W-phase coil (V_{rms})	131.233	262.466	393.700	524.933

3.3.2 Gap Distance between the Magnet Pairs

To show the significance of the gap distance between the magnet pairs, there were seven sets of gap distance between the magnet pairs done: 14mm; 16mm; 18mm; 20mm; 22mm; 24mm; and, 26mm. Other parameters such as magnet grade used, the number of coil turns per phase, material used on rotor and stator remained constant so that the best results for the gap distance between the magnet pairs could be obtained. The number of coil turns per phase was set to 500 coil turns per phase, the magnet grade used was N48 Neodymium magnet and the material used on the rotor and stator was plastic.

Figure 3.5 shows the magnetic flux density contour plot on the ironless electricity generator. As shown in the Figure 3.1, different colours indicate the magnetic flux distribution within the area. The purple colour region in Figure 3.5 indicates that there was no magnetic flux density distribution within the area since the value of the magnetic flux density was 0T. The lighter the blue colours were, the more intense the magnetic flux distribution within the area in Figure 3.4 as the value of magnetic flux density distribution fluctuated from $5 \times 10^{-2} \text{T}$ to $4 \times 10^{-1} \text{T}$.

Figure 3.6 shows the magnetic flux of FEM coil for the ironless electricity generator while Figure 3.7 shows the circuit voltage for the ironless electricity generator with 14mm gap distance between the magnet pairs. The legends in the Figure 3.6 and Figure 3.7 are the same as the ones in Figure 3.2 and Figure 3.3, respectively. Black colour indicates U-phase coil output, while red and green colours are for the V-phase output and the W-phase output, respectively. The dotted lines in Figure 3.6 and Figure 3.7 show the RMS value for the U-phase coil, V-phase coil and W-phase coil, respectively. In Figure 3.6, the magnetic flux of FEM coil for each phase had amplitudes of approximately 0.55Wb/phase. For the RMS value for the magnetic flux in FEM coil as shown in Figure 3.6, the value was approximately 0.415Wb/phase. The amplitude and RMS value of the circuit voltage as shown in the Figure 3.7 were approximately 220V/phase and 164V/phase, respectively. Figure 3.8 illustrates the torque of the rotors of the ironless coreless electricity generator in 14mm gap distance analysis. During the analysis, the torque of the rotors fluctuated between 5.25Nm and -4.9Nm. As shown in Figure 3.8, the RMS value of the torque of the rotors was 2.95Nm.

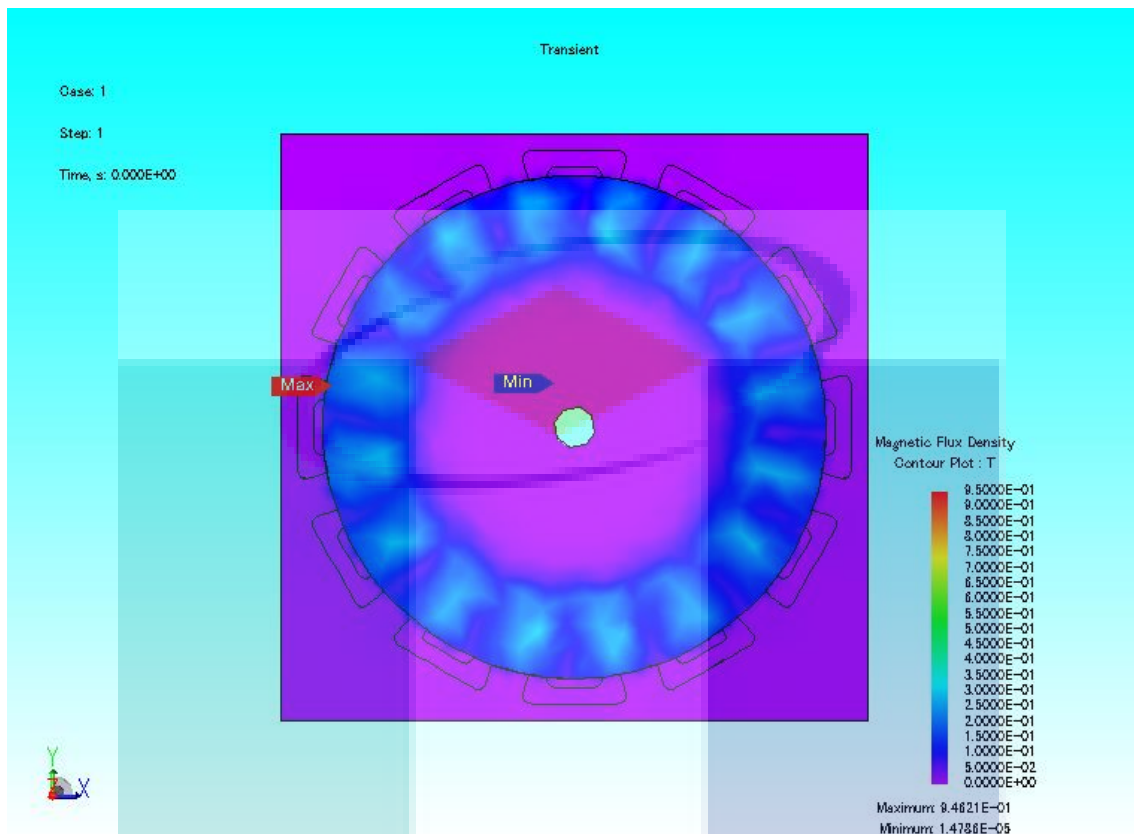


Figure 3.5: Magnetic Flux Density Contour Plot for 14mm Gap Distance Analysis

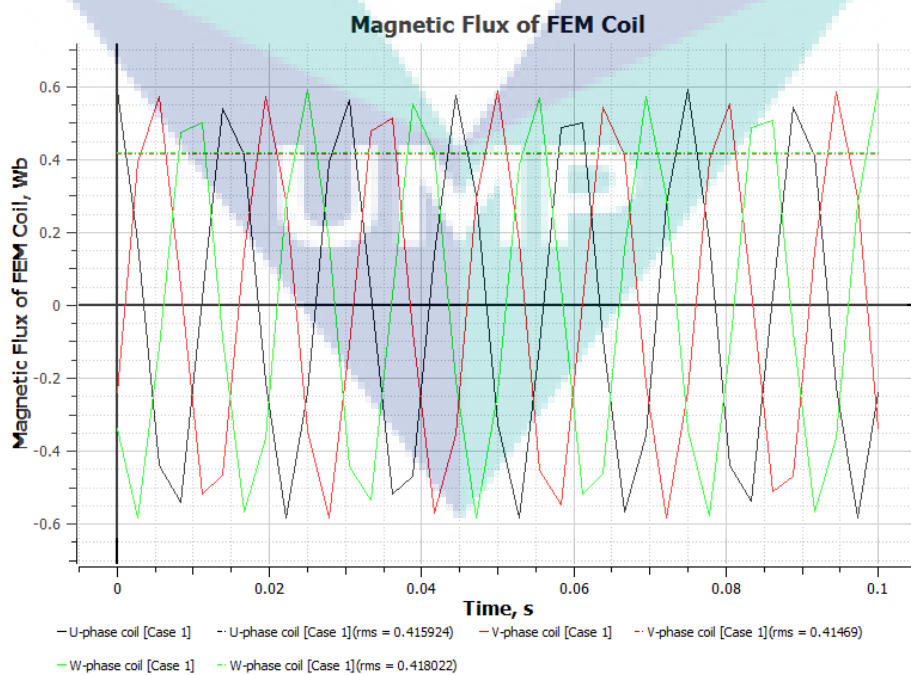


Figure 3.6: Magnetic Flux of FEM Coil for 14mm Gap Distance Analysis

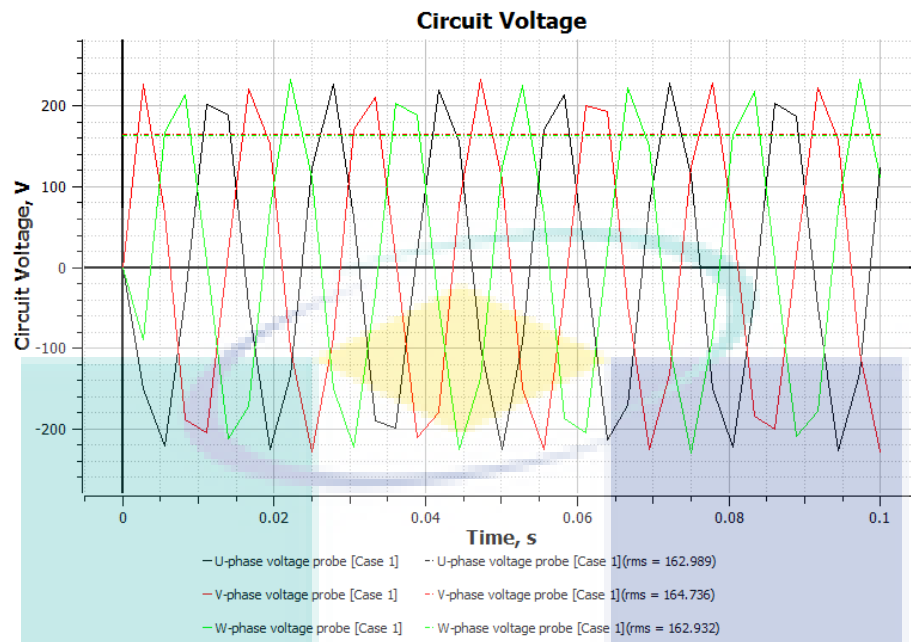


Figure 3.7: Circuit Voltage for 14mm Gap Distance Analysis

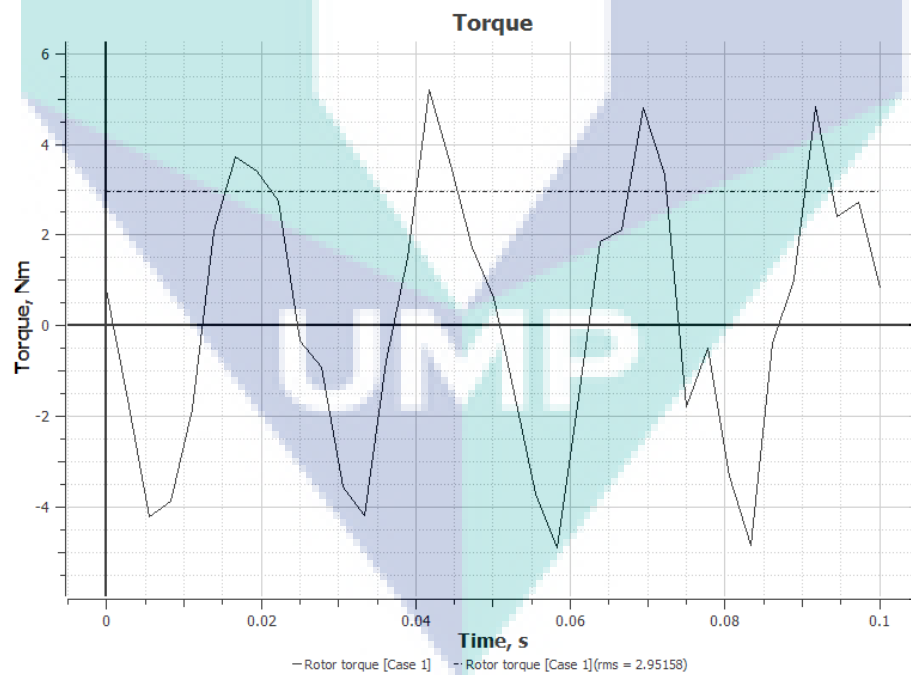


Figure 3.8: Torque for 14mm Gap Distance Analysis

Table 3.2 shows the summary of the finite element analysis on the gap distance between the magnet pairs. In Table 3.2, what is interesting in these data is that the torque

of the rotors of the ironless coreless electricity generator showed a downward trend as the gap distance between the magnet pair increased. During 14mm gap distance test, the torque RMS value of the rotors was 2.951Nm. When the gap distance increased to 16mm, the torque RMS value of the rotors decreased to 2.893Nm. The torque RMS value of the rotors was then further decreased to 2.838Nm when the gap distance increased to 18mm. In 20mm gap distance test, the torque RMS value of the rotors dropped significantly to 2.367Nm. The RMS value of torque of the rotors further dropped to 2.291Nm during the 22mm gap distance test. The torque RMS of the rotors decreased to 2.098Nm when the gap distance increased to 24mm. During the 26mm gap distance analysis, the RMS value of the torque of the rotors of the ironless coreless electricity generator decreased to 1.819Nm.

In the gap distance between magnet pair analysis, the magnetic flux and the circuit voltage of the three-phase coil of the ironless coreless electricity generator was in decreasing trend while the gap distance between the magnet pairs is increase. As shown in 14mm gap distance test, the magnetic flux RMS value per phase was 0.415Wb/phase. The magnetic flux RMS value decreased to approximately 0.386Wb/phase for 16mm gap distance test. The magnetic flux RMS value further decreased to around 0.361Wb/phase for 18mm gap distance test. When the experiment proceeded with the 20mm gap distance test, the magnetic flux RMS value per phase decreased to 0.337Wb/phase. For the 22mm gap distance test, the magnetic flux RMS value was reduced to 0.335Wb/phase. The magnetic flux RMS value per phase then further dropped to 0.294Wb/phase when the 24mm gap distance test was carried out. During the 26mm gap distance test, the lowest value of magnetic flux RMS value per phase amongst all the test results was obtained, which was approximately 0.274Wb/phase.

For the circuit voltage in the gap distance test, the circuit voltage output decreased when the gap distance between the magnets pairs increased. In the 14mm gap distance test, the circuit voltage RMS value was approximately 163V/phase. The circuit voltage RMS value decreased to 152V/phase when 16mm gap distance test was carried out. The circuit voltage RMS then further dropped to 142V/phase during the 18mm gap distance test. In 20mm gap distance test, the circuit voltage RMS value was approximately 132V/phase, indicating a lower value compared to that of the 18mm gap

distance test. For 22mm gap distance test, the circuit voltage RMS value was 131V/phase. The RMS value for the circuit voltage then continued to decline to 116V/phase in 24mm gap distance test. In the 26mm gap distance test, the circuit voltage RMS was 109V/phase, which was the lowest amongst all values in the gap distance tests.

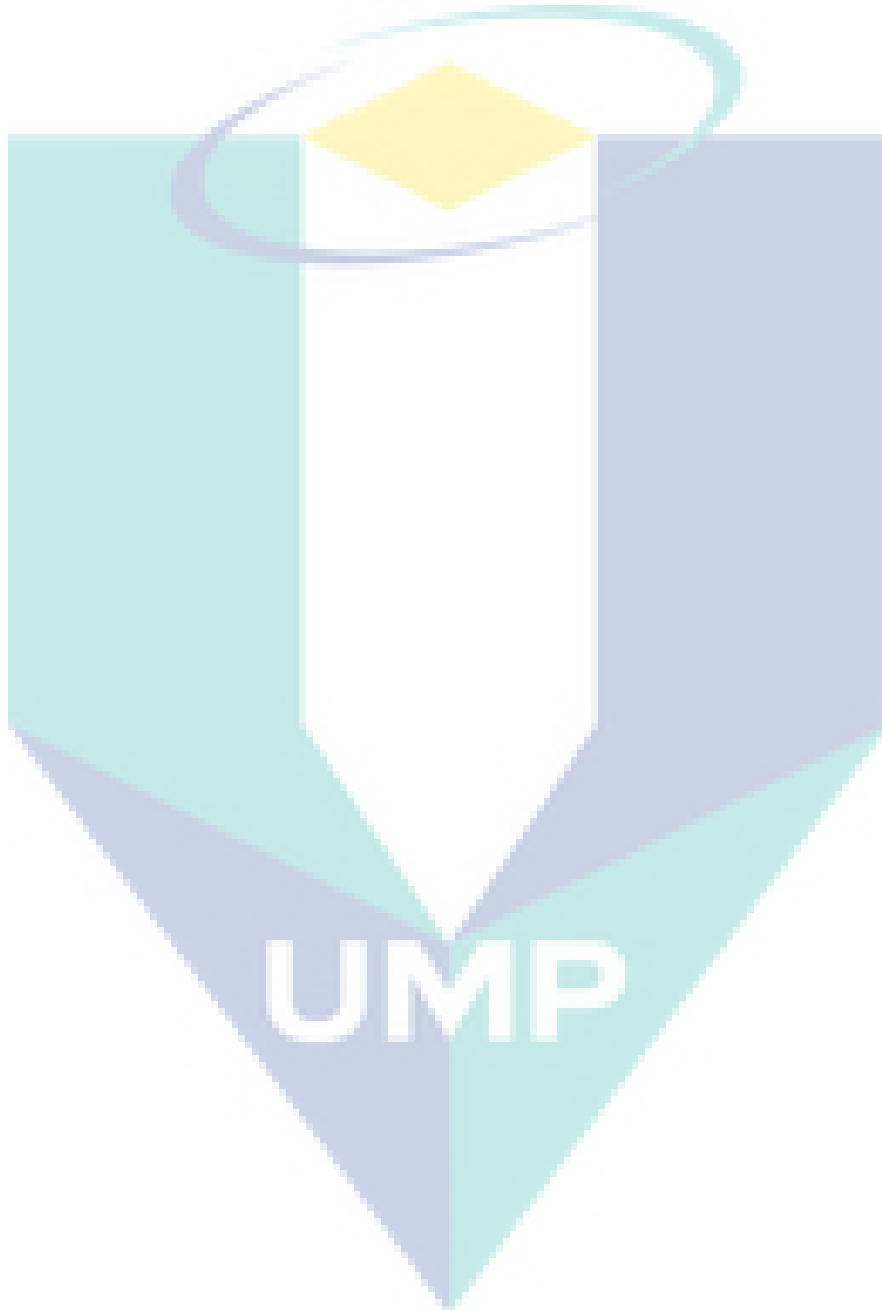


Table 3.2: Summary of finite element analysis on the gap distance between magnet pairs

	14mm Gap Distanc e	16mm Gap Distanc e	18mm Gap Distanc e	20mm Gap Distanc e	22mm Gap Distanc e	24mm Gap Distanc e	26mm Gap Distanc e
Number of coil turns per phase	500						
Magnet grade used	N48 Neodymium Magnet						
Material used on rotor and stator	Plastic						
Rotational speed of rotor	500RPM						
Rotor Torque (Nm _{rms})	2.951	2.893	2.838	2.367	2.291	2.098	1.819
Magnetic flux for U-phase coil (Wb _{rms})	0.416	0.386	0.361	0.337	0.335	0.294	0.274
Magnetic flux for V-phase coil (Wb _{rms})	0.415	0.385	0.358	0.336	0.334	0.294	0.275
Magnetic flux for W-phase coil (Wb _{rms})	0.418	0.388	0.362	0.340	0.338	0.296	0.277
Circuit voltage for U-phase coil (V _{rms})	162.989	151.330	141.315	131.901	131.531	115.031	107.439
Circuit voltage for V-	164.736	152.881	142.304	133.684	132.844	116.692	109.364

phase coil (V_{rms})							
Circuit voltage for W- phase coil (V_{rms})	162.932	151.248	141.110	132.625	131.233	115.526	108.128

3.3.3 Magnet Grade Used on Magnet Pairs

There were five sets of analysis on the magnet grade test. The magnet grades used were N42, N45, N48, N50 and N52 Neodymium. Other parameters such as the number of coil turns per phase, gap distance between the magnet pairs and material used on the rotor and stator remained constant so that the results for magnet grade tests could be obtained accurately. The number of coil turns per phase was set to 500 coil turns per phase and the gap distance between the magnet pairs was set to 20mm while the material used on rotor and stator was plastic.

Figure 3.9 shows the magnetic flux density contour plot on the ironless electricity generator, while Figure 3.10 and Figure 3.11 show the magnetic flux of FEM coil for the ironless electricity generator and the circuit voltage for the ironless electricity generator with N42 Neodymium Magnet, respectively. For the magnetic flux distribution for the magnet grade simulation in Figure 3.7, the colour purple indicates that there was no distribution in the area whereas the highlighted area had magnetic flux distribution value of 0T. The lighter the blue colour, the stronger the magnetic flux distribution as the value of magnetic flux density distribution fluctuated from $3.9474 \times 10^{-2}T$ to $3.1579 \times 10^{-1}T$.

As shown in Figure 3.10 and Figure 3.11, the indication was the same as the coil turns per phase analysis and the gap distance analysis where the black colour was for U-phase coil output, red and green colours were for V-phase coil output and the W-phase coil output, respectively. The dotted lines were the RMS output for U-phase coil, V-phase coil and W-phase coil output, respectively. In Figure 3.10, the magnetic flux within FEM coils for all three-phase each had an amplitude of approximately 0.45Wb/phase. The RMS value for the magnetic flux within FEM coils for the three-phase connection of the ironless coreless electricity generator was around 0.3Wb/phase.

The amplitude and the RMS value for the circuit voltage were approximately 160V/phase and 119V/phase respectively, as shown in Figure 3.11. Figure 3.12 shows the torque of the rotors of the ironless coreless electricity generator in which N42 Neodymium Magnet was used to run the analysis. As illustrated in the figure, the torque of the rotors fluctuated between 0.9Nm and -3.4Nm. The RMS value of the torque of the rotors was around 1.958Nm for this analysis.

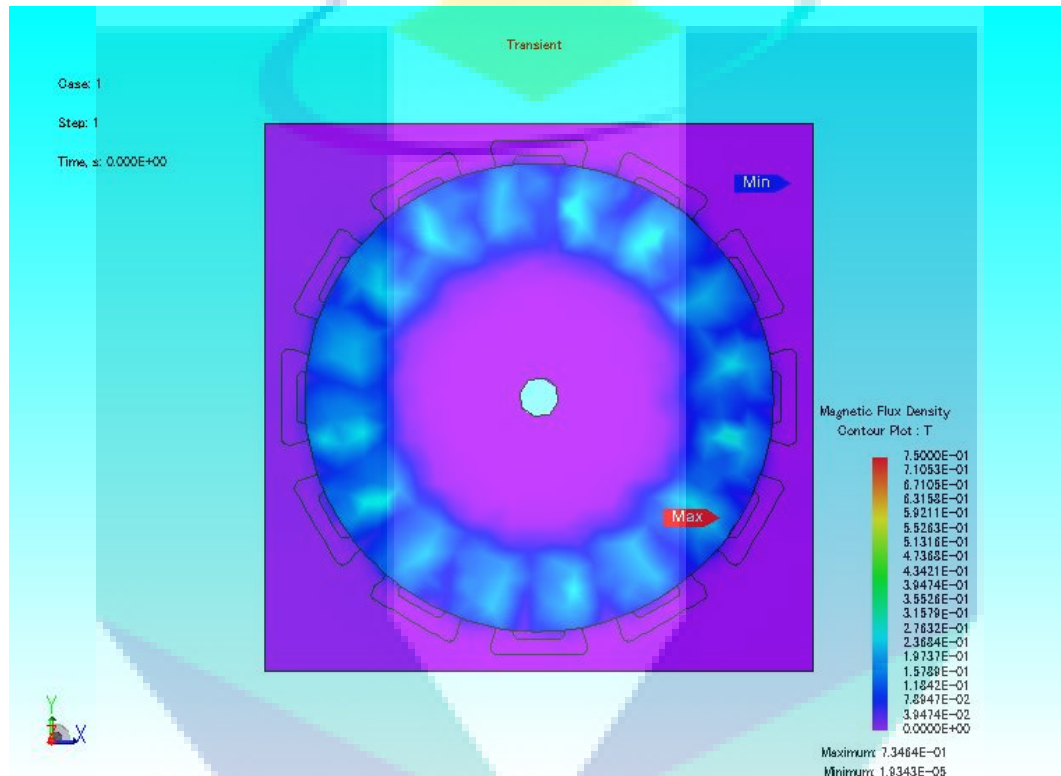


Figure 3.9: Magnetic Flux Density Contour Plot for N42 Neodymium Magnet Analysis

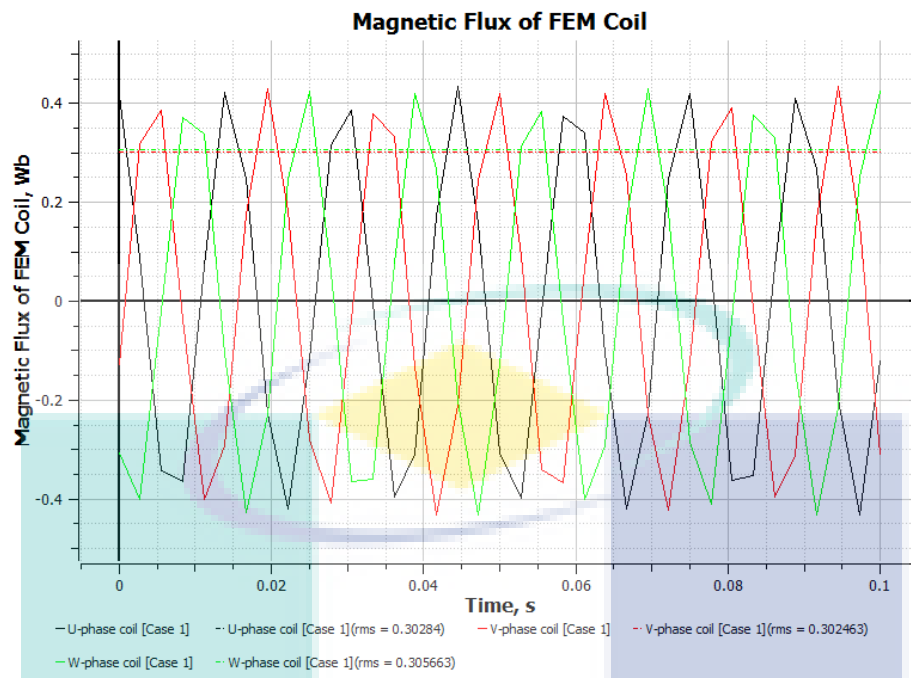


Figure 3.10: Magnetic Flux of FEM Coil for N42 Neodymium Magnet Analysis

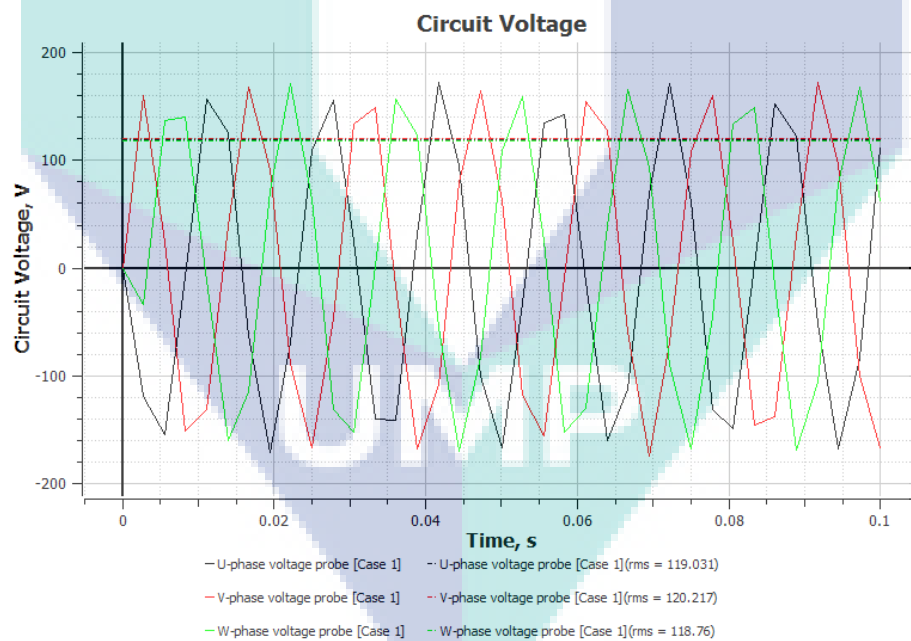


Figure 3.11: Circuit Voltage for N42 Neodymium Magnet Analysis

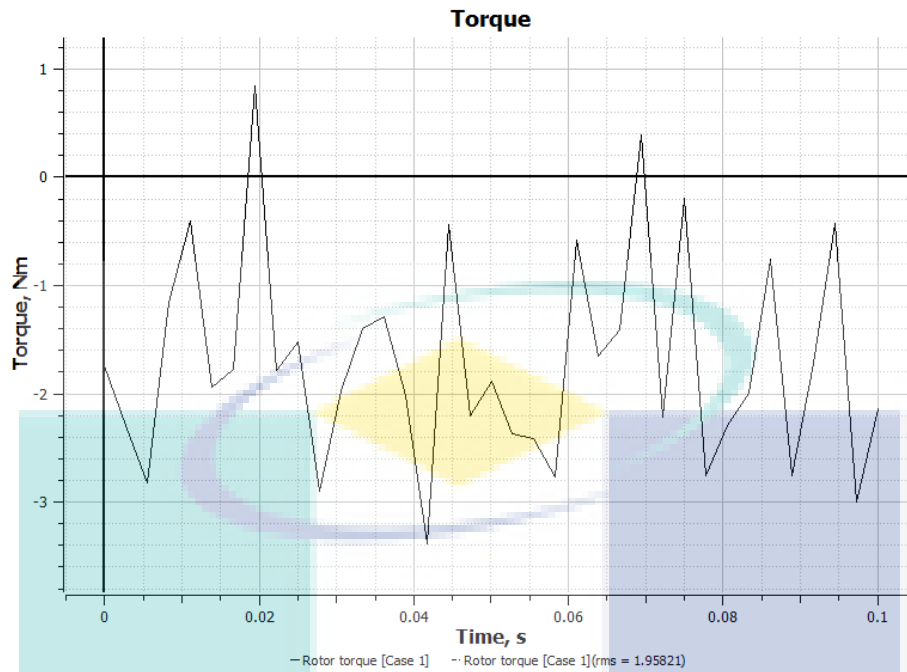


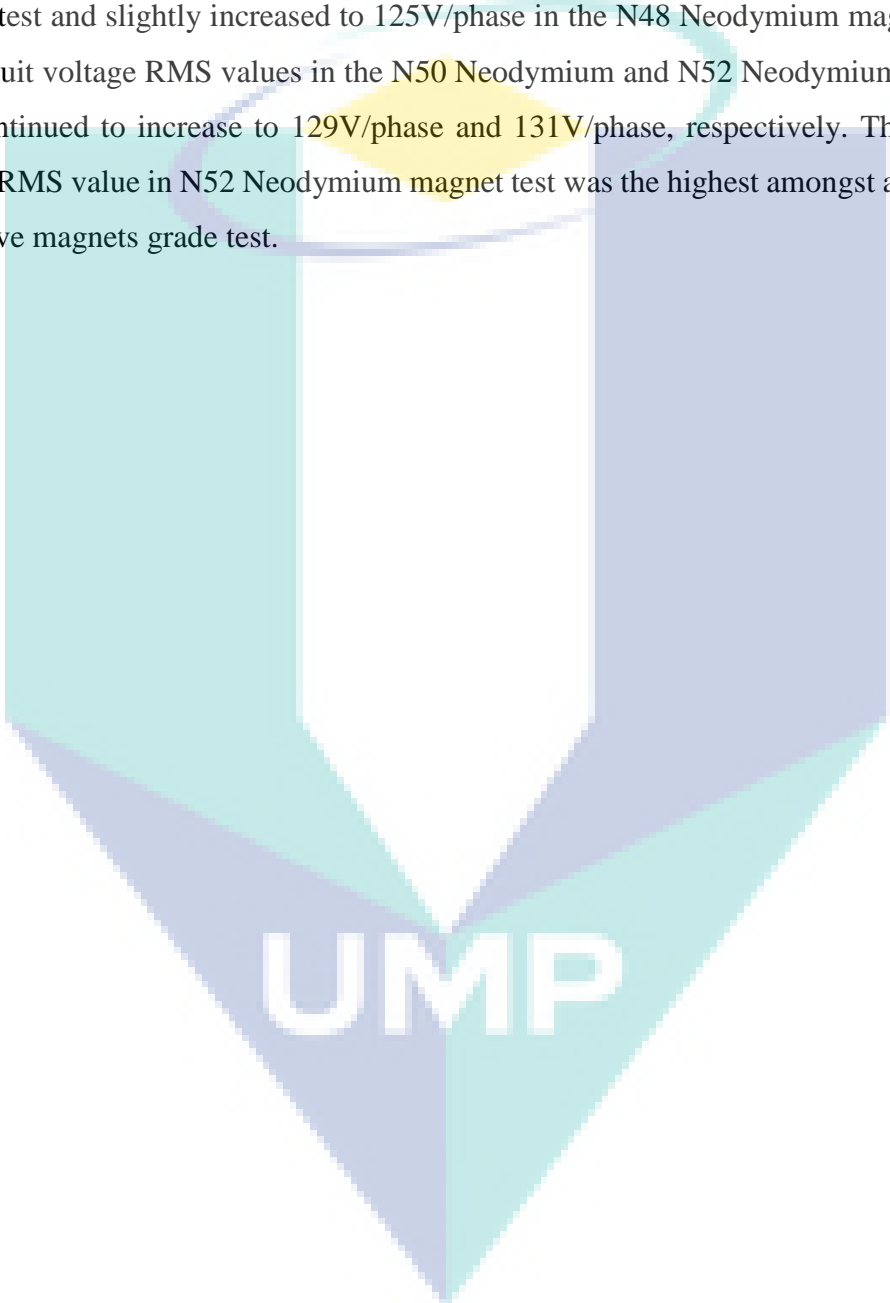
Figure 3.12: Torque for N42 Neodymium Magnet Analysis

Table 3.3 shows the summary of the finite element analysis on magnet grade used on magnet pairs. From Table 3.3, the torque of the rotors of the ironless coreless electricity generator shows an upward trend when the magnet grade used was increased. When N42 Neodymium Magnets was used in the analysis, the RMS value of torque of the rotors was 1.958Nm. The RMS value of the torque of the rotors then increased to 2.103Nm when N45 Neodymium Magnet was used. The RMS value of the torque of the rotors further increased to 2.165Nm when the N48 Neodymium Magnet was used in the analysis. When the N50 Neodymium Magnet and the N52 Neodymium Magnet were used in the magnet grade analysis, the RMS values of torque of the rotors rose to 2.293Nm and 2.391Nm, respectively.

In the magnet grade analysis, the magnetic flux and the circuit voltage in the three-phase coil showed an increasing trend from N42 Neodymium magnet to N52 Neodymium magnet. As indicated in the magnetic flux RMS value in the N42 Neodymium magnet test, a value of around 0.303Wb/phase was obtained. The magnetic flux RMS value increased to 0.314Wb/phase in the N45 Neodymium magnet test and further increased to 0.318Wb/phase in the N48 Neodymium magnet test. The N50 Neodymium magnet test produced a value of approximately 0.328Wb/phase for the

magnetic flux RMS value while the N52 Neodymium magnet test produced a value of 0.335Wb/phase, which was the highest value amongst all values in the five tests.

Meanwhile, the circuit voltage RMS value for in the N42 Neodymium magnet test was 119V/phase. This value increased to 123V/phase in the N45 Neodymium magnet test and slightly increased to 125V/phase in the N48 Neodymium magnet test. The circuit voltage RMS values in the N50 Neodymium and N52 Neodymium magnet tests continued to increase to 129V/phase and 131V/phase, respectively. The circuit voltage RMS value in N52 Neodymium magnet test was the highest amongst all values in the five magnets grade test.

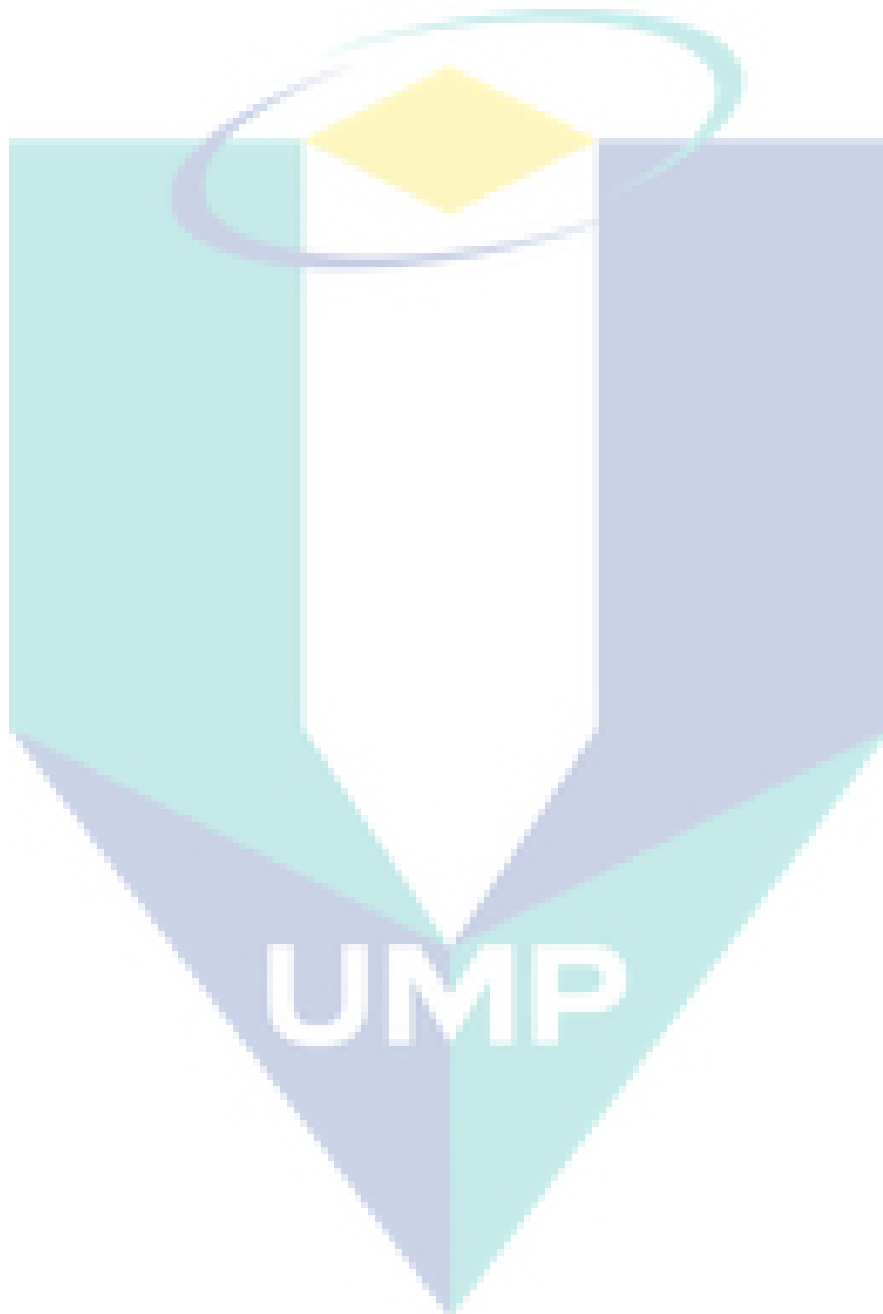


UMP

Table 3.3: Summary of the finite element analysis on magnet grade used on magnet pairs

	N42 Neodymium magnet	N45 Neodymium magnet	N48 Neodymium magnet	N50 Neodymium magnet	N52 Neodymium magnet
Number of coil turns per phase			500		
Gap distance between magnet pairs			20mm		
Material used on rotor and stator			Plastic		
Rotational speed of rotor			500RPM		
Rotor torque (Nm_{rms})	1.958	2.103	2.165	2.293	2.391
Magnetic flux for U-phase coil (Wb_{rms})	0.303	0.314	0.318	0.328	0.335
Magnetic flux for V-phase coil (Wb_{rms})	0.302	0.313	0.318	0.327	0.334
Magnetic flux for W-phase coil (Wb_{rms})	0.306	0.316	0.321	0.331	0.338
Circuit voltage for U-phase coil (V_{rms})	119.031	123.338	125.159	128.800	131.531
Circuit voltage for V-phase coil (V_{rms})	120.217	124.570	126.408	130.086	132.844

Circuit voltage for W-phase coil (V_{rms})	118.760	123.060	124.876	128.509	131.233
--	---------	---------	---------	---------	---------



3.3.4 Discussion on the Simulation Results

During the test on coil turns per phase, the torque on the rotors of the ironless coreless electricity generator was remained constant when the coil turns per phase increase. It was because there was no adjustment made on the rotors, for example, to make the rotors heavier, and thus, the torque of the rotors remained constant. Both magnetic flux within the circuit and circuit voltage showed an upward trend with the increase in the coil turns per phase. This is because as the number of coil turns per phase increased, there would be increasing number of magnetic flux cutting process by the coil and thus, magnetic flux and circuit voltage within the three-phase coil would also increase. An increase in coil turns would cause the output of the generator, the cost as well as the size to increase. Since in this research was concerned with developing a table size ironless coreless electricity generator, 500 coil turns per phase was chosen because it required less space and minimal cost.

The circuit voltage RMS value declined while the gap distance between the magnets pairs increased in the gap distance analysis. The reason behind this is because when the distance between magnet pairs increased, the magnetic strength between the magnet pairs decreased, which caused the quality of the magnetic flux cut to drop and thus, magnetic flux and circuit voltage generated in three phase coil would decrease. If the gap distance was too close, there could be a chance that rubbing might occur between the rotor and stator, which would reduce the efficiency of the ironless coreless electricity generator. By considering this error, the gap distance between the magnet pairs of 26mm was chosen to prevent such problem from happening.

The magnetic flux RMS value and circuit voltage RMS value showed increasing trends with the increase in the grade of the magnet used in the magnet grade analysis. The reason behind it is because amongst these five grades of magnet, N52 had the strongest magnetic field and it did produce better quality magnetic flux during the three-phase coil cutting through the magnetic field. In the market, N50 Neodymium magnet and N52 Neodymium magnets can be easily obtained. N52 Neodymium magnet was the choice for making the electricity generator because it could produce better quality of the magnetic flux compared to that of the other grades. Although using N52

Neodymium magnet on ironless coreless electricity generator did increase the torque of the generator, the output of the generator did compensate on such weakness.

During the gap distance analysis, the torque of the rotors of the ironless coreless electricity generator showed downward trend as the gap distance increased. The reason behind it is because when the magnet pairs moved further away, the magnetic force between it became weakened and made the pulling force between the rotors weaker. In the magnet grade analysis, the torque of the rotors of the ironless coreless electricity generator increased when the magnet grade used on the analysis was stronger. Such phenomena occurred because when the stronger magnet was used on the rotors, it made the pulling force between the rotors became stronger. When the pulling force between the rotors was stronger, more energy would be required to spin. Thus, this would increase the torque of the rotors.

3.4 OPTIMUM PARAMETER FOR THE IRONLESS CORELESS ELECTRICITY GENERATOR

With these all four sets of parameter, namely, the number of coil turns per phase, gap distance between the magnet pairs, magnet grade used on magnet pairs and material used on rotor and stator, the best parameters were chosen to develop the electricity generator. Closed circuit finite element analysis with 80 ohm of resistance in each phase was carried out in electricity generator using these parameters as a reference for testing. Based on the literature review, plastic was chosen as the material. It is because plastic would be cheaper than aluminium and would not cause the redirection of the magnetic flux between the magnets. The chosen parameters were 500 coil turns per phase, 20mm gap distance, N52 Neodymium magnet and plastic as the material to be used on rotor and stator with rotational speed of rotor of 500rpm.

Figure 3.13 shows the magnetic flux density contour plot on the ironless electricity generator. The purple colour region of the Figure 3.13 illustrates that there was no magnetic flux density distribution since the value of magnetic flux density distribution in that region was 0T. For the light blue and blue regions in Figure 3.13, the lighter the blue colour was, the higher the magnetic flux density distribution was as the

value of magnetic flux density distribution fluctuated from $4.4737 \times 10^{-2} \text{T}$ to $3.5789 \times 10^{-1} \text{T}$.

Figure 3.14 shows the magnetic flux of FEM coil for the ironless electricity generator. The magnetic flux of FEM coil recorded an amplitude of approximately 0.4Wb/phase. The RMS value for the magnetic flux of FEM coil as shown in Figure 3.14 was around 0.287Wb/phase. Figure 3.15 shows the circuit voltage for the ironless electricity generator indicating an amplitude of around 5.5V/phase. For the RMS value of the circuit voltage, the value was 4.1161V/phase.

Figure 3.16 shows the torque of the ironless electricity generator. The initial torque was as high as 10Nm but later dropped to 5Nm. Figure 3.17 illustrates the current produced by the ironless electricity generator. The amplitude for the current produced by the generator was approximately 1.8A/phase while the RMS value for the current produced by the ironless coreless electricity generator was around 1.335A for each phase. Figure 3.18 shows the electric power produced by the ironless electricity generator. The electric power generated by the three-phase connection of the ironless coreless electricity generator fluctuated from around 30W to 200W. The electric power used by the load fluctuated between -30W and -200W. The RMS values for the electric power generated and electric power used were both approximately 128W. Figure 3.19 shows the joule losses of the ironless electricity generator with optimum parameter. The initial joule losses reached up to 33W and later remained between 30W and 34W. The RMS value of the joule losses was 30.748W. The losses were due to the resistance within the coils in the stator as the wire coils itself had the electrical resistance properties.

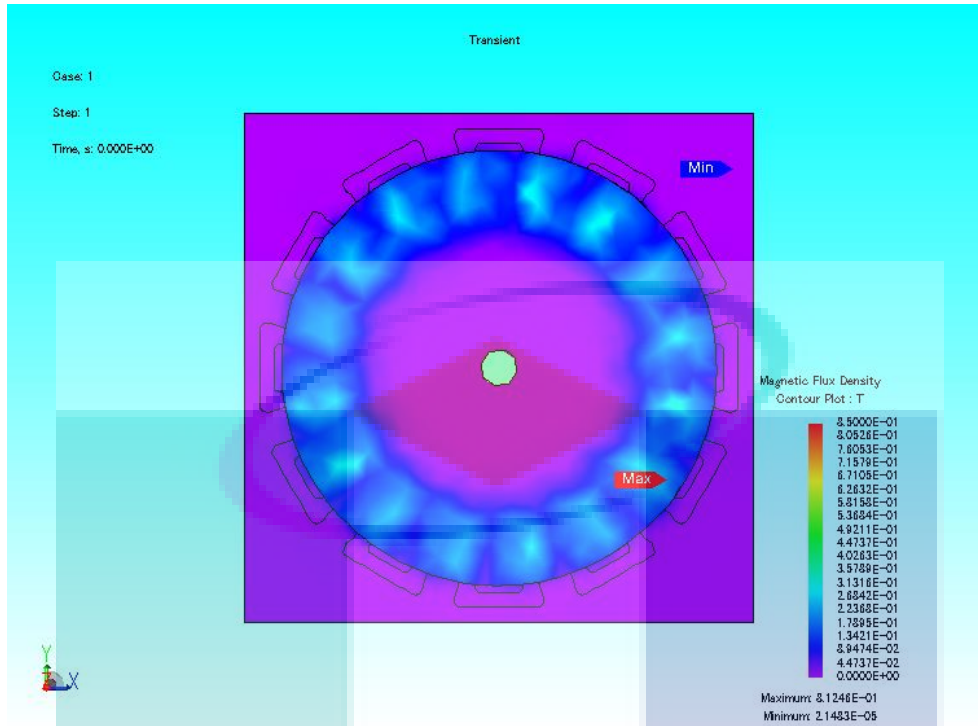


Figure 3.13: Magnetic Flux Density Contour Plot for Optimum Parameter Design

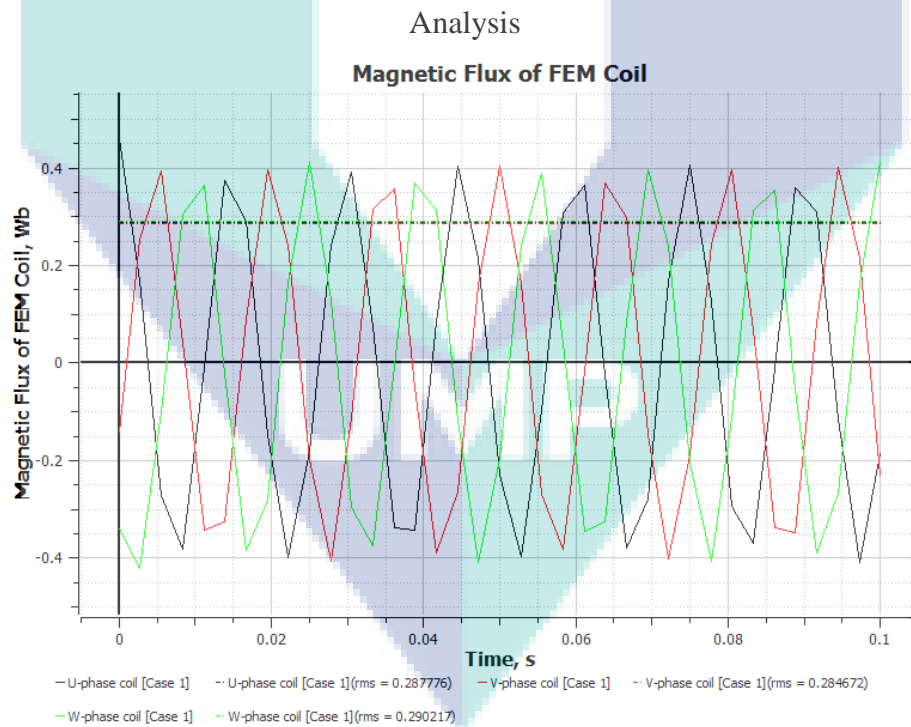


Figure 3.14: Magnetic Flux of FEM Coil for Optimum Parameter Design Analysis

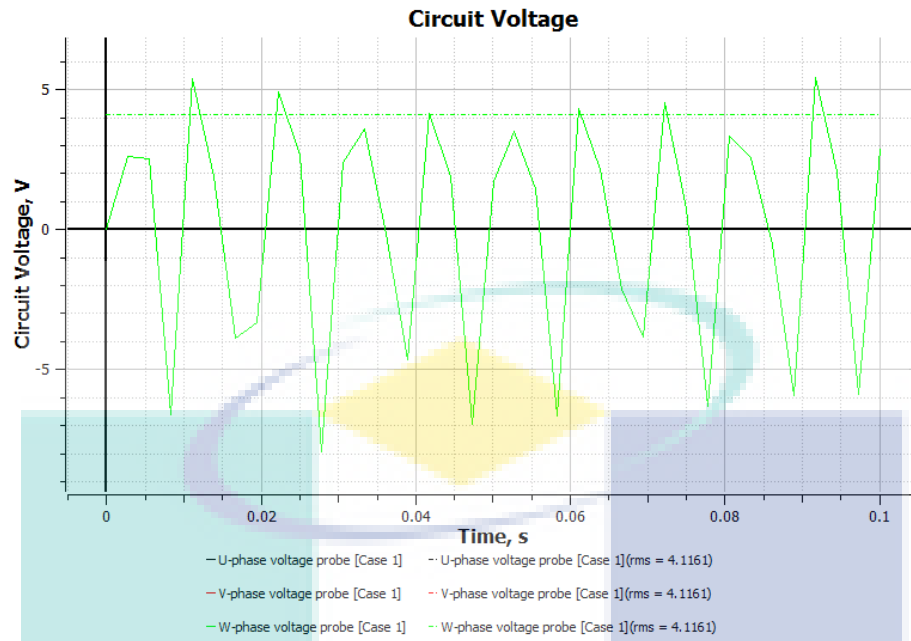


Figure 3.15: Circuit Voltage for Optimum Parameter Design Analysis

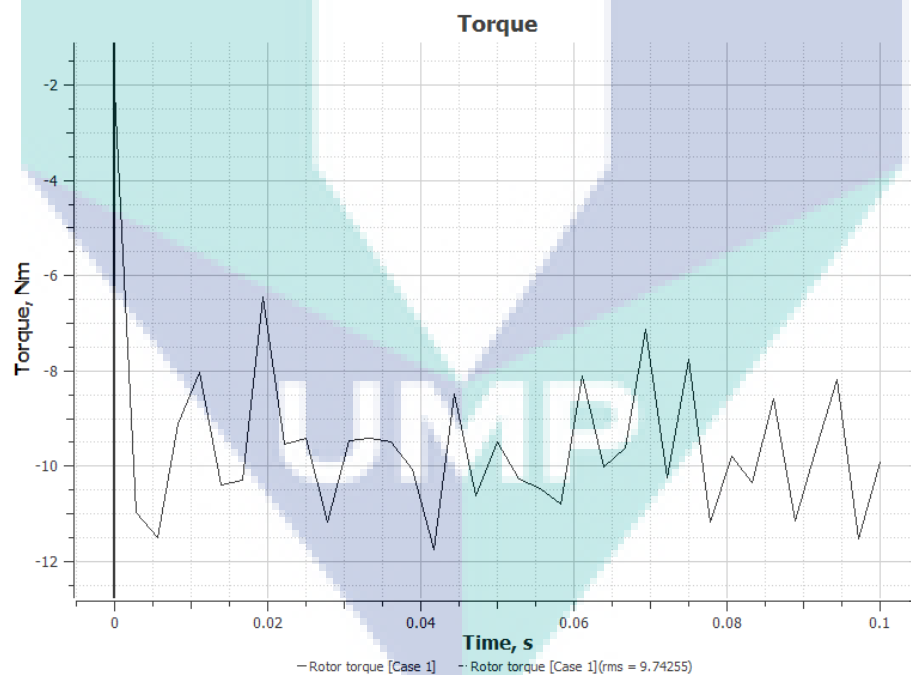


Figure 3.16: Rotor Torque for Optimum Parameter Design Analysis

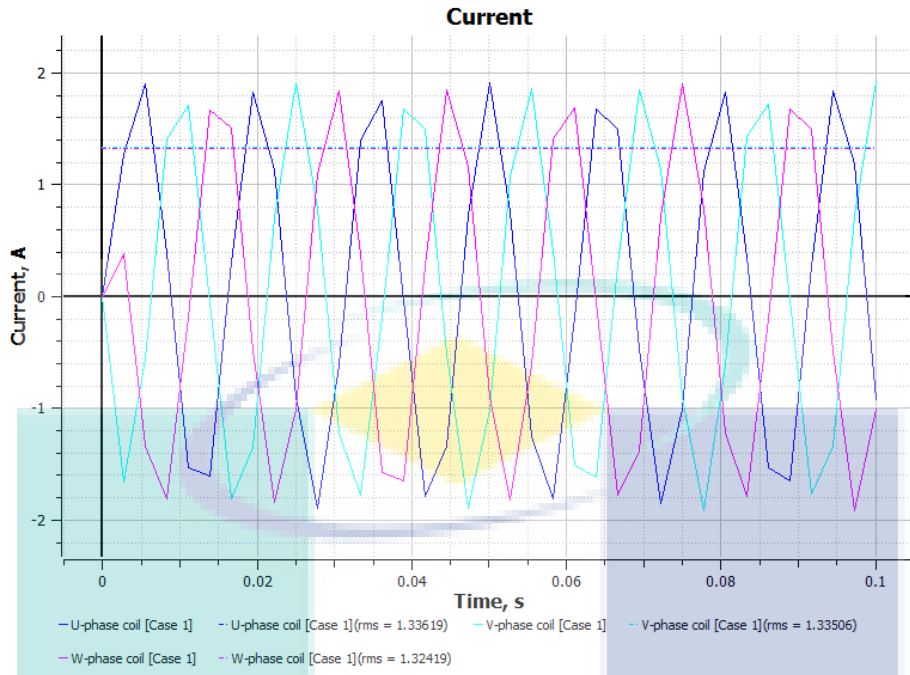


Figure 3.17: Current for Optimum Parameter Design Analysis

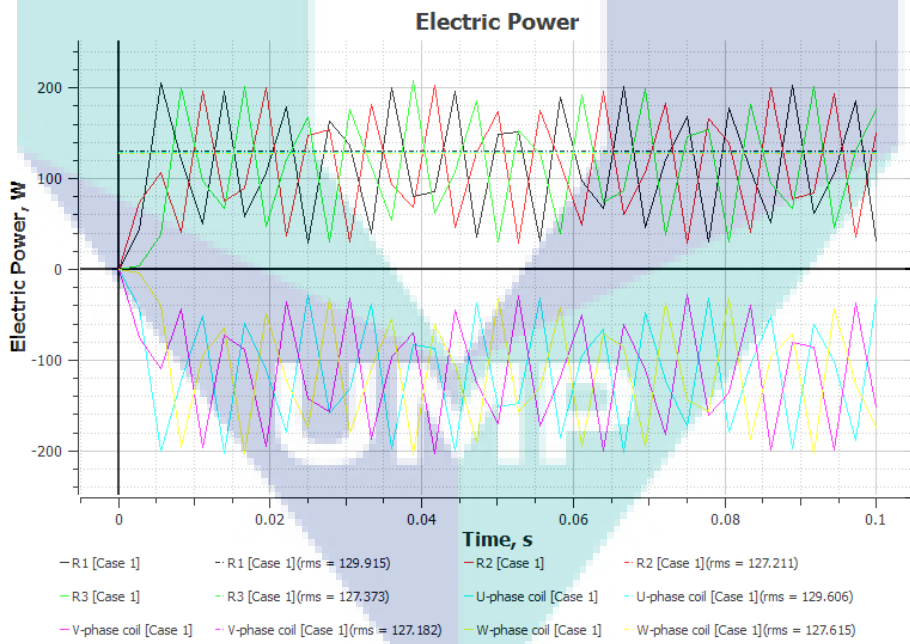


Figure 3.18: Electric Power for Optimum Parameter Design Analysis

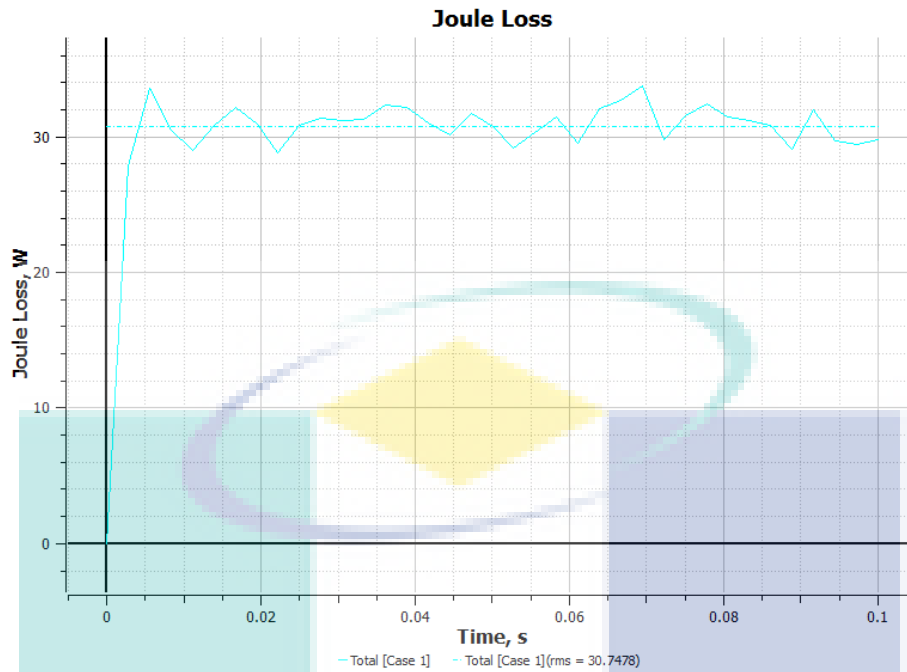


Figure 3.19: Joule Loss for Optimum Parameter Design Analysis

It should be noted that in the closed circuit, other additional types of data such as current, electric power and joule loss were obtained. This is because without the resistance in the circuit, the calculation of the current, electric power and joule loss could not be completed. Eq. 3.2 and Eq. 3.3 would be used as the basic formula required in calculating current and electric power, respectively.

$$I = \frac{V}{R} \quad (3.2)$$

$$P = I^2 R \quad (3.3)$$

The simulated mechanical power would be considered as input power for the ironless coreless electricity generator as this power would be required to operate the generator. By using the Eq. 2.9 as stated in Chapter 2 of this thesis, mechanical power can be calculated easily. To obtain ω , the value of rotational speed of rotors in rad/s, Eq. 3.4 was applied, where N is the rotational speed of rotor set on the JMAG Designer software. The calculated simulated mechanical power produced was 510.12W.

$$\omega = \frac{2\pi N}{60} \quad (3.4)$$

Figure 3.15 illustrates the closed circuit voltage output for the ironless coreless electricity generator. It was noted that the closed circuit voltage was much lower than the open circuit voltage. This is because in the closed circuit, some voltage was used on the load or resistor, which caused a decrease in the voltage output.

Figure 3.16 shows the initial high negative value change in the torque. This is because when the ironless coreless electricity generator started to rotate, much energy would be required to move the rotor. After a while, the torque of the ironless coreless electricity generator showed high and stable negative value, which was good because high amount of torque would be required to stop the rotor from spinning. This also indicated that the rotor had enough energy and functioned as a flywheel.

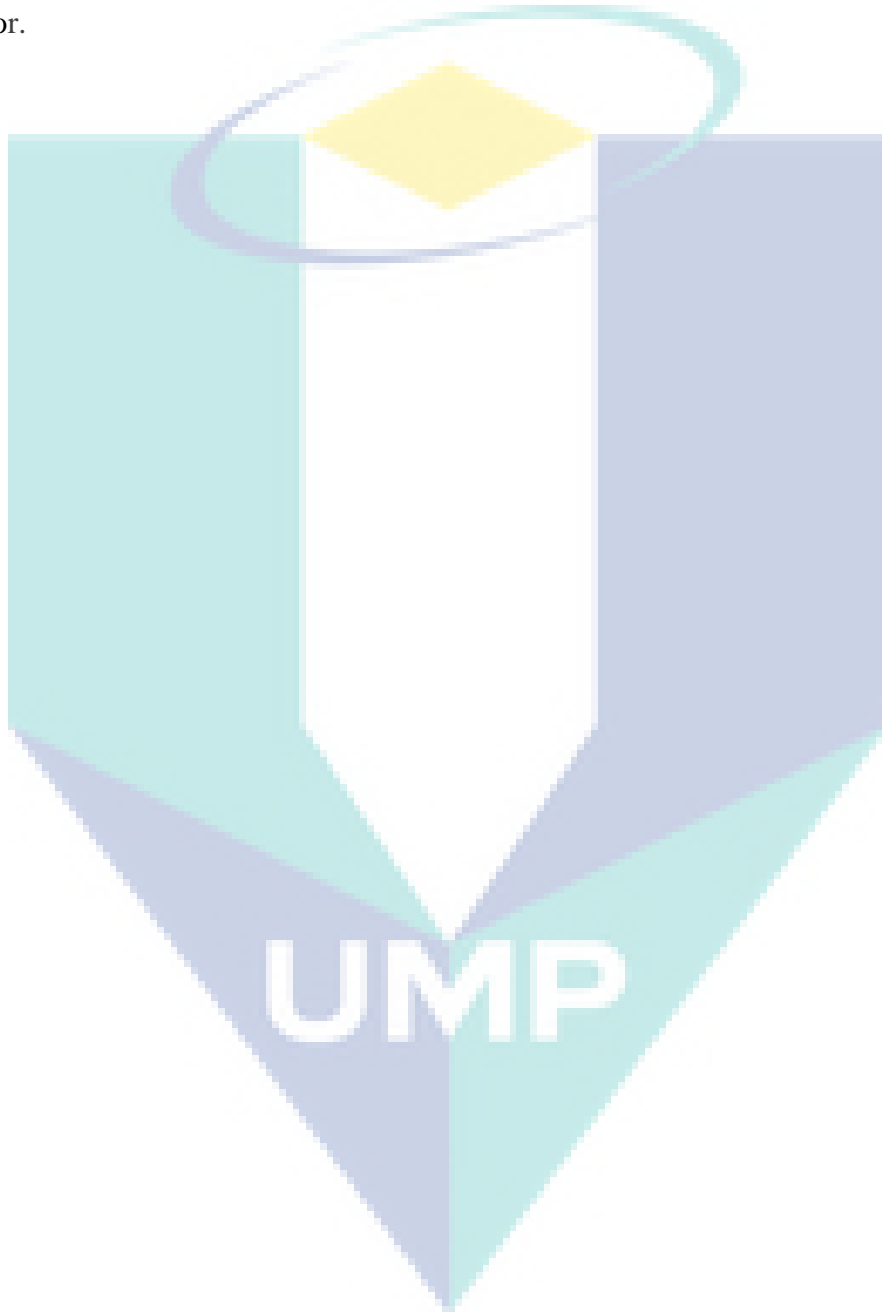
The ironless coreless electricity generator as the power plant and the resistors in this simulation could be considered as the load or electrical appliances. The power plant generates electricity for consumers to use for domestic uses such as in light bulbs, heaters and refrigerators. Figure 3.18 shows the electric power generated by the three-phase coils of the ironless electricity generator. The electric power generated by the ironless coreless electricity generator would be used by the resistors.

When electricity is transferred from the power plant to consumers, some losses occur during this process. This is because the wire itself has the resistance which converts electricity into heat energy and this heat energy is wasted into the surrounding area. Figure 3.19 shows the amount of joule loss generated during the generation of electricity, as heat would also be generated within the coil itself, causing the loss of power to surrounding area.

3.5 SUMMARY OF PRELIMINARY FINDINGS

The purpose of the finite element analysis in this research was to obtain the optimum parameters to be used to fabricate the ironless electricity generator. The results

in this finite element analysis showed that the optimum parameters to be used were: 500 coil turns per phase; 20mm gap distance between the magnet pairs; N52 Neodymium magnet grade; and, plastic as the material used on rotor and stator. Another finite element analysis would also be conducted on the optimum parameter design so that the results could be used as the datum to fabricate the ironless coreless electricity generator.



CHAPTER 4

DEVELOPMENT WORKS FOR IRONLESS CORELESS ELECTRICITY GENERATOR

4.1 INTRODUCTION

After the software analysis on the ironless coreless electricity generator was completed, development works based on the optimum simulation results gained from the JMAG Designer software began. The development works were divided into two stages, namely, the development works for the ironless electricity generator and the development works on the test bed to test the ironless electricity generator. Most of the fabrication works used CNC machine to produce the real model of the ironless coreless electricity generator. All the parts were assembled using mechanical screw and bolt after all the parts were ready for assembly. Before the fabrication work began, structural analysis was done on the ironless coreless electricity generator. By using Solidworks Simulation, a function embedded within the Solidworks software, the structural analysis was done so that it would help to detect the weak point of the ironless coreless electricity generator model.

4.2 STRUCTURAL ANALYSIS ON IRONLESS CORELESS ELECTRICITY GENERATOR

After the optimum parameter for the ironless coreless electricity generator model was chosen based on the result gained from the simulation by using JMAG Designer software, the model then underwent structural analysis by using Solidworks Simulation. There were three tests which had been carried out to test the ironless coreless electricity generator model, namely, the von Mises stress test, the displacement test and the strain test.

Figure 4.1 shows the results of von Mises stress test on the ironless coreless electricity generator model which had maximum von Mises stress on the rotating shaft where it intersected with the ironless coreless electricity generator. The colour indication of this maximum point was red. The maximum value of this high von Mises stress was 256426.2Nm^2 . Other parts of the rotating shaft had a value fluctuating between 42766.2Nm^2 and 170962.2Nm^2 as the colour indication was green to yellowish green. It was anticipated that the value of the maximum von Mises stress would not be as high as in the structural analysis. This is because during the real experiment, at the end of the long excessive length of rotating shaft, the prime mover or the motor would become the support and reduce the von Mises stress within the rotating shaft. As for the ironless coreless electricity generator model itself, it had minimum von Mises stress within itself, with the value from 34.2Nm^2 to 21400.2Nm^2 and the colour indication was blue.

Figure 4.2 indicates the results of displacement test on the ironless coreless electricity generator model. From these results, the displacement resultant (URES) was the highest on the end of the long excessive length of rotating shaft. The colour indication for this point was red. It had the value of $7.510 \times 10^{-3}\text{mm}$. The other points of the rotating shaft had considerable amount of URES value indicated by light blue to yellow, with the value of between $1.252 \times 10^{-3}\text{mm}$ to $6.258 \times 10^{-3}\text{mm}$. Although the URES value was small on the shaft, the URES value was anticipated to be much lower. This is because during the real experiment, the long excessive length of rotating shaft would be supported by the prime mover, thus reducing the unsupported length of

rotating shaft. The ironless coreless electricity generator model itself had lower URES value compare to the rotating shaft, as the colour indication was only dark blue and light blue, with the URES value of between 1×10^{-30} and 1.877×10^{-3} .

Figure 4.3 shows the results of the strain test on the ironless coreless electricity generator model. As illustrated in Figure 4.3, unlike in the von Mises stress test and displacement test, the rotating shaft had surprisingly low equivalent strain (ESTRN) value. The colour indication was blue, with the value of between 1.586×10^{-9} and 2.368×10^{-6} . As for the ironless coreless electricity generator model, the colour indication was dark blue to light blue, with the ESTRN value from 1.586×10^{-9} to 9.467×10^{-6} .

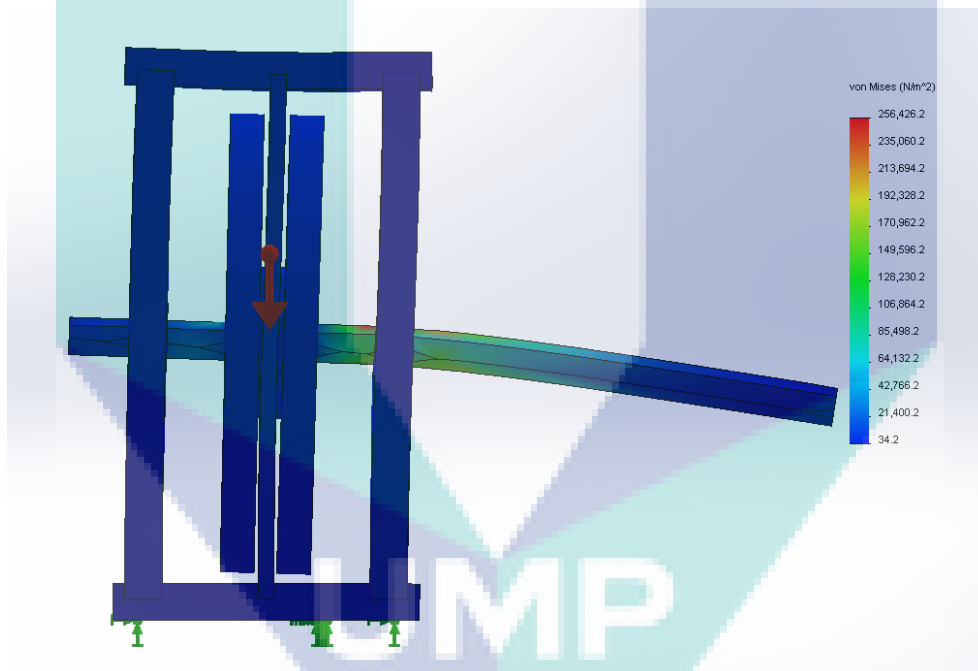


Figure 4.1: Results of the von Mises stress test on the ironless coreless electricity generator

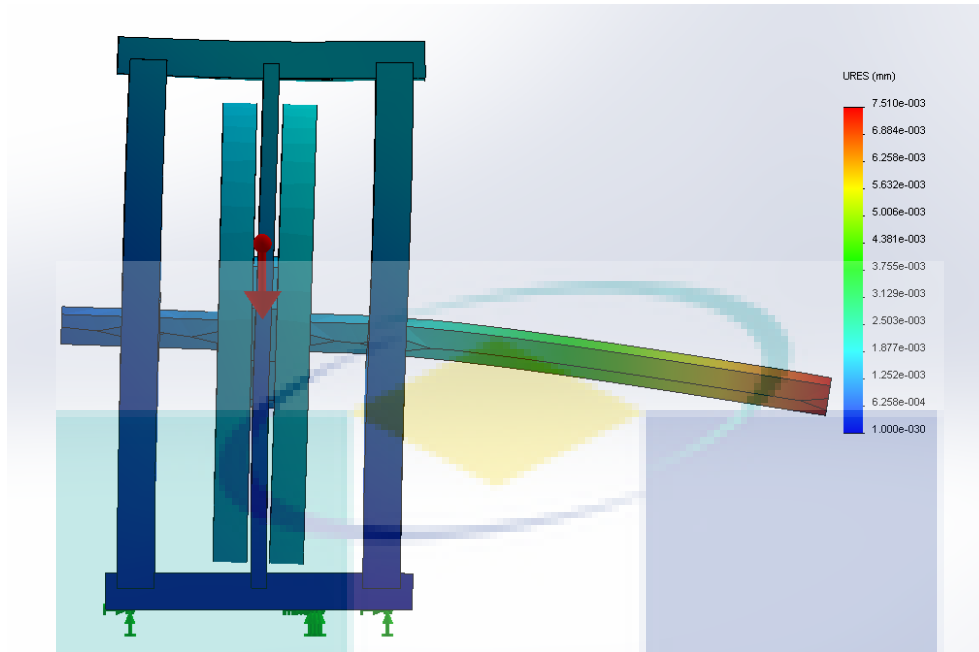


Figure 4.2: Results of the displacement test on the ironless coreless electricity generator

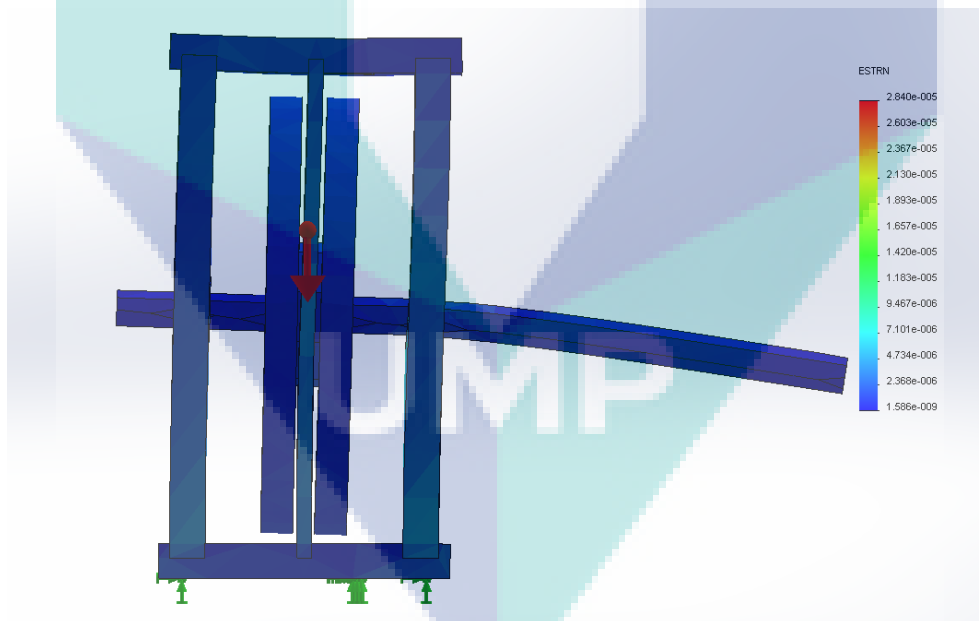


Figure 4.3: Results of the strain test on the ironless coreless electricity generator

4.3 FABRICATION FOR THE IRONLESS CORELESS ELECTRICITY GENERATOR

The designed model was converted into “.dwg” format and then transferred to the Draftsight software for some adjustment such as alignment for the mid-point. The modified model was then converted into R13 drawing format so that it could be used in the Mastercam X5, the software used to communicate with the CNC machine. The converted file was processed further using this Mastercam X5 software.

In the Mastercam X5 software, the machining sequence, tool used and cutting parameter were set accordingly. Cutting the hole as large as the rotating shaft diameter would require the use of 16mm flat end mill. With the consideration of the plastic material for 16mm flat end mill cutting, the following settings were used so that the plastic material would not be damaged: feed rate of the machine = 300; spindle speed of the cutting tools = 1800; the plunge rate of the cutting tools = 80. The depth of cut using 16mm flat end mill as cutting tool was set to 2mm max rough step as this cutting tool could withstand such depth.

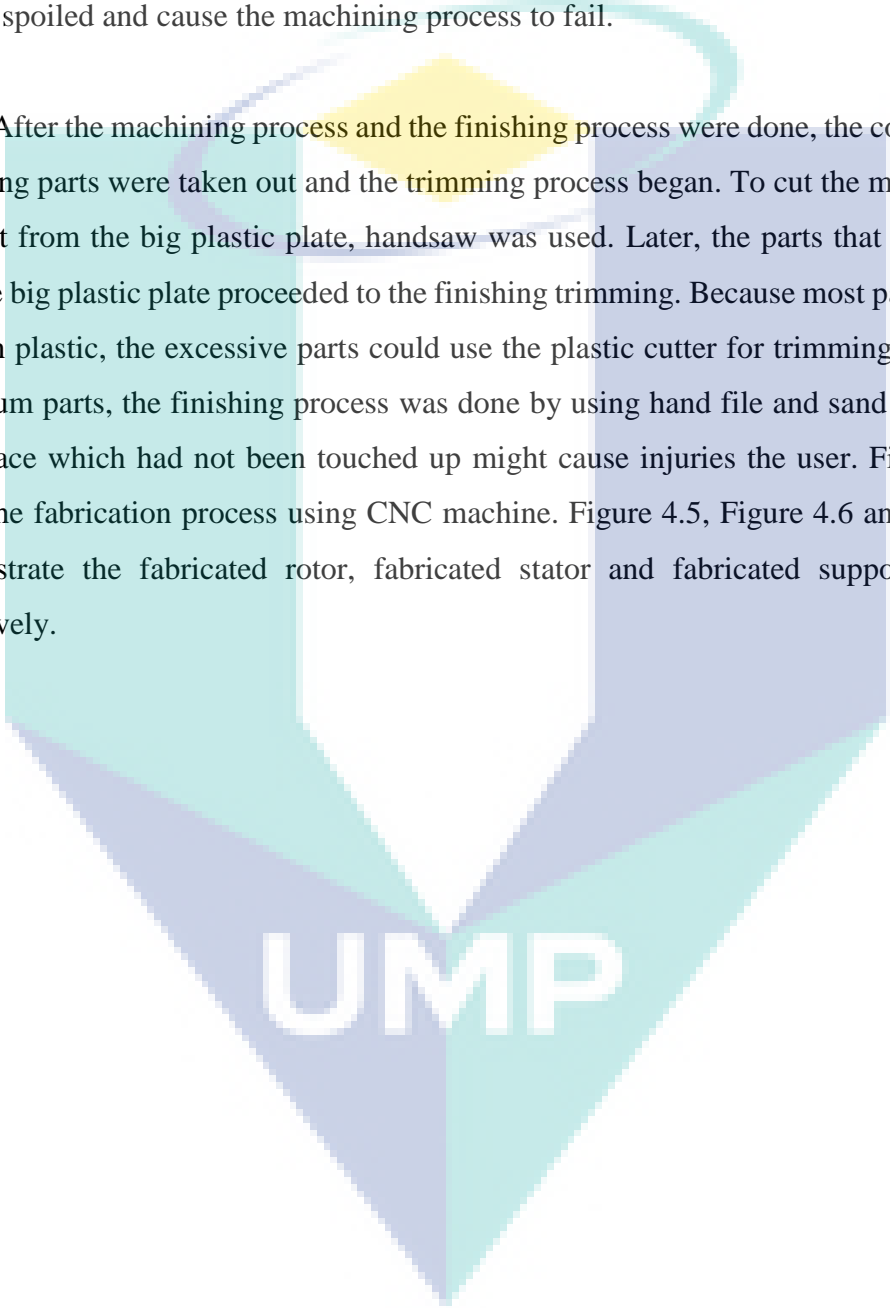
To cut smaller holes, 8mm flat end mill was used and the following settings were applied: feed rate = 300; spindle speed = 2100; and, the plunge rate = 80. The depth of cut was set to between 1mm and 1.5mm as its strength was less compared to that of the 16mm flat end mill. If the threaded hole was required on the design, for example, threaded hole of 6mm diameter, 5mm drill was used to drill the machining parts initially. After that, the 5mm hole was then threaded using 6mm hand tap manually.

For the linking parameters, the cutting tools retract was set to 10mm above the cutting surface, the feed plane was set to 5mm above the cutting surface, the top of stock of the cutting surface was set to 0mm and the total depth of cut was set according to how deep the cutting had to be done on the machining parts.

Once this was done, the modified model was converted into a language that could be read by CNC machine via the Mastercam X5 software. By clicking *SEND*, the CNC machine was ready to receive the program. The machining material, plastic, was

then accurately clamped on the machining bed of the CNC machine, followed by the zero position setting for the machining parts. When all was ready, the machining process began. The coolant must be ensured to have been sprayed on the tip of the cutting tools. This was necessary to make sure that the cutting tools were cold and prevented the tools from overheating. If the cutting tools became overheated, they could become spoiled and cause the machining process to fail.

After the machining process and the finishing process were done, the completed machining parts were taken out and the trimming process began. To cut the machining parts out from the big plastic plate, handsaw was used. Later, the parts that were cut from the big plastic plate proceeded to the finishing trimming. Because most parts were made on plastic, the excessive parts could use the plastic cutter for trimming. For the aluminium parts, the finishing process was done by using hand file and sand paper as the surface which had not been touched up might cause injuries the user. Figure 4.4 shows the fabrication process using CNC machine. Figure 4.5, Figure 4.6 and Figure 4.7 illustrate the fabricated rotor, fabricated stator and fabricated support plate, respectively.

The logo for UMP (Universiti Malaysia Perlis) is a large, stylized letter 'U' shape. The top part of the 'U' is a yellow diamond. The left and right sides of the 'U' are light blue, and the bottom part is a darker blue. The letters 'UMP' are written in white, bold, sans-serif font across the bottom of the 'U' shape.

UMP



Figure 4.4: Fabrication using CNC machine

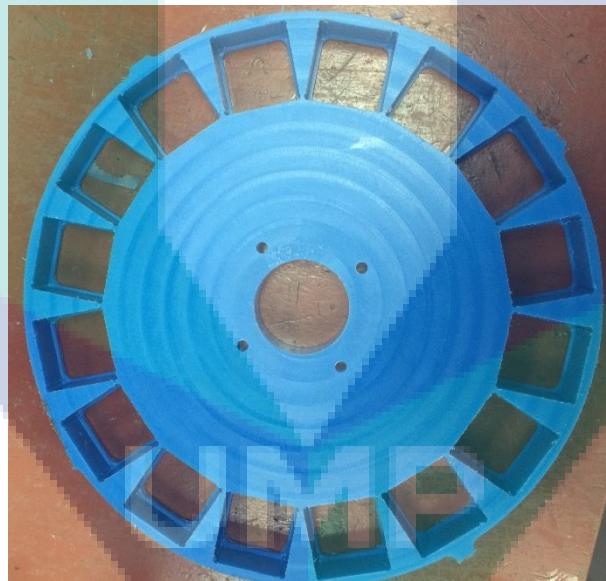


Figure 4.5: Fabricated rotor



Figure 4.6: Fabricated stator



Figure 4.7: Fabricated support plate

Making the coil for the stator needs time and stamina. This is because it had to be neat so that the losses could be reduced. Also, each coil would require 125 turns for each coil to be wrapped. To ease the wrapping of the coil turns and increase the accuracy on coiling, a special jig was used. With the help of the coiling jig which was specifically developed to do the coiling, the workload became less because it did reduce the difficulties in adjusting the wrapping position.

Prior to the making of the coil, the core which held the coil in place was spread with a layer of grease so that the disassembly process from the core after the coil could be done with ease. For the design in this research, each layer of coil consisted of 10 wraps and 13 layers with the final layer of 5 wraps, which resulted in 125 wraps per coil. It should be noted that after finishing each layer, glue or epoxy had to be applied on the layer. This is because with the bonding strength of adhesive between the coils, the completed coil strength increased and thus making the completed coils firm and strong. After 12 sets were completed, the coils were assembled with the stator. Three-phase star connection was made after all the coils were assembled on the stator. Figure 4.8 shows the special jig used to do the coiling. Figure 4.9 and Figure 4.10 illustrate the top view and the side view of the coil with core, respectively. Figure 4.11 shows the completed stator with the coils assembled on it.

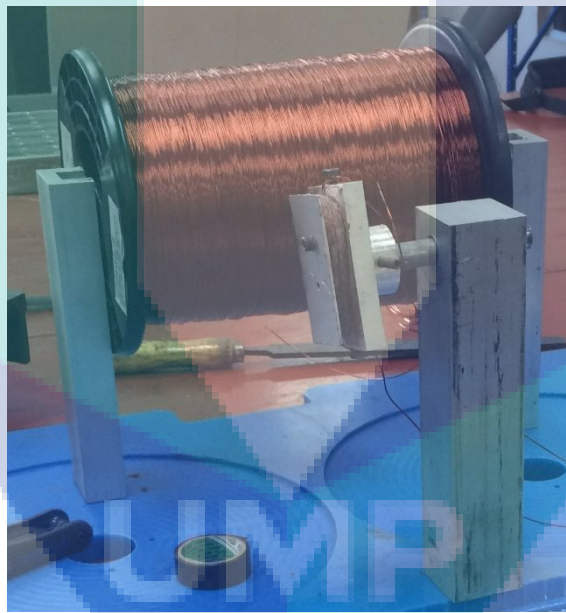


Figure 4.8: Jig used to do the coiling

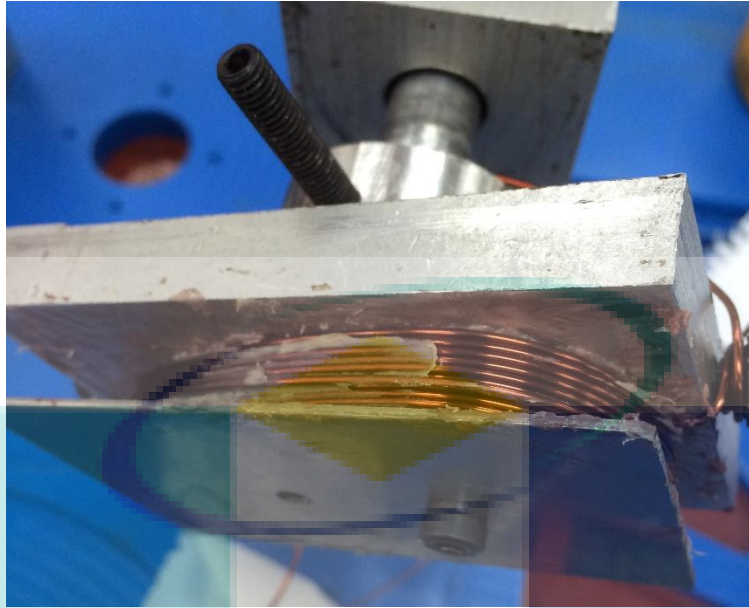


Figure 4.9: Top view for the coil with core



Figure 4.10: Side view for the completed coil with core



Figure 4.11: Coil assembled on the stator

The calculation for the line voltage and line current produced by the three-phase star or wye connection circuit of the ironless coreless electricity generator was done as indicated in the Eq. 4.1 and Eq.4.2, respectively, where V_L would represent the line voltage; V_ϕ , the phase voltage; I_L , the line current; and, I_ϕ , the phase current.

$$V_L = \sqrt{3}V_\phi \quad (4.1)$$

$$I_L = I_\phi \quad (4.2)$$

Line voltage in a polyphase system would be the voltage between two given phases while phase voltage would be the voltage between the given phase and neutral. It should be noted that neutral would be available in star connection but not in delta connection. The same would apply to the line current and phase current. In a balanced wye connection, the line voltage would be equal to the square root of three times phase voltage and line current would be equal to the phase current. For example, if the phase voltage and the phase current was 100V and 3A respectively, the line voltage and line current would be 173.2V and 3A, respectively.

Magnets were the vital parts for this research. Without the magnets, no electricity could be generated in this research. The shipment of magnets came in bulk. To assemble the magnets into the rotor, the first step was to disassemble the magnet bulk into single quantities. Since the Neodymium magnet was so strong that could not be removed by using bare hand, another jig was made specifically to disassemble the magnet from the bulk. The special jig made to perform such task used shear force to separate single unit of Neodymium magnet from the bulk.

After disassembling the magnets from the bulk into single quantities, the magnets were then pushed into the rotor by using mallet. The assembly process was carried out pole by pole. For example, the north pole was firstly assembled on stator and after all was done on the north pole, the assembly for the south pole was then carried out. By using a compass, the poles for the magnet could be easily identified. After all the magnets were in place, the back of the rotor was covered and tightened with aluminium plate to ensure the magnets would be fixed to the rotor. Figure 4.12 shows the special jig used to disassemble Neodymium magnet from the magnet bulk. Figure 4.13 indicates the magnet assembly process into the rotor.



Figure 4.12: Jig used to disassemble magnet from bulk



Figure 4.13: North pole assembled into rotor

After all the parts of ironless coreless electricity generator were assembled, next was the assembly process for the generator. Firstly, the shaft support was pressed into the rotor. A few units of screw were placed without tightening them to ensure the position for shaft support and rotor would be aligned. After that, stator was placed between the rotors and the shaft support was pressed into the second rotor.

For the support plate, the bearing was pushed into the designated space on the side support plate and at the bottom so that both of the support plates were locked with top bottom support plate. Then, the shaft was connected through the support plate, the rotor and the shaft support. After the stator was aligned in the middle, the top plate was screwed to keep it locked. Figure 4.14 illustrates the finished prototype of the ironless coreless electricity generator.

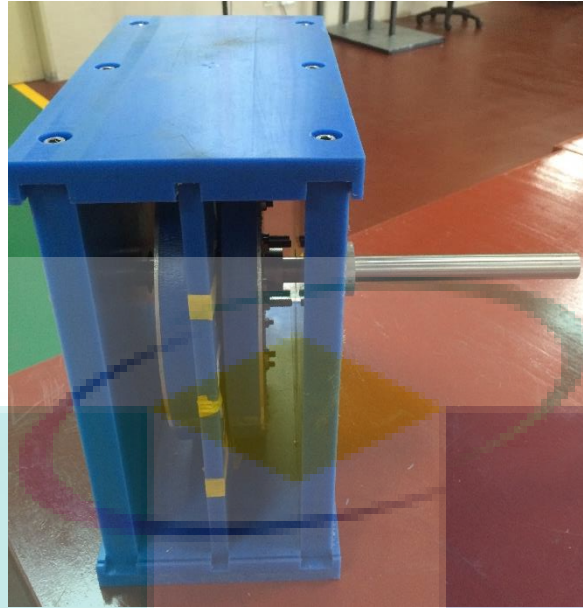


Figure 4.14: Assembled ironless coreless electricity generator

4.4 TEST BED ASSEMBLY

Development of the test bed was rather straightforward. It consisted of the bottom plate which had adjustable height mounting to cause the motor to spin the ironless coreless electricity generator. The motor mounting height had to be adjustable because with this function, the motor or prime mover could be aligned horizontally and accurately with less worry of having to redo the machining on the test bed required. After the alignment of the motor or prime mover was done, the bolt and nuts on the four corners of each screw were tightened to ensure the stiffness of the motor support.

The ironless coreless electricity generator was placed on the other side of mounting placement. The ironless coreless electricity generator was able to move horizontally before it was tightened in its place. This was to ensure that the connection in the motor or prime mover was secured in its place. After the shaft was horizontally aligned with the motor, a specially made connector was used to tighten the shaft connection between the motor and the ironless coreless electricity generator. During the experiment, the inverter was used to convert the direct current into alternating current since the motor or prime mover used three-phase connection to power up. Figure 4.15

shows the completed assembly of test bed with motor and ironless coreless electricity generator.



Figure 4.15: Test bed used to test the ironless coreless electricity generator

UMP

CHAPTER 5

OPEN CIRCUIT TEST ON IRONLESS CORELESS ELECTRICITY GENERATOR

5.1 INTRODUCTION

This chapter describes the open circuit test on the fabricated ironless coreless electricity generator. Fabricated generator was mounted on a test bed and a driver motor was attached to drive the generator. The motor used was three-phase induction and controlled by variable frequency drive (VFD/inverter). The preliminary test, which was an open circuit test or unloaded test, was conducted. The test was meant to qualify the ironless coreless electricity generator capabilities when no load was attached. In the experiment, the three-phase wire from the stator of the generator was connected to each channel of the oscilloscope. The ground in each phase was connected together. The output voltage and frequency produced by the ironless coreless electricity generator were captured on the oscilloscope. Each phase waveform produced pure sine wave signal and was analysed in terms of the phase frequency, peak voltages, root mean square (RMS) voltages, and produced currents. A few experiments with different rotational speed settings were conducted and with the results produced by the generator, the relationship curve between the voltage output and the rotational speed was obtained. It was anticipated that the outcome of this experiment would be that the output voltage of the generator was directly proportional to the rotational speed of the rotors. When the rotational speed increased, this would also increase the magnetic flux cutting rate

of the stator. After obtaining such results, the ironless coreless electricity generator experiment proceeded to the next test, which was the closed circuit test.

5.2 MATERIAL AND EQUIPMENT

In the open circuit test for the ironless coreless electricity generator, a 2-horsepower three-phase induction motor was used to function as the prime mover to rotate the rotor of the generator. This induction motor had a rating no-load rotational speed of 1400RPM, input voltage of 220V to 240V for delta connection, input voltage of 380V to 415V for star connection, rating current of 5.64A to 6.15A for delta connection and rating current of 3.26A to 3.56A for star connection with efficiency of 75.5% if the load usage was below half of the motor but 78.5% if the load usage was above three quarters of the motor. Figure 5.1 shows the specification of the induction motor.



Figure 5.1: Specification of the three-phase induction motor

Since the motor was using alternating current supply to power up, the inverter was used to convert the direct current supply into alternating current supply so that the motor was able to operate. The inverter had an efficiency of 96% when working within the rated load. Wires were used to connect the power source to the inverter. They were also used to connect the inverter to the motor. To measure the wave frequency and the voltage output of the three-phase circuit of the ironless coreless electricity generator, the oscilloscope was used. The oscilloscope was connected to the end of the three-phase circuit by using wires. The tachometer was used to measure the rotational speed of the rotors of the generator. Figure 5.2 illustrates the tachometer used to measure the rotational speed of the rotor. Figure 5.3 shows the inverter used in the open circuit test.



Figure 5.2: Tachometer used to measure rotational speed of rotors



Figure 5.3: Inverter used in the open circuit test

5.3 EXPERIMENTAL SETUP AND PROCEDURES

Before connecting the circuit to the induction motor, it was first aligned with the ironless coreless electricity generator. The centres of motor shaft should be around 189mm from the surface of test bed in order to align them with the shaft of the ironless coreless electricity generator. The plate which supported the motor was then tightened using M8 bolts and nuts after the height of motor was set. The distance between the ironless coreless electricity generator and the motor was aligned horizontally by adjusting the generator. The bottom surface of the ironless coreless electricity generator was then locked on the test bed using M8 bolts and nuts. After the induction motor was well aligned with the generator, the connection between the induction motor and the generator was tightened with specifically made socket using socket cup point grub screws.

After the test bed was completely set up, the three-phase induction motor was connected using star connection as it could support higher voltage. The inverter was connected to power supply and the motor after the ironless coreless electricity generator and the motor were in place. The three-phase circuit of the ironless coreless electricity generator was then connected to the oscilloscope. When all the mechanical assembly

and electrical assembly were done, the experiment began. After the power supply was switched on, a specified amount of power transferred to the motor was set by the inverter. The input power of the motor was controlled by the inverter using frequency input in the inverter. Once the setting was done and the rotational speed of the rotor was stabilized, the rotational speed of the rotor was observed using tachometer and recorded. To clearly obtain the graphical output wavelength from the oscilloscope, the x -axis was set to 10 milliseconds per column and y -axis was set to 20V or 50V per row, depending on the output voltage of the experiment. When the rotors were rotating, wave frequency and the output voltage were produced (see Figure 5.4 until Figure 5.8). When everything was observed to have been completed, screenshots of the oscilloscope were taken and the data were transferred into the computer for data extraction process.

5.4 RESULTS OF THE OPEN CIRCUIT TEST

In the open circuit test, there were five experiments carried out with various rotational speed settings. Figure 5.4 (a) -(e) show the results of experiment screenshots from the oscilloscope while Table 5.1 shows the compiled results for the test in experiment and simulation modes. The Figure 5.5 shows the comparison of the results for the experimental and simulation modes of the test. Figure 5.4 (a) -(e) show three colours, namely, purple, yellow and teal, to indicate different waveforms in the graph. Each colour represented the output for U-phase voltage output, V-phase voltage output and W-phase voltage output, respectively. Figure 5.4 (a) indicates the three-phase voltage output of the first run of the experiment under rotational speed of 113.4 RPM. It should be noted that there were several dotted lines within Figure 5.4 (a). The x -axis represented 10 milliseconds per column while the y -axis represented 20 volts per row. As illustrated in the graph from the oscilloscope, the peak-to-peak value of the three-phase voltage output was approximately 44 volts. After the processing of such data by the oscilloscope, the RMS value for the voltage output around 29 volts with wave frequency of approximate 15.2 Hertz were obtained.

Figure 5.4 (b) shows the three-phase voltage output results obtained from the second run of the experiment under rotational speed of 171.8 RPM. The x -axis of the Figure 5.4 (b) indicates 10 milliseconds per column, while the y -axis of the Figure 5.4

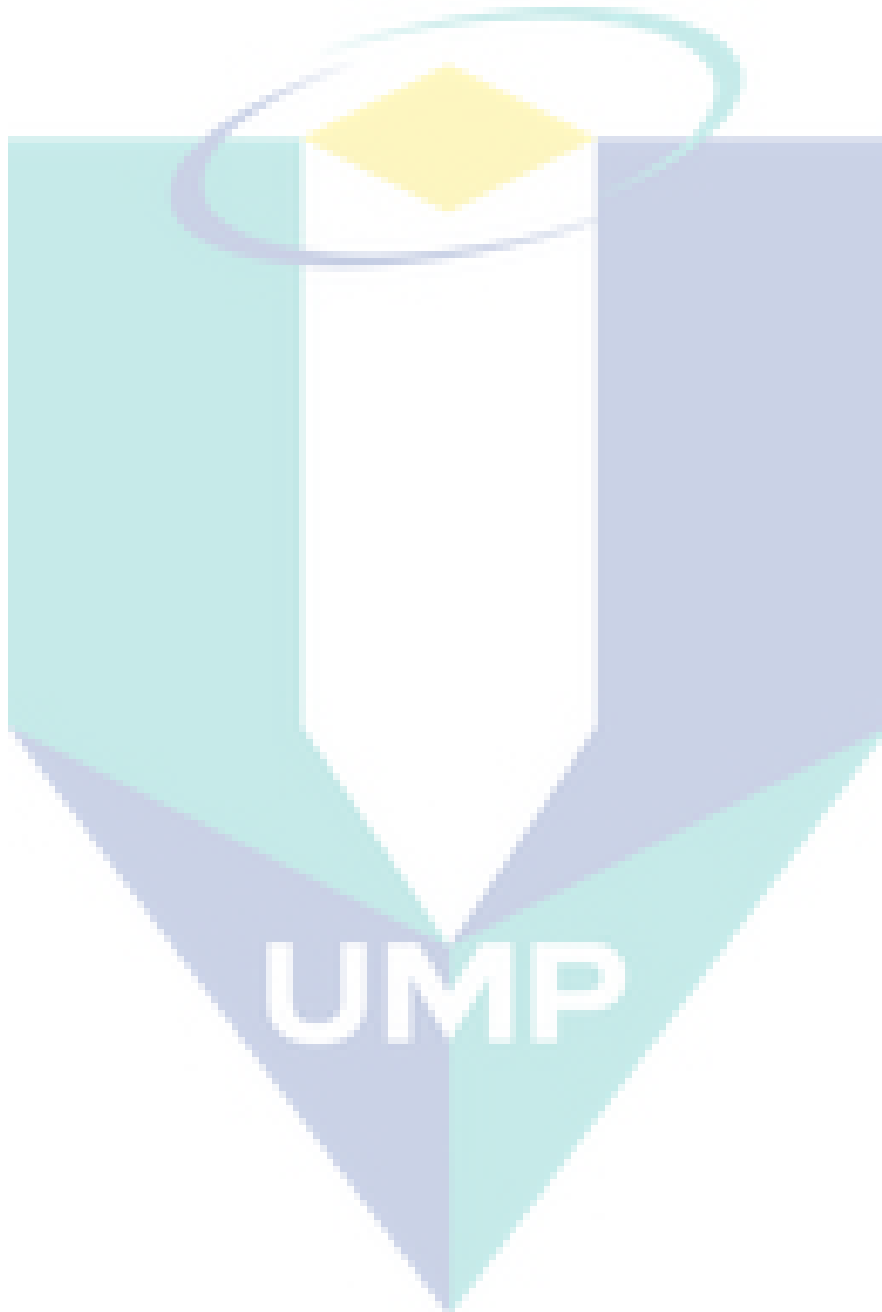
(b) shows that there were 50 volts per row. With regard to the results obtained from the oscilloscope in the second run of the unloaded test, the peak-to-peak value of the three-phase voltage output of the ironless coreless electricity generator was around 70 volts. The outcome of the processed data by the oscilloscope shows that the RMS value of the voltage output in the second run of the unloaded test was approximately 46 volts with wave frequency of around 23.3 Hertz.

Figure 5.4 (c) illustrates the three-phase voltage output results obtained from the third run of the unloaded test on the ironless coreless electricity generator under rotational speed of 233.5 RPM. The x -axis in this figure shows 10 milliseconds per column, while the y -axis indicates that the value per row was 50 volts. Based on the results obtained from the third run, the peak-to-peak value of the three-phase voltage output of the ironless coreless electricity generator was approximately 90 volts. After the data obtained in the third experiment were processed by the oscilloscope, it was observed that the RMS value of the voltage output on the third experiment was around 60 volts with the wave frequency of around 31.3 Hertz.

Figure 5.4 (d) indicates the three-phase voltage output results obtained from the fourth run of the unloaded test on the ironless coreless electricity generator under rotational speed of 293.6 RPM. The x -axis shows that the value per column was 10 milliseconds, while the y -axis shows that the value of each row was 50 volts. The peak-to-peak value of the three-phase voltage output of the ironless coreless electricity generator after the fourth experiment was around 110 volts. The RMS value of the voltage output in the fourth experiment was approximately 77 volts with the wave frequency of around 39.2 Hertz. Similarly, the RMS value and the wave frequency were obtained based on the data processed by the oscilloscope.

Meanwhile, the three-phase voltage output obtained from the fifth run of the unloaded test on the ironless coreless electricity generator under rotational speed of 352.8 RPM is shown in Figure 5.4 (e). The x -axis in the Figure 5.4 (e) shows that the value of each column was 10 milliseconds, while the y -axis indicates that the value of each row was 50 volts. Based on the results gained from the fifth unloaded experiment, the peak-to-peak value of the three-phase voltage output of the ironless coreless electricity generator was around 130 volts. Based on the data processed by the

oscilloscope, it was observed that the RMS value of the three-phase voltage output of the ironless coreless electricity generator was approximately 93 volts with the wave frequency of around 47.2 Hertz.



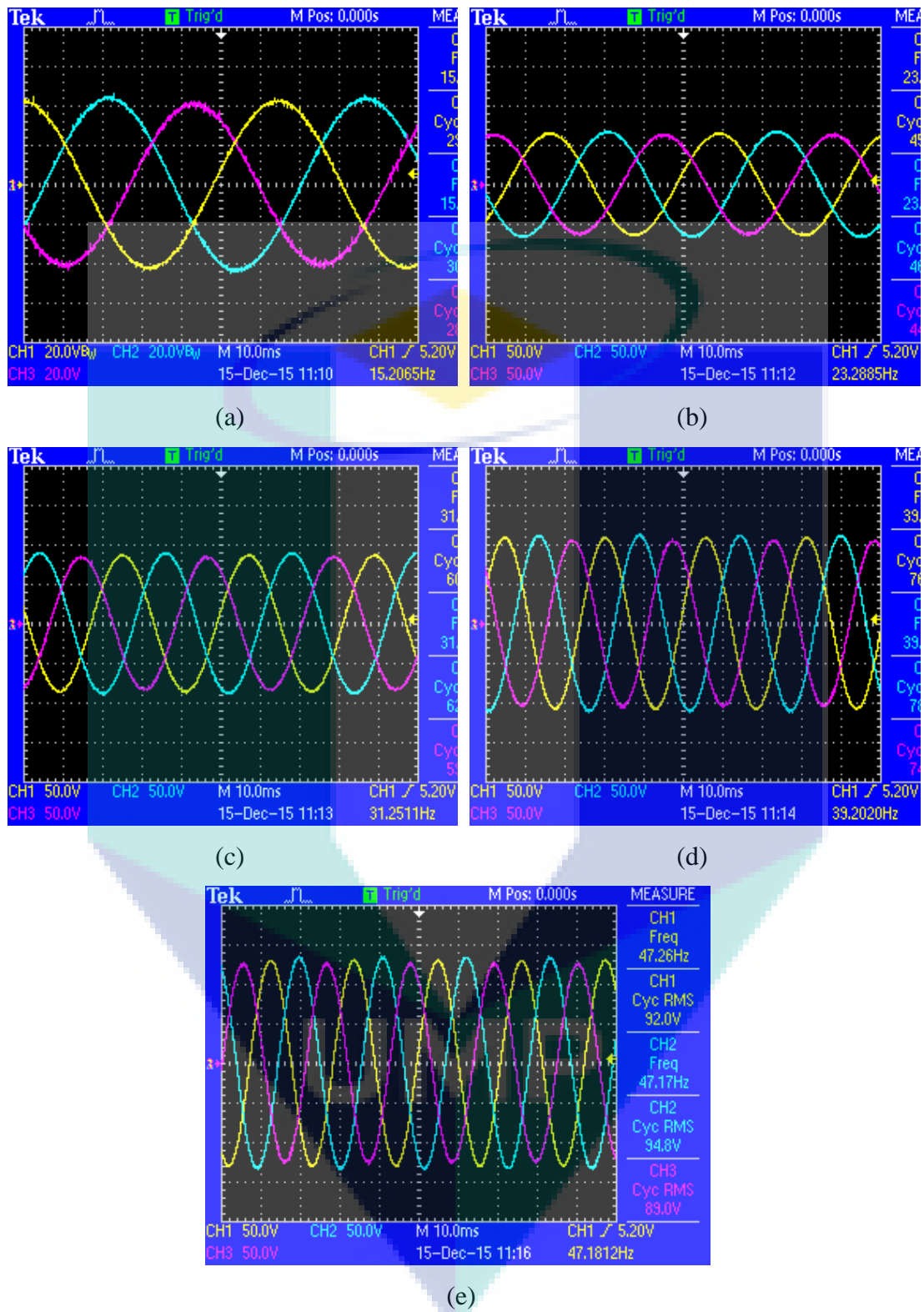


Figure 5.4: Phase voltages and characteristics for rotational speed of a) 113.4 RPM, b) 171.8 RPM. c) 233.5 RPM, d) 293.6 RPM and e) 352.8 RPM

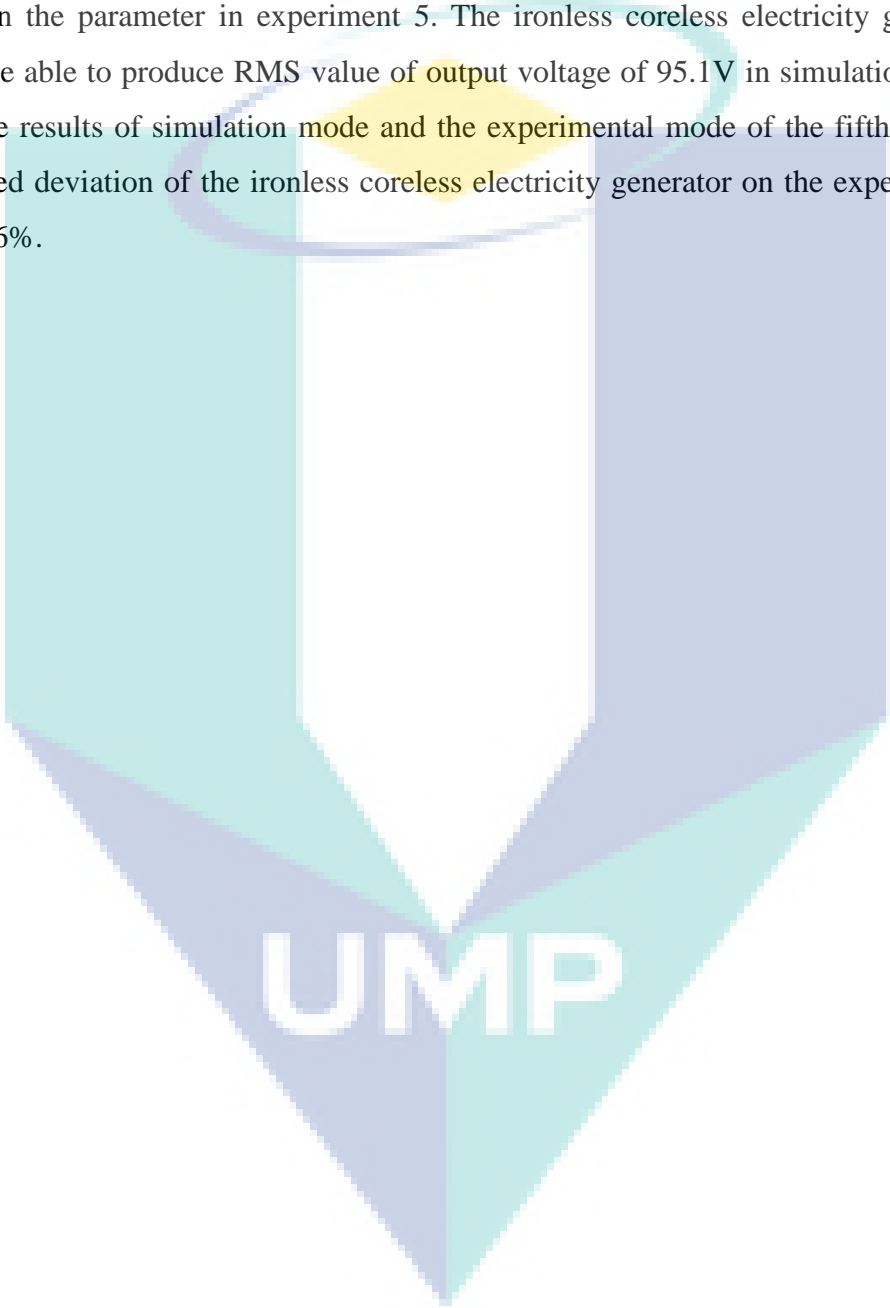
Table 5.1 summarizes the results of open circuit test from experiment 1 to experiment 5 as illustrated in Figure 5.4 (a) - (e). In experiment 1, the rotational speed used was 113.4RPM. It produced wave frequency of 15.2Hz with RMS value of output voltage of 29.5V. Based on the similar variable to run the simulation, the simulated result of the RMS value of output voltage was 31.8V. Based on the results in both simulation mode and experimental mode, the deviation of the ironless coreless electricity generator in experiment 1 was 7.23%.

In the second run of the experiment, the rotational speed of 171.8RPM was used. The ironless coreless electricity generator using this rotational speed was able to produce wave frequency of 23.28Hz with the RMS value of output voltage of 45.6V. Based on the same parameter, the simulated result showed that the ironless coreless electricity generator would be able to produce 48.1V. By comparing the two results in the simulation mode and experimental mode in experiment 2, the deviation of the ironless coreless electricity generator in this run was 5.20%.

For the third run of the open circuit test for the ironless coreless electricity generator, the rotational speed of 233.5 RPM was used. Based on the constant variable, the rotational speed of the rotor on this experiment, the three-phase circuit of the ironless coreless electricity generator was able to produce wave frequency of 31.25Hz with the RMS value of the three-phase output voltage of 60.9V. By using same parameter for the simulation mode, the three-phase circuit of the generator would be able to produce RMS value of 63.9V. By comparing the two results in the simulation mode and the experimental mode of experiment 3, the deviation of the ironless coreless electricity generator was 4.69%.

In the fourth open circuit experiment on the ironless coreless electricity generator, the rotational speed of the rotors was set to 293.6 RPM. By using such speed on the rotors of the generator, the wave frequency of 39.25Hz and RMS value of output voltage of 76.5V was produced by the three-phase circuit of the generator. By using the exact parameter in the simulation, the ironless coreless electricity generator would be able to produce RMS value of output voltage of 81V with such rotor speed. By comparing the simulated output voltage and experimental output voltage, the deviation of the ironless coreless electricity generator on the experiment 4 was 5.56%.

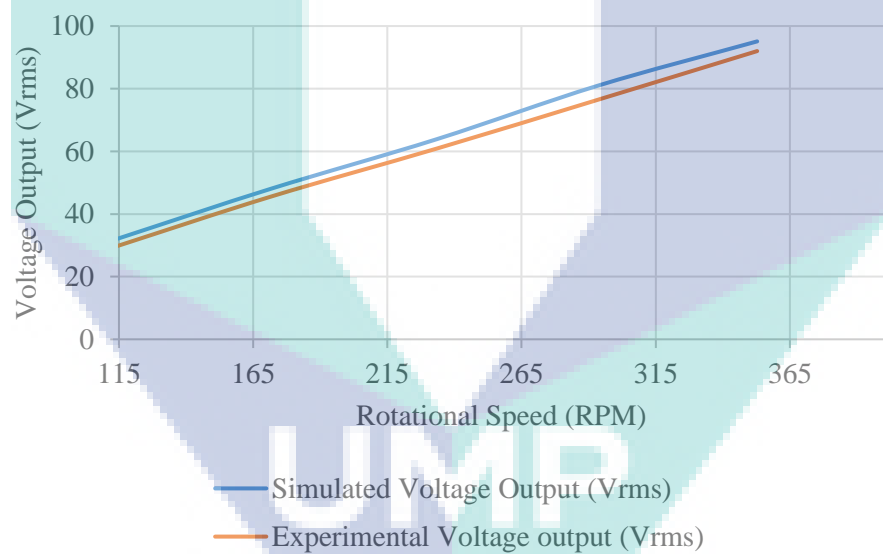
In the fifth and final open circuit experiment on the ironless coreless electricity generator, the rotational speed of 352.8 RPM was used. During experiment 5, the wave frequency of 47.21Hz and RMS value of output voltage of 92V was produced by the three-phase circuit of the ironless coreless electricity generator. The simulation was run based on the parameter in experiment 5. The ironless coreless electricity generator would be able to produce RMS value of output voltage of 95.1V in simulation mode. With the results of simulation mode and the experimental mode of the fifth test, the calculated deviation of the ironless coreless electricity generator on the experiment 5 was 3.26%.

The logo for UIMP (Universitas Islam Malang) is a large, downward-pointing arrow shape. It is composed of several overlapping geometric shapes in shades of teal, light blue, and white. The letters 'UIMP' are written in a bold, white, sans-serif font across the bottom of the arrow.

UIMP

Table 5.1: The results for the experiment mode with different rotational speed settings

	Open Circuit test 1	Open Circuit test 2	Open Circuit test 3	Open Circuit test 4	Open Circuit test 5
Rotational speed (RPM)	113.4	171.8	233.5	293.6	352.8
Wave Frequency (Hz)	15.20	23.28	31.25	39.25	47.21
Simulated Output Voltage (V_{rms})	31.8	48.1	63.9	81.0	95.1
Experimental Output voltage (V_{rms})	29.5	45.6	60.9	76.5	92.0
Deviation (%)	7.23	5.20	4.69	5.56	3.26

**Figure 5.5:** Voltage output versus rotational speed of the rotor for ironless coreless electricity generator

5.5 DISCUSSIONS

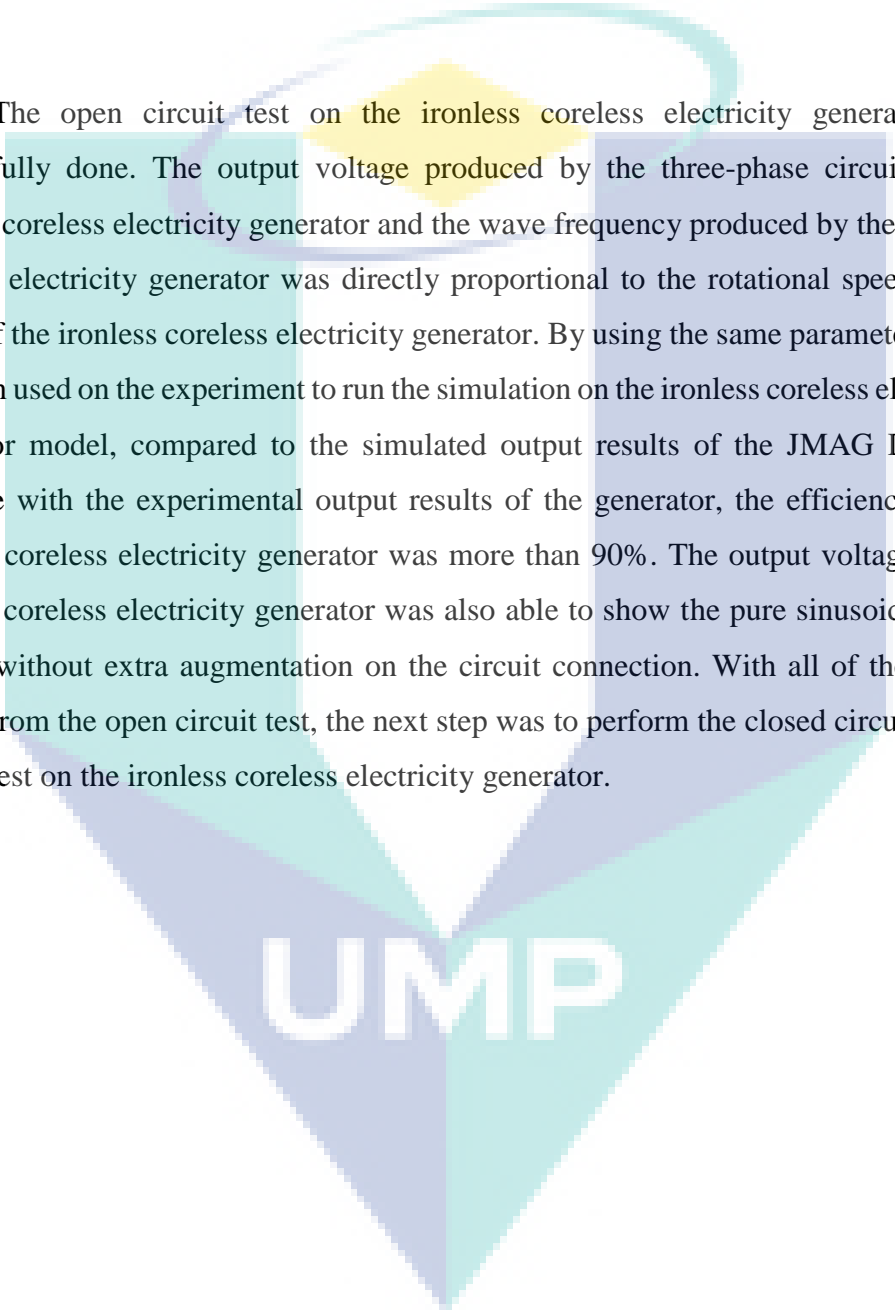
As shown in the illustrations (see Figure 5.4 to Figure 5.8), it was noted that the frequency of wave became increasingly frequent and the output voltage produced by the three-phase circuit of the ironless coreless electricity generator increased within the time frame when the rotational speed of the rotors of the ironless coreless electricity generator increased. This is because when the rotors of the generator were spinning faster, the frequency of magnetic flux cutting in the three-phase circuit on the stator of the ironless coreless electricity generator increased proportionally. When there was more magnetic flux cut by the three-phase circuit in the stator, the voltage per phase and wave frequency of each phase produced by the ironless coreless electricity generator also increased. This explanation for the open circuit test is similar and agrees with that of Chalmers and Spooner's research findings on an axial flux permanent magnet generator for a gearless wind energy system (Chalmers & Spooner, 1999). By applying the rotational speed of the rotors of the generator and the frequency output produced by the rotors as indicated in Eq. 2.16 in Chapter 2 of this thesis, the calculated result was in good agreement with the ironless coreless electricity generator design, that is, 16 poles applied on a rotor.

The results showed the three-phase voltage output for all five experiments in the open circuit test was pure sinusoidal wave. Normally, the experimental results for other generators would not show such outcome without having done the augmentation on the output of the electricity generator. This was the selling point of this ironless coreless electricity generator because without adding extra equipment to produce or modify the output became pure sinusoidal wave, the losses in the system would be minimal. The statement regarding to the losses was supported by the findings of Tamura's research on calculation method of losses and efficiency of wind generators (Tamura, 2012). In Table 5.1, compared with the simulation results, the experimental results seemed to be slightly lower. This is because the simulation of the ironless coreless electricity generator was generated based on the ideal condition, which did not include system losses such as the bearing losses, slipping losses as well as the frictional losses on the test bed. Undeniably, there were some losses such as bearing losses and frictional losses in the system. The losses in the real experiment results were the causes of the lower

voltage output compared to that of the simulation results. The results of the open circuit test were found to be similar and in good agreement with the results of Chen and Pillay's (2005) research in terms of no load voltage versus speed test (Chen & Pillay, 2005).

5.6 SUMMARY OF THE CHAPTER

The open circuit test on the ironless coreless electricity generator was successfully done. The output voltage produced by the three-phase circuit of the ironless coreless electricity generator and the wave frequency produced by the ironless coreless electricity generator was directly proportional to the rotational speed of the rotors of the ironless coreless electricity generator. By using the same parameter which had been used on the experiment to run the simulation on the ironless coreless electricity generator model, compared to the simulated output results of the JMAG Designer software with the experimental output results of the generator, the efficiency of the ironless coreless electricity generator was more than 90%. The output voltage of the ironless coreless electricity generator was also able to show the pure sinusoidal wave pattern without extra augmentation on the circuit connection. With all of the results gained from the open circuit test, the next step was to perform the closed circuit test or loaded test on the ironless coreless electricity generator.

The logo for UMP (Universiti Malaysia Perlis) is a large, stylized letter 'U' composed of several overlapping triangles in shades of teal and light blue. The letters 'UMP' are printed in a bold, white, sans-serif font across the center of the 'U' shape.

UMP

CHAPTER 6

CLOSED CIRCUIT TEST ON IRONLESS CORELESS ELECTRICITY GENERATOR

6.1 INTRODUCTION

In this chapter, the results of the closed circuit test on the ironless coreless electricity generator will be presented and discussed. After the open circuit test was done, the closed circuit test or loaded test was performed to test the ironless coreless electricity generator. The reason to perform the closed circuit test was to experiment the capabilities of the fabricated ironless coreless electricity generator under loaded conditions. In the closed circuit test, the generator was connected to the rectifier which enabled the three-phase output to be converted into direct current. After being connected to the rectifier, the rectifier was then connected to the DC electronic load unit in which the resistive load used to test the ironless coreless electricity generator was controlled. The output voltage, as well as the output power from the ironless coreless electricity generator, were able to be monitored by using this DC electronic load unit. Other than that, the oscilloscope was used to measure the input current for the motor. Various rotational speed constant resistive load tests and maximum power point tracking tests were carried out to examine the capability of the fabricated ironless coreless electricity generator. During the various rotational speed constant resistive load tests, the power generated by the ironless coreless electricity generator was directly proportional to the rotational speed of the rotors. For the maximum power point tracking

test, the results showed that the optimal resistive load for the ironless coreless electricity generator was around the range of between 34 ohms and 35 ohms.

6.2 MATERIAL AND EQUIPMENT

In the closed circuit test on the ironless coreless generator, the same motor was used in the open circuit test, with a 2-horsepower three-phase induction motor was used to function as the prime mover to rotate the rotor of the generator. This induction motor with the following settings was used as the prime mover for the generator in this experiment: rating rotational speed of 1400RPM, rating voltage of 220V to 240V for delta connection, rating voltage of 380V to 415V for star connection, rating current of 5.64A to 6.15A for delta connection and rating current of 3.26A to 3.56A for star connection. The DC electronic load was used to supply load to the ironless coreless electricity generator. It was also able alternate the load manually which would be handled by the generator. The inverter was also used to control the power supplied to the motor. In the closed circuit test, the rectifier was used to convert the alternating current generated by the ironless coreless electricity generator into the direct current. This was because the DC electronic load unit was only able to connect by using direct current connection. Figure 6.1 shows the display of the DC electronic load used to test the ironless coreless electricity generator in the closed circuit experiment. Figure 6.2 shows the rectifier used in the closed circuit test.



Figure 6.1: DC electronic load used in the close circuit test



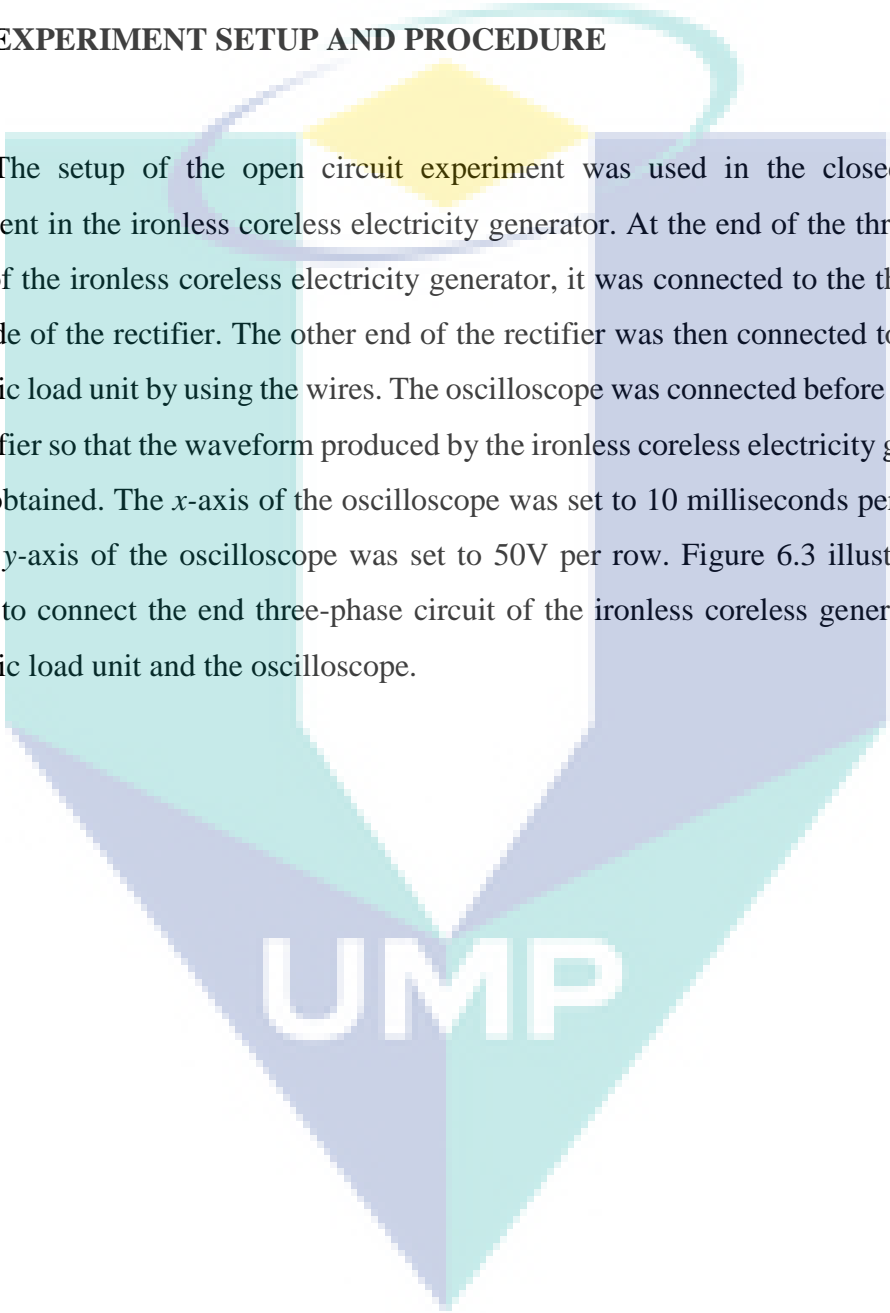
Figure 6.2: Rectifier used in the closed circuit test

UMP

The oscilloscope was used to verify the waveform profiles for both before and after the voltage was generated by the ironless coreless electricity generator passing through the rectifier. When the experiment began, the tachometer was used to measure the rotational speed of the rotors of the ironless coreless electricity generator.

6.3 EXPERIMENT SETUP AND PROCEDURE

The setup of the open circuit experiment was used in the closed circuit experiment in the ironless coreless electricity generator. At the end of the three-phase circuit of the ironless coreless electricity generator, it was connected to the three-way input side of the rectifier. The other end of the rectifier was then connected to the DC electronic load unit by using the wires. The oscilloscope was connected before and after the rectifier so that the waveform produced by the ironless coreless electricity generator can be obtained. The x -axis of the oscilloscope was set to 10 milliseconds per column and the y -axis of the oscilloscope was set to 50V per row. Figure 6.3 illustrates the method to connect the end three-phase circuit of the ironless coreless generator, DC electronic load unit and the oscilloscope.

The logo for UIMP (Universiti Malaysia Perlis) is a large, stylized letter 'V' shape. The top part of the 'V' is a yellow diamond. The left and right sides of the 'V' are light blue, and the bottom part is a darker blue. The letters 'UIMP' are written in white, bold, sans-serif font across the bottom of the 'V' shape.

UIMP

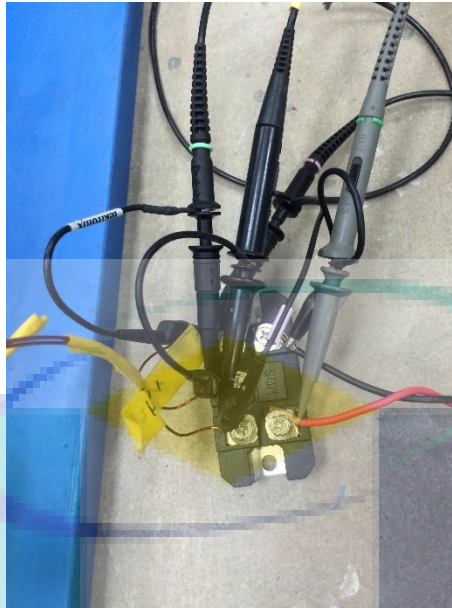


Figure 6.3: Method to connect ironless coreless generator, DC electronic load unit and oscilloscope

When the setup was completed, the closed circuit test was performed on the ironless coreless electricity generator. After the power source was switched on, the frequency input was set on the inverter and the inverter was turned on. The motor and the rotors of the ironless coreless electricity generator started to spin. The load value was then set at the DC electronic load unit. For the various rotational speed constant load tests, the load value was set to 100 ohms. As for the maximum power point tracking test, the load value was alternate to obtain the highest output voltage, power and current for the ironless coreless electricity generator. After that, the rotational speed settings of the rotors were measured using the tachometer and recorded accordingly. Screenshots of the waveform of the output voltage were also taken using the oscilloscope and transferred into the computer for further analysis. The reading of the voltage produced by the ironless coreless electricity generator, the current produced by the ironless coreless electricity generator as well as the power produced by the ironless coreless electricity generator from the DC electronic load unit were also recorded for data processing. The power input for the inverter was also measured using the current probe and voltage probe and the results were obtained by reading the output from the oscilloscope. The procedures were repeated by using various frequency inputs in the inverter as they altered the rotational speed settings of the rotors of the ironless coreless

electricity generator. Figure 6.4 illustrates the flow chart of the closed circuit test and its setup.

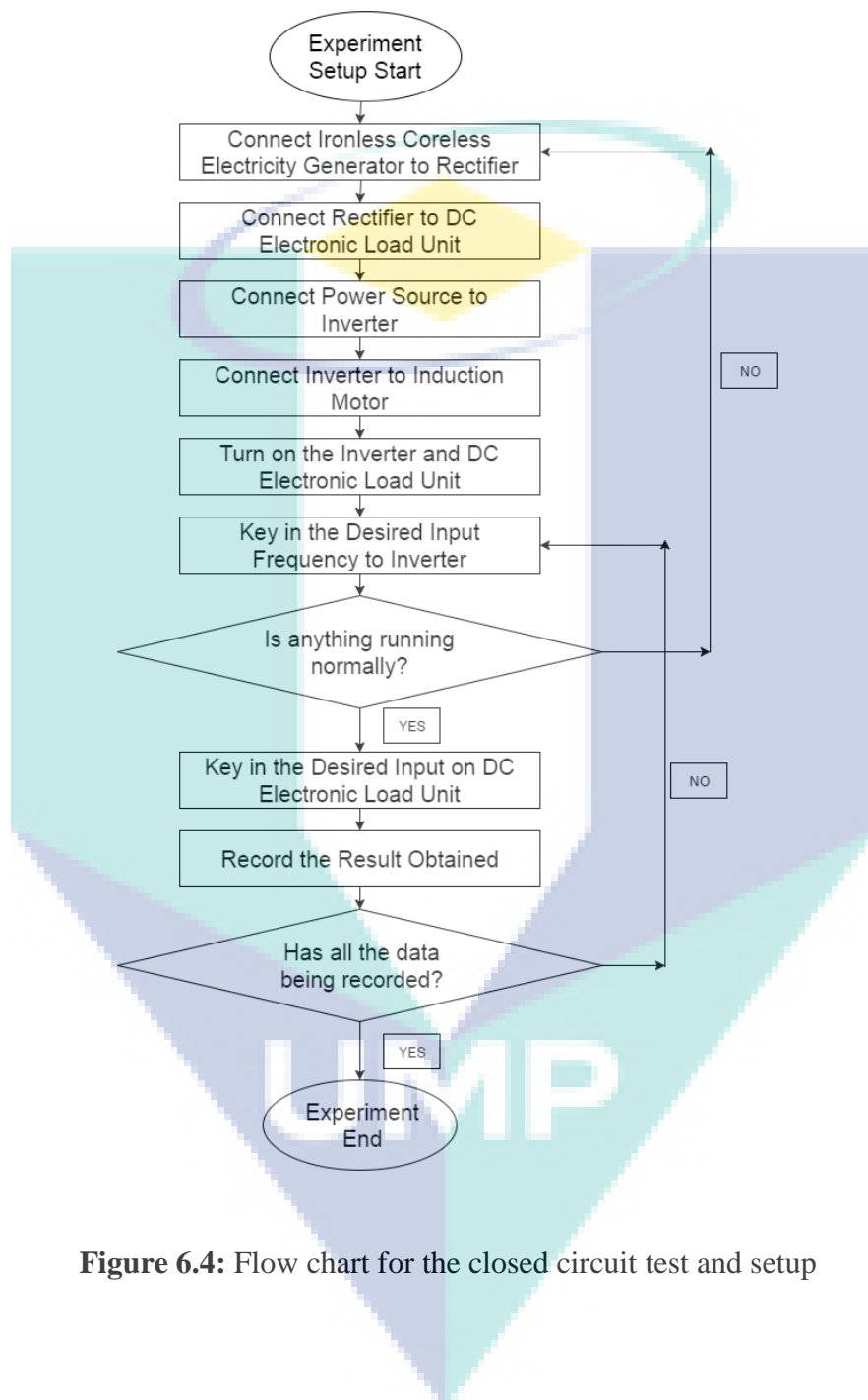


Figure 6.4: Flow chart for the closed circuit test and setup

6.4 RESULTS FOR THE CLOSED CIRCUIT TEST

In the closed circuit test for the ironless coreless electricity generator, to measure the output voltage, power and output current of the ironless coreless electricity generator for the closed circuit test, the three-phase output of the ironless coreless electricity generator, the alternating current (AC), was converted to output similar to the direct current (DC) so that it could be used on the DC electronic load unit. The rectifier was used to convert the alternating current into a similar pattern as the direct current. Figure 6.5 illustrates the voltage produced by the ironless coreless electricity generator before and after conversion by the rectifier. The colours purple, yellow and teal waves were the three-phase voltage output for the ironless coreless electricity generator while the green wave is the output which was similar to the direct current after passing through the rectifier. The peak-to-peak value of the voltage output before conversion by the rectifier was approximately 80V. After the voltage output was converted by the rectifier, the voltage fluctuated between 70V and 80V.

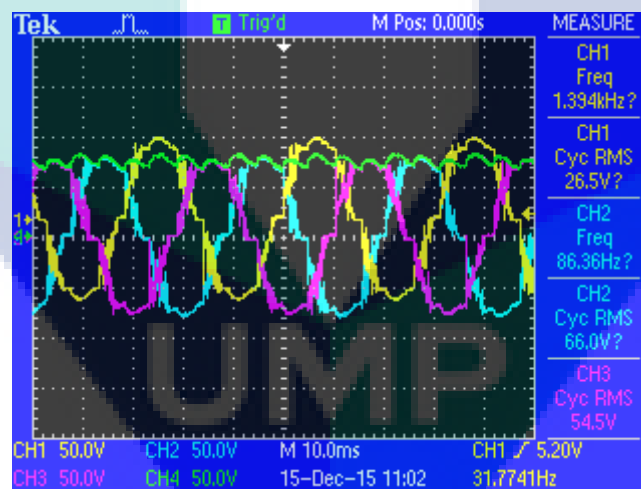


Figure 6.5: The voltage output before and after conversion by the rectifier

In order to calculate the torque used on the generator and the efficiency of the generator, the power output of the prime mover had to be obtained. By applying Eq. 2.7, the power output of the inverter and power output of the prime mover could be calculated as the efficiency of the inverter and motor could be obtained from the datasheet of each part respectively after the power input before the inverter was measured. After obtaining the power output of the prime mover, the calculated value was simply applied to Eq. 2.9 while for the efficiency of the ironless coreless electricity generator, since power input of the ironless coreless electricity generator was equal to the power output of the prime mover, the efficiency of the generator could be calculated using Eq. 2.7 as mentioned in Chapter 2 of this thesis.

6.4.1 Various rotational speed constant load tests

In the various rotational speed constant load tests, the load used by the ironless coreless electricity generator was set as constant variable, which was 100 ohm. The rotor speed was the manipulated variable, while the power generated, voltage produced, the current produced, the torque produce and the efficiency by the ironless coreless electricity generator were the responding variables. Based on derivation in Eq. 2.9 and Eq. 2.10, the torque of the ironless coreless electricity generator could be calculated using Eq. 6.1.

There were 12 sets of experiments carried out in the various rotational speed constant load tests. In the first run, rotational speed of 104RPM was used on the rotor of the ironless coreless electricity generator. With such rotational speed, the ironless coreless electricity generator was able to produce output power of 10.7W, output voltage of 33V, output current of 0.3A, torque of 3.01Nm and efficiency of 32.59%. Rotational speed of 118RPM was used on the rotors of the generator during the second test. The generator was able to produce output power of 13.8W, output voltage of 38V, output current of 0.36A, torque of 3.03Nm and efficiency of 36.83% with such rotational speed.

In the third experiment, rotational speed of 131RPM was set on the rotor of the ironless coreless electricity generator. The generator was able to produce output power

of 17.3W, output voltage of 43V, output current of 0.41A, torque of 2.86Nm and efficiency of 44.04% with 131RPM. The fourth experiment was using 145RPM on the rotors of the generator. With such speed, the generator was able to produce output power of 21.4W, output voltage of 46V, output current of 0.46A, torque of 2.73Nm and efficiency of 51.53%. For the fifth experiment, rotational speed of 158RPM was used on the rotors of the generator. The generator was able to produce the output power of 25.2W, output voltage of 51V, output current of 0.5A, torque of 2.70Nm and efficiency of 56.35%. The sixth experiment was using rotational speed of 171RPM on the rotors of the generator and with this rotational speed, the generator was able to produce an output power of 30.3W, output voltage of 55V, output current of 0.546A, torque of 2.77Nm and efficiency of 61.03%.

In the seventh test, rotational speed of 184RPM was used on the rotors of the generator. The generator was able to produce output power of 35.9W, output voltage of 60V, output current of 0.592A, torque of 2.72Nm and efficiency of 68.41% under such rotational speed. The eighth test was using 198RPM on the rotors of the generator. An output power of 41.3W, output voltage of 64.5V, output current of 0.636A, torque of 2.83Nm and efficiency of 70.43% was able to produce by the generator under the provided rotational speed. The ninth test was using 211RPM on the rotor of the generator and it was able to produce output power of 46.9W, output voltage of 69V, output current of 0.682A, torque of 2.87Nm and efficiency of 73.95% under such condition. In the tenth test, the generator was able to produce output power of 52.1W, output voltage of 72V, output current of 0.727A, torque of 2.91Nm and efficiency of 76.39% when the rotational speed of 224RPM was supplied to the rotors of the generator. Rotational speed of 238RPM was supplied to the rotors of the generator during the eleventh test. The generator was able to produce output power of 59.5W, output voltage of 77V, output current of 0.771A, torque of 3.06Nm and efficiency of 77.96% during this test. In the last test for the various rotational speed constant load test, rotational speed of 250RPM was used on the rotors of the generator. With such rotational speed, output power of 66.1W, output voltage of 81V, output current of 0.814A, torque of 3.24Nm and efficiency of 77.95% was able to produce by the generator. Table 6.1 summarizes the results of power output while Table 6.2 summarizes the result of power input, power after inverter and power after motor for

the various rotational speed constant load tests. Meanwhile, Table 6.3 summarizes the results for torque and efficiency for the various rotational speed constant load tests.

Table 6.1: Results for power output in various rotational speed constant load tests

load (ohm)	Speed (RPM)	Power output for generator(W)	voltage (V)	current (A)
100	104	10.7	33	0.3
100	118	13.8	38	0.36
100	131	17.3	43	0.41
100	145	21.4	46	0.46
100	158	25.2	51	0.5
100	171	30.3	55	0.546
100	184	35.9	60	0.592
100	198	41.3	64.5	0.636
100	211	46.9	69	0.682
100	224	52.1	72	0.727
100	238	59.5	77	0.771
100	250	66.1	81	0.814

UMP

Table 6.2: Results for power input, power after inverter and power after motor in various rotational speed constant load tests

load (ohm)	Speed (RPM)	Power input (W)	Power after inverter (W)	Power after motor (W)
100	104	45.3	43.48	32.83
100	118	51.7	49.63	37.47
100	131	54.2	52.03	39.28
100	145	57.3	55.00	41.53
100	158	61.7	59.23	44.72
100	171	68.5	65.76	49.64
100	184	72.4	69.50	52.47
100	198	80.9	77.66	58.63
100	211	87.5	84	63.42
100	224	94.1	90.33	68.20
100	238	105.3	101.08	76.32
100	250	117	112.32	84.80

Table 6.3: Results for torque and efficiency in various rotational speed constant load tests

load (ohm)	Speed (RPM)	Power input for generator (W)	Power output for generator(W)	Torque (Nm)	Efficiency (%)
100	104	32.83	10.7	3.01	32.59
100	118	37.47	13.8	3.03	36.83
100	131	39.28	17.3	2.86	44.04
100	145	41.53	21.4	2.73	51.53
100	158	44.72	25.2	2.70	56.35
100	171	49.64	30.3	2.77	61.03
100	184	52.47	35.9	2.72	68.41
100	198	58.63	41.3	2.83	70.43
100	211	63.42	46.9	2.87	73.95
100	224	68.20	52.1	2.91	76.39
100	238	76.32	59.5	3.06	77.96
100	250	84.80	66.1	3.24	77.95

Figure 6.6 shows the graph for the power generated by ironless coreless electricity generator versus rotational speed of the rotors of the generator. The output power generated by the generator from around 10W increased to around 65W when the

rotational speed of the rotors of the generator rose from 105RPM to 250RPM. Figure 6.7 shows the current produced by the ironless coreless electricity generator versus the rotational speed of rotor is plotted. The graph in Figure 6.7 is positively skewed as the output current of the generator increased from 0.3A to 0.8A when the rotational speed of the rotors of the generator increased from 105RPM to 250RPM. Voltage produced by the ironless coreless electricity generator versus the rotational speed of rotor graph was plotted and the graph is shown in Figure 6.8. In Figure 6.8, the graph is also positively skewed as the output voltage produced by the ironless coreless electricity generator increase from 33V to around 80V when the rotational speed of the rotors of the ironless coreless electricity generator rose from 105RPM to 250RPM. Figure 6.9 shows the plotted graph for torque of the ironless coreless electricity generator versus rotational speed of the rotors. Figure 6.10 illustrates efficiency versus rotational speed of the rotors of the generator in which the efficiency increased from around 33% to around 78% when the rotational speed of the rotor increased from 105RPM to 250RPM.

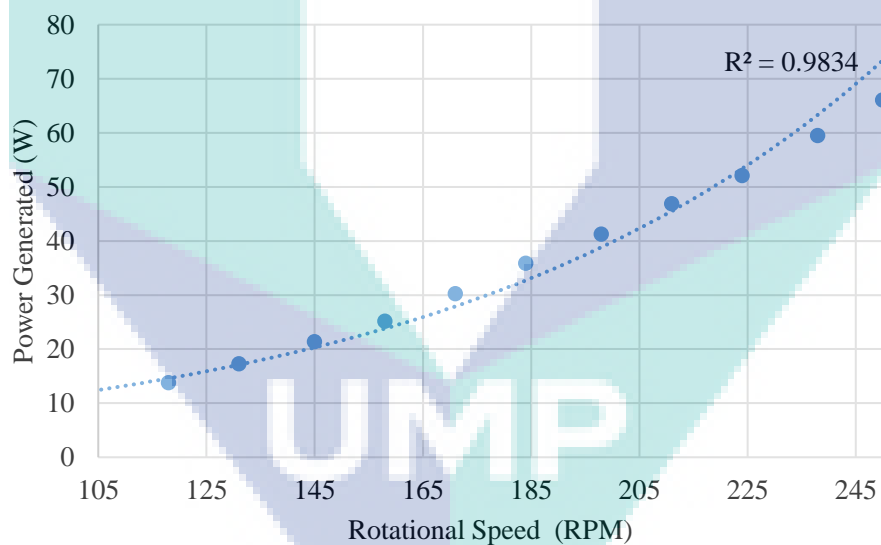


Figure 6.6: Power generated by ironless coreless electricity generator versus rotational speed graph

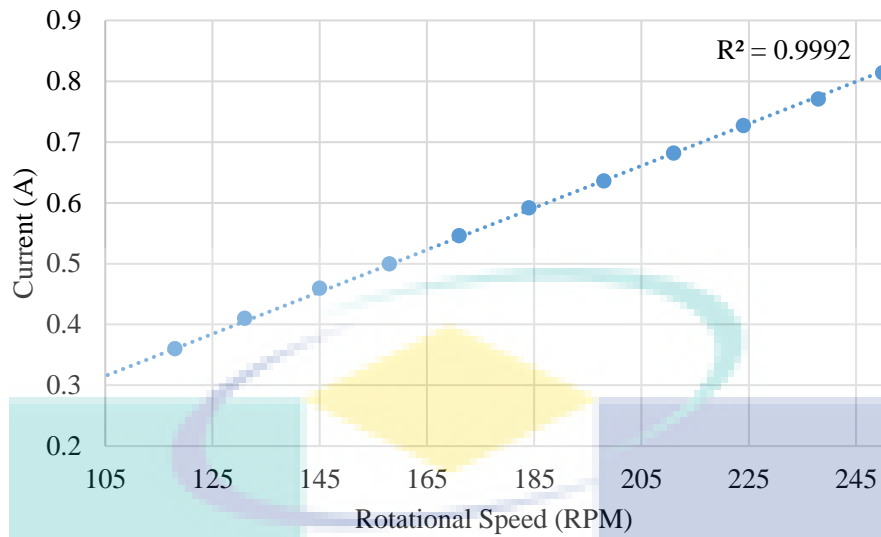


Figure 6.7: Current generated by the ironless coreless electricity generator versus rotational speed graph

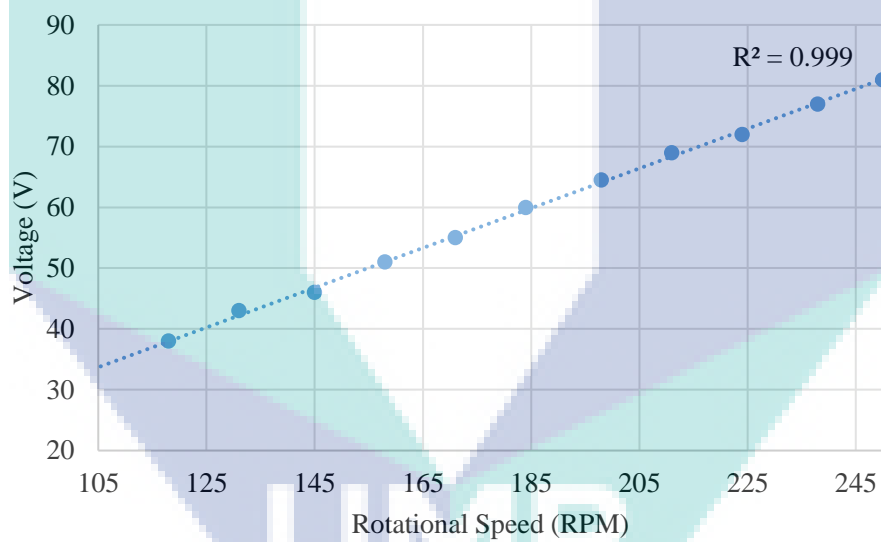


Figure 6.8: Voltage produced by the ironless coreless electricity generator versus rotational speed graph

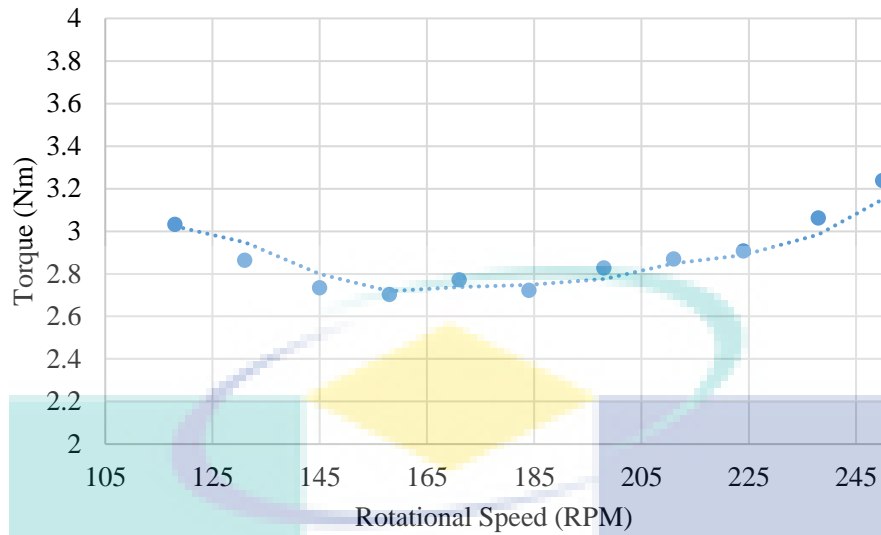


Figure 6.9: Torque of the ironless coreless electricity generator versus rotational speed graph

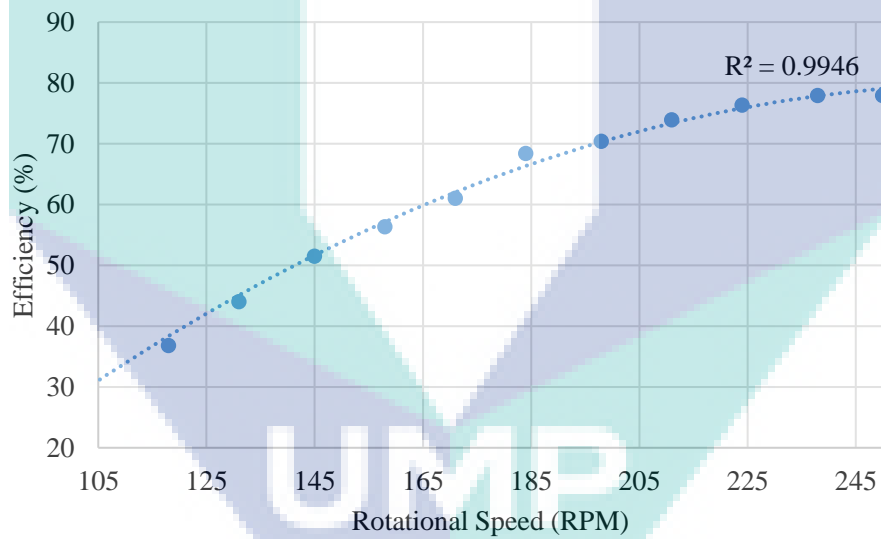


Figure 6.10: Efficiency of the ironless coreless electricity generator versus rotational speed graph

6.4.2 Maximum power point tracking test

In the maximum power point tracking test, the fabricated ironless coreless electricity generator underwent the load used by the ironless coreless electricity generator optimization to maximize the power generated, voltage produced and the current produced by the ironless coreless electricity generator when the rotational speed of the rotor increased throughout the test. Nine experiments were conducted for the maximum power point tracking test on the ironless coreless electricity generator.

In the first test, when rotational speed of 167RPM was used on the rotor of the ironless coreless electricity generator, the optimum load was 34.4 ohms as during this rotational speed with this amount of load, the generator was able to produce highest amount of output power, output voltage and output current compare to other amount of load. The output power generated was 72W, output voltage generated was 50V, output current generated was 1.44A, torque was 6.96Nm and efficiency was 59.13%. In the second test, with the rotational speed of the rotors of 189RPM, the optimum load was 34.96ohms and with such parameter, the generator was able to produce output power of 92W, output voltage of 56V, output current of 1.64A, torque of 6.96Nm and efficiency of 66.81%. In the third test, with the rotational speed of 207.5RPM and optimum load of 35.2 ohms, the generator was able to generate output power of 118W, output voltage of 64V, output current of 1.84A, torque of 7.40Nm and efficiency of 73.33%.

In the fourth test on the maximum power point tracking test, with the rotational speed of 223RPM used on the rotors of the ironless coreless electricity generator and the optimum load in this speed was 34.4 ohms, the generator was able to generate output power of 140W, output voltage of 70V, output current of 2A, torque of 8.16Nm and efficiency of 73.44%. For the fifth test, the rotational speed of rotor was 240.7RPM, with the optimum load of 34.6 ohms in this rotational speed. With such parameter, the generator was able to produce output power of 164W, output voltage of 76V, output current of 2.16A, torque of 8.77Nm and efficiency of 74.19%. The rotational speed of rotors of the generator was set to 258.1RPM during the sixth test and with such speed, the optimum load for the generator was 34.96 ohms. The generator was able to generate

output power of 192W, output voltage of 82V, output current of 2.34A, torque of 9.22Nm and efficiency of 77.01% under such condition.

In the seventh test of the maximum power point tracking test, rotational speed of 277RPM was used on the rotors of the ironless coreless electricity generator with optimum load of 34.96 ohms under such rotational speed. The generator was able to create output power of 220W, output voltage of 88V, output current of 2.5A, torque of 9.92Nm and efficiency of 76.46% during the seventh test. For the eighth test, the rotational speed of the rotors of the generator was 305RPM and with such speed, the optimum load for the generator was 34.72 ohms. Output power of 250W, output voltage of 94V, output current of 2.66A, torque of 10.10Nm and efficiency of 77.51% was produced by the generator during the eighth test. In the last test of the maximum power point tracking test on the ironless coreless electricity generator, the rotational speed of the rotors was 318RPM. The optimum load for the generator using 318RPM rotational speed was 35.08 ohms. Output power of 280W, output voltage of 100V, output current of 2.8A, torque of 10.82Nm and efficiency of 77.73% were generated within such parameters. Table 6.4 summarizes the results for power output, while Table 6.5 summarizes the results for power input, power after inverter and power after motor for the maximum power point tracking test on the ironless coreless electricity generator. Table 6.6, summarizes the results of torque and efficiency for the maximum power point tracking test on ironless coreless electricity generator.

Table 6.4: Results for power output in maximum power point tracking test

Speed (RPM)	Power output for generator(W)	Voltage (V)	Current (A)	load (ohm)
167	72	50	1.44	34.4
189	92	56	1.64	34.96
207.5	118	64	1.84	35.2
223	140	70	2.00	34.4
240.7	164	76	2.16	34.6
258.1	192	82	2.34	34.96
277	220	88	2.50	34.96
305	250	94	2.66	34.72
318	280	100	2.80	35.08

Table 6.5: Results for power input, power after inverter and power after motor in maximum power point tracking test

Speed (RPM)	Power input(W)	Power after inverter (W)	Power after motor (W)
167	168	161.28	121.77
189	190	182.4	137.71
207.5	222	213.12	160.91
223	263	252.48	190.62
240.7	305	292.8	221.06
258.1	344	330.24	249.33
277	397	381.12	287.75
305	445	427.2	322.54
318	497	477.12	360.23

Table 6.6: Results for torque and efficiency in maximum power point tracking test

Speed (RPM)	Power input for generator (W)	Power output for generator(W)	Torque (Nm)	Efficiency (%)
167	121.77	72	6.96	59.13
189	137.71	92	6.96	66.81
207.5	160.91	118	7.40	73.33
223	190.62	140	8.16	73.44
240.7	221.06	164	8.77	74.19
258.1	249.33	192	9.22	77.01
277	287.75	220	9.92	76.46
305	322.54	250	10.10	77.51
318	360.23	280	10.82	77.73

Figure 6.11 illustrates the power generated by the ironless coreless electricity generator versus the rotational speed of the rotor graph. As shown in Figure 6.11, the graph is positively skewed as the output power generated by the ironless coreless electricity generator increased from 75W to 380W when the rotational speed of the rotors of the generator increased from 170RPM to 318RPM.

Figure 6.12 and Figure 6.13 show the current produced by the ironless coreless electricity generator versus rotational speed of the rotor graph and the voltage produced by the ironless coreless electricity generator versus rotational speed of rotor graph, respectively. As illustrated in the Figure 6.12, the output current produced by the generator increased from 1.5A to 2.8A when the rotational speed of the rotors of the generator increased from 170RPM to 318RPM. Figure 6.13 provides an explanation to justify when the rotational speed of rotors of the generator rose from 170RPM to 318RPM, the output voltage generated by the ironless coreless electricity generator increased from 52V to 100V.

Figure 6.14 shows the graph for the optimum resistive load used by the ironless coreless electricity generator versus rotational speed graph. From the Figure 6.14, it is clear that when the resistive load was around 35 ohms, the ironless coreless electricity

generator produced highest output power, output voltage and output current when the rotational speed of the rotors of the generator was 170RPM to 318RPM.

Figure 6.15 illustrates the torque of the ironless coreless electricity generator versus rotational speed graph. The torque of the ironless coreless electricity generator was positively skewed from around 6.8Nm to around 10.5Nm when the rotational speed of the ironless coreless electricity generator increased from 170RPM to 318RPM.

Figure 6.16 shows the efficiency of the ironless coreless electricity generator versus the rotational speed graph. The efficiency of the ironless coreless electricity generator increased gradually from around 59% until around 75% and after achieving 75% efficiency, the generator became less efficient as the rotational speed of the rotors increased from 170RPM to 318RPM.

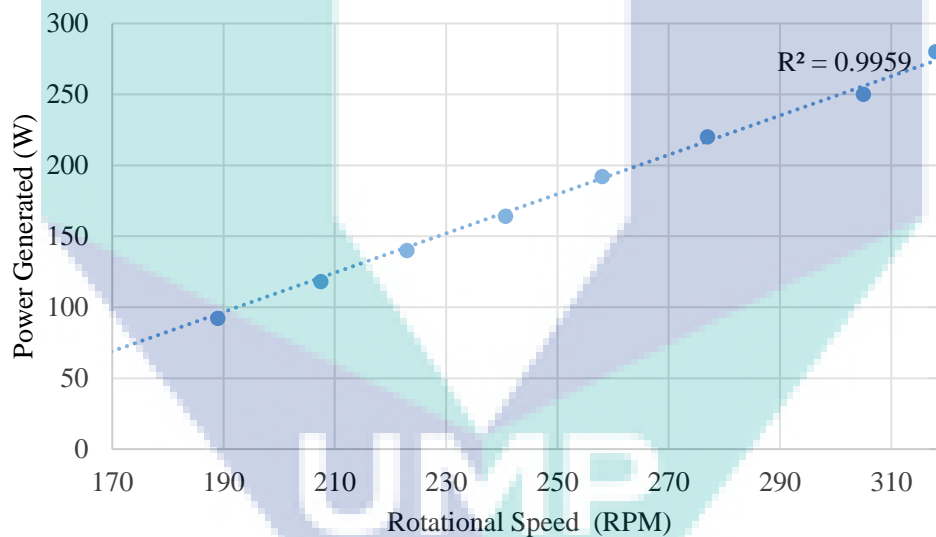


Figure 6.11: Power generated by the ironless coreless electricity generator versus rotational speed graph for maximum power point tracking test

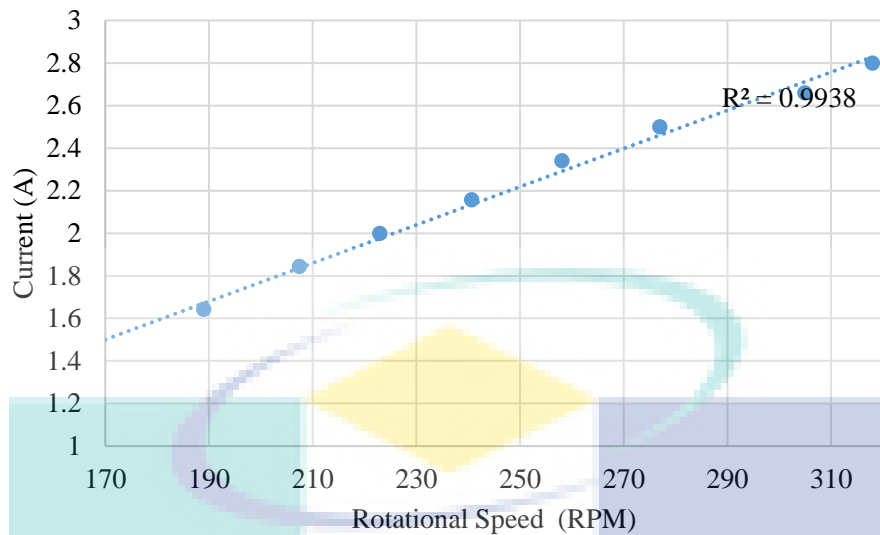


Figure 6.12: Current versus rotational speed graph for maximum power point tracking test

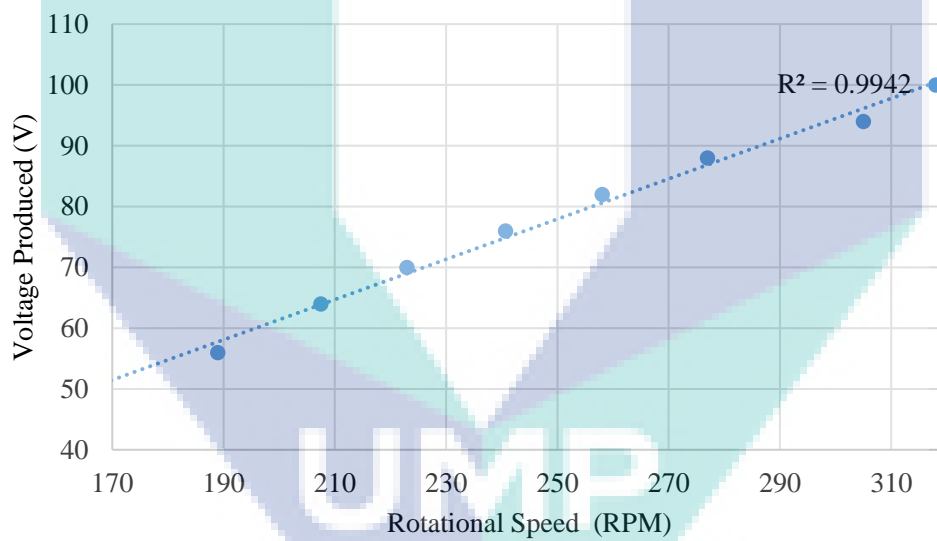


Figure 6.13: Voltage produced by the ironless coreless electricity generator versus rotational speed graph for maximum power point tracking test

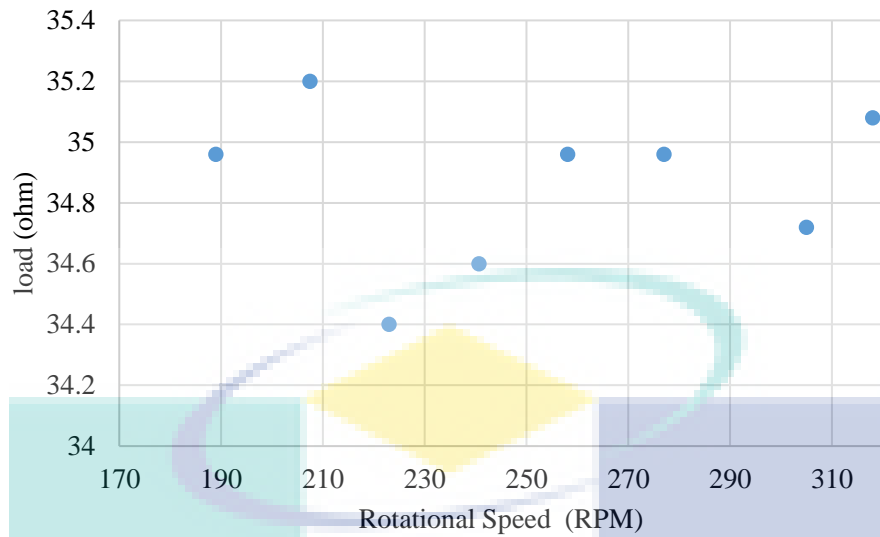


Figure 6.14: Optimum resistive load versus rotational speed graph for maximum power point tracking test

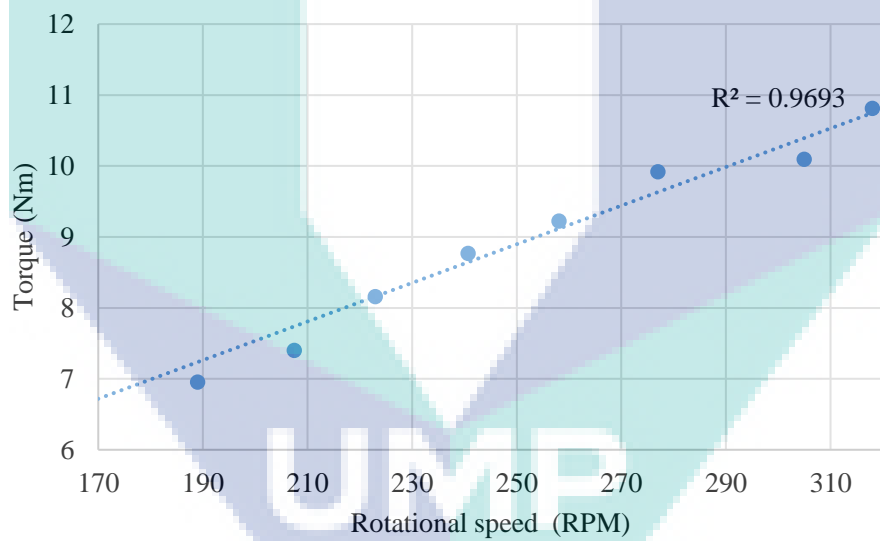


Figure 6.15: Torque versus rotational speed graph for maximum power point tracking test

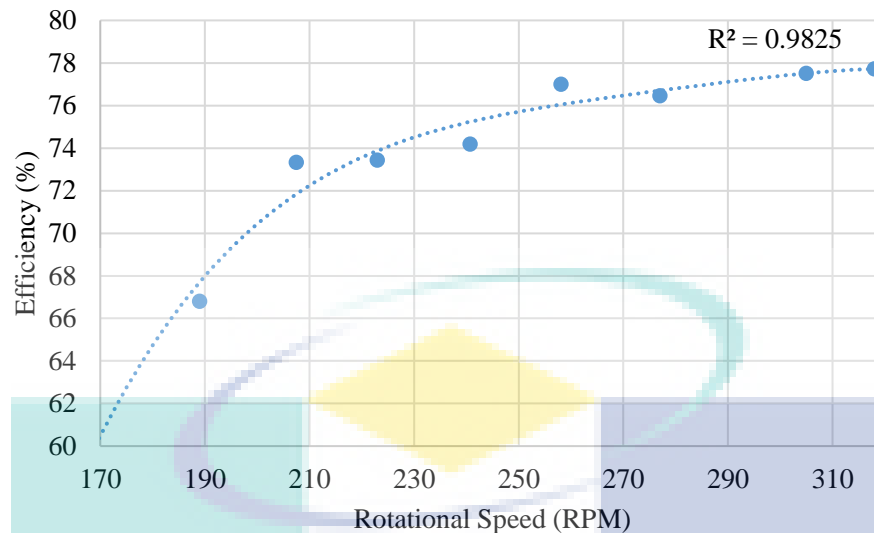


Figure 6.16: Efficiency versus rotational speed graph for maximum power point tracking test

6.5 DISCUSSION

In the closed circuit test on the fabricated ironless coreless electricity generator, there was a ripple within the waveform obtained from the oscilloscope. The waveform obtained during the test was not so smooth compared to the waveform obtained during the open circuit test. It is believed that there was some noise or interference which had occurred within the system itself when the system was connected to the rectifier. This was because when the circuits was connected to the silicon-controlled rectifiers or power thyristors, “notching” effects occurred, and when these devices were doing switching operation, it caused sharp inverted spikes during commutation or transfer of conduction from one phase to the next (Vijayaraghavan, Brown & Barnes, 2008).

During the closed circuit test on the ironless coreless electricity generator, the voltage produced by the ironless coreless electricity generator after passing through the rectifier was not as smooth as the DC output voltage. After the output voltage produced by the generator passed through the rectifier, the sine wave was filtered and became the waveform as the green colour wave as shown in Figure 6.4. Although by only using such rectifier do had good technical properties such as low ripple on output voltage, simple construction on the circuit created to generate electricity and low cost to buy the

rectifier (Vodovozov & Jansikene, 2006), to further filter the output power produced by the ironless coreless electricity generator, the inductor and capacitor should be used (Liang, Yang & Chen, 2007; Nishimura et al., 2008) after the rectifier so that the filtered output voltage of the ironless coreless electricity generator will be smoother.

In the various rotational speed constant load tests carried out on the ironless coreless electricity generator, when the rotational speed of the rotors of the generator increased, the power generated by the ironless coreless electricity generator also increased. Likewise, for the ironless coreless electricity generator, when the rotational speed of the rotor in the ironless coreless electricity generator increased, the magnetic flux cutting rate for the coil connected using three-phase star connection on the stator also increased. When such phenomena occurred, more voltage and current would be produced by the three-phase coil on the stator of the ironless coreless electricity generator. Based on Eq. 3.3, assuming that the load used by the ironless coreless electricity generator was constant, when the current produced by the ironless coreless electricity generator increased, the power generated by the ironless coreless electricity generator also increased. The results for the various rotational speed constant load tests for the ironless coreless electricity generator in this research showed similar trend with the results in Chung and Yew's research for their coreless axial-flux permanent-magnet generator for small wind turbines (Chung & You, 2014).

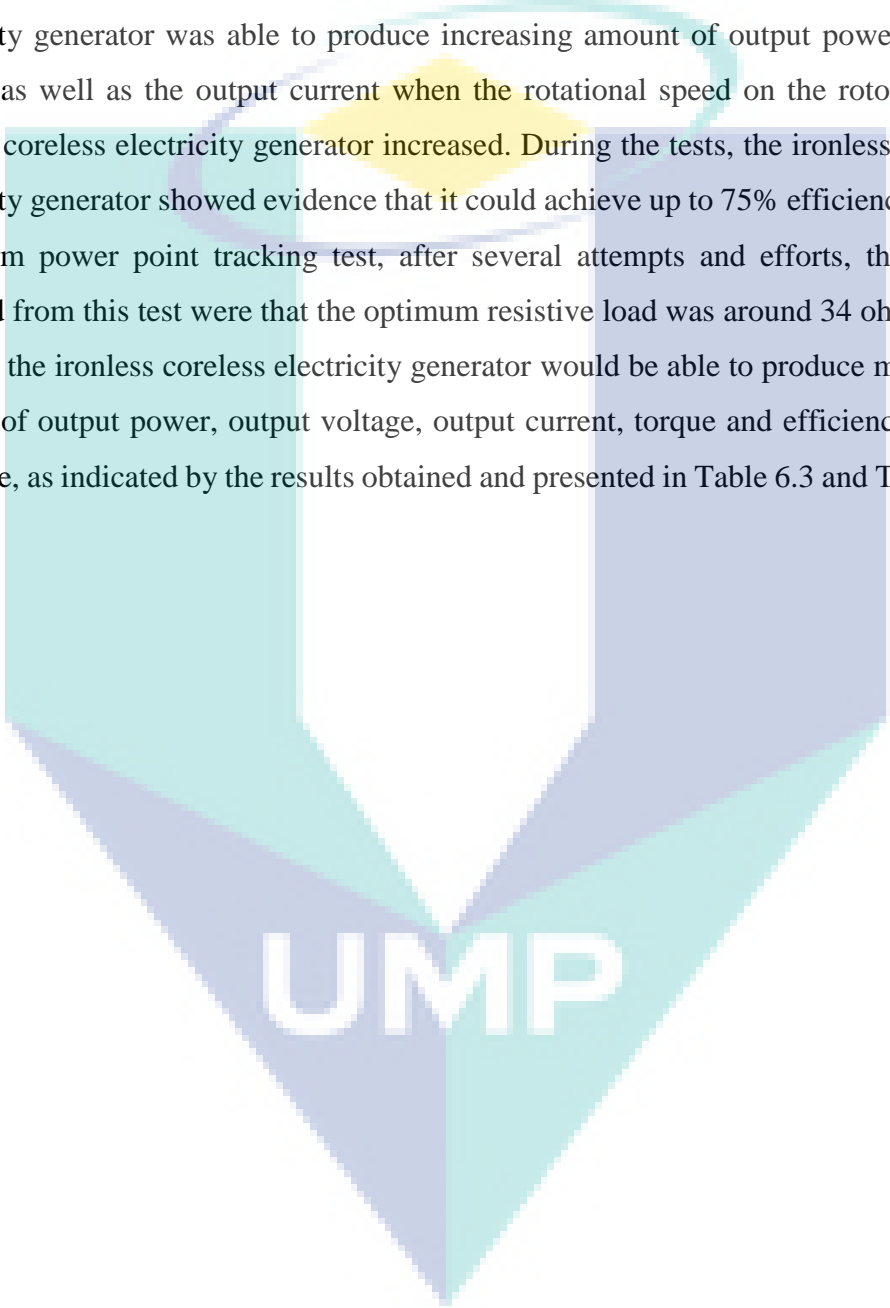
The reason to conduct the maximum power point tracking test was because the maximum power point could be achieved by the permanent magnet synchronous generator by varying the generator's load (Abdullah et al., 2012). The results of the maximum power point tracking test were similar with the results of the various rotational speed constant load tests. This is because the after several times and some efforts to obtain the optimum resistive load which was most suitable for the fabricated ironless coreless electricity generator, the difference of the resistive load used by the ironless coreless electricity generator was small throughout the maximum power point tracking test. Since the resistive load used by the ironless coreless electricity generator was almost constant, the only thing that would affect the output of the ironless coreless electricity generator would be the rotational speed of the rotor. For the fabricated ironless coreless electricity generator in this research, the optimum range of the resistive load was between 34 ohm and 35 ohm.

In the maximum power point tracking test, the torque of the ironless electricity generator increased when the rotational speed increased. When the rotational speed of the ironless coreless electricity generator increased, the power output of the generator also increased. As the power output of the generator became higher, the counter electromotive force between the rotors and stator of the generator would likely be higher. With this, the resistance of rotors and stator would increase, thus, more force would be required to operate the generator and thus, producing a higher torque. According to Zhang et al. (2013), in their research, when the power was higher, the torque density would increase and the power density would decrease.

It was noted that in the constant load various rotational speed tests and the maximum power point tracking test, the efficiency of the ironless coreless electricity generator only increased to around 75% as the rotational speed of the rotors of the generator kept increasing. This is because the ironless coreless electricity generator itself had reached its maximum efficiency when its efficiency was around 75%. It had been anticipated that the efficiency of the ironless coreless electricity generator would still be around 75% although there would be increment on the rotational speed of the rotor of the ironless coreless electricity generator itself. The trend of the efficiency of fabricated ironless coreless electricity generator was in good agreement with that in Polinder et al.'s (2006) research as the efficiency of DFIG3G, DDSG and DDPMG in their research since the generators would stay constant when they reached their maximum capabilities.

6.6 SUMMARY OF THE CHAPTER

In this chapter, there were two closed circuit tests performed on the ironless coreless electricity generator, namely, the various rotational speed constant load tests and the maximum power point tracking test. In both tests, the ironless coreless electricity generator was able to produce increasing amount of output power, output voltage as well as the output current when the rotational speed on the rotors of the ironless coreless electricity generator increased. During the tests, the ironless coreless electricity generator showed evidence that it could achieve up to 75% efficiency. In the maximum power point tracking test, after several attempts and efforts, the results obtained from this test were that the optimum resistive load was around 34 ohms to 35 ohms as the ironless coreless electricity generator would be able to produce maximum amount of output power, output voltage, output current, torque and efficiency within the range, as indicated by the results obtained and presented in Table 6.3 and Table 6.4.



UMP

CHAPTER 7

CONCLUSION AND RECOMMENDATION

7.1 CONCLUSIONS

At the end of the research, the ironless coreless electricity generator was successfully fabricated after the fundamental studies on coreless electricity generator had been done. The fundamental studies on generators were conducted to gain knowledge on the design of the generator, magnet to be used on the generator, the connection of wire to be used to obtain better output and the software to be used for the analysis of the designed ironless coreless electricity generator. After designing the generator, it went through series of analysis using JMAG Designer software to obtain the optimum parameters to be used on the ironless coreless electricity generator which was going to be fabricated. The fabricated ironless coreless electricity generator was then tested on test bed mounted with the induction motor. On the test bed, open circuit test and closed circuit test were performed. In the open circuit test, the ironless coreless electricity generator was able to obtain an efficiency of up to 90%. For the closed circuit test, numerous tests such as the various rotational speed constant resistive load tests and the maximum power point tracking test were performed to determine the capability of the fabricated ironless coreless electricity generator. In the maximum power point tracking test, the fabricated generator was able to obtain output power of 280W when the rotational speed of the generator was 318RPM. Table 7.1 shows the objectives of the present study and how these objectives were achieved.

Table 7.1: Summary of the Research Objectives and How These Objectives Were Achieved for the Development of the Ironless Coreless Electricity Generator

Objectives	Achievements
To analyse the design and characteristics of an ironless coreless electricity generator	Before starting to design on the ironless coreless electricity generator, fundamental studies were conducted to obtain good insights on what aspects to consider when designing the generator (e.g., the connection on wire to use, design of rotors and stator, magnet to be used on rotors and software to be used on doing the analysis).
To develop an ironless coreless electricity generator	After the ironless coreless electricity generator was designed, the designed generator underwent a series of analyses to obtain the optimum parameters for the generator and based on the parameters, adjustment on the designed generator was made. When the design was finalized, the ironless coreless electricity generator was fabricated using CNC machine. An AFPM ironless coreless electricity generator with 2 rotors consisting of 16 poles, a stator with 12 coils was connected using three-phase wye connection.
To analyse the performance of the ironless coreless electricity generator	The open circuit test and closed circuit tests were conducted on the fabricated ironless coreless electricity generator on test bed so that the performance of the generator could be analysed. During the open circuit test, the efficiency of the fabricated AFPM coreless ironless electricity generator could reach up to around 90%. During the closed circuit test, in maximum power point tracking test, the optimum load to be used on the generator was around 35 ohms, with the rotational speed of 318RPM, the generator could produce output power of 280W.

7.2 RECOMMENDATIONS

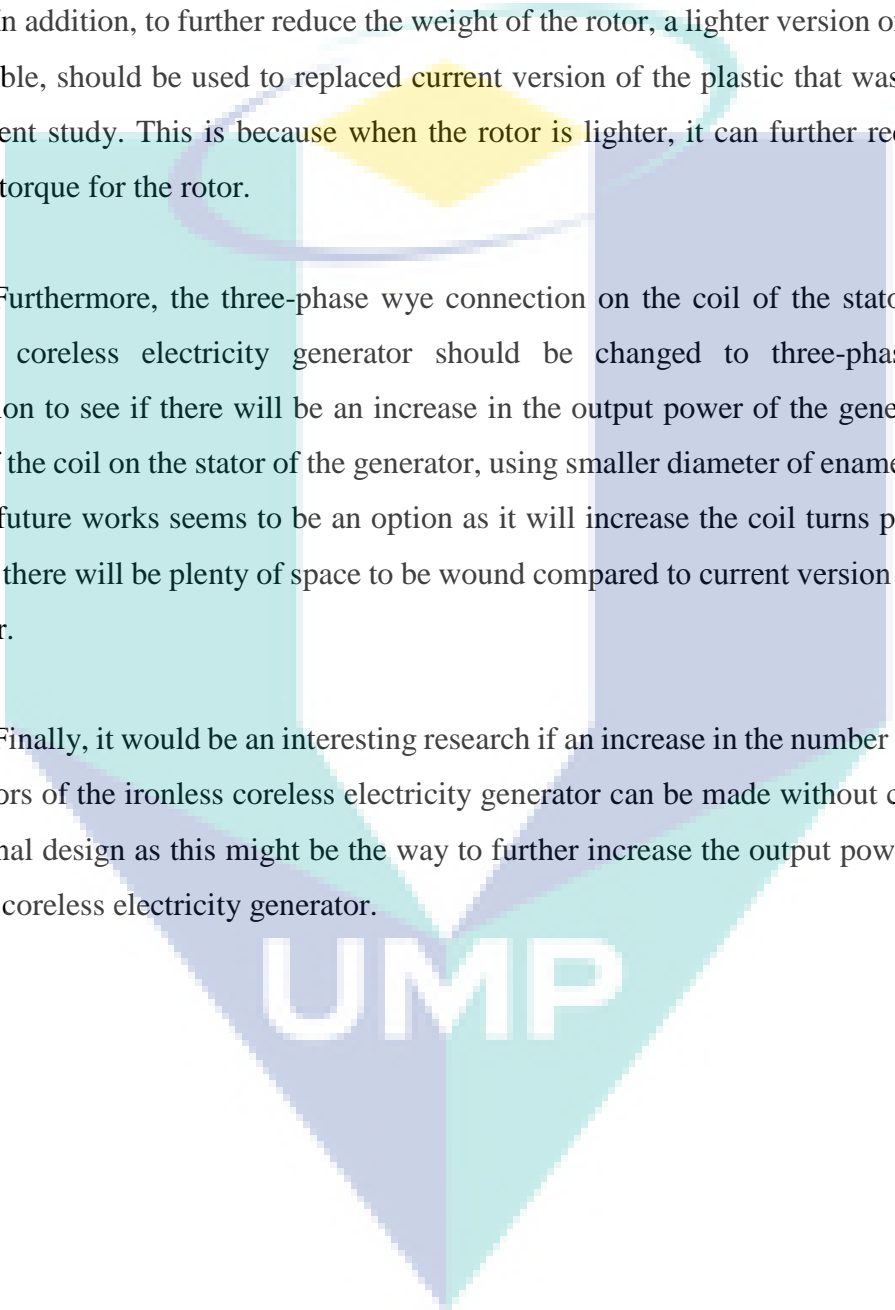
There are a few recommendations which can be done to improve the current version of ironless coreless electricity generator in this research. First of all, to further improve the efficiency of the ironless coreless electricity generator, it is suggested that

a different method such as three-dimensional printing method to fabricate rotor of the ironless coreless electricity generator should be used. It is believed that by using such method, the stability of the rotor can be improved and thus, reducing the losses within the ironless coreless electricity generator.

In addition, to further reduce the weight of the rotor, a lighter version of plastic, if available, should be used to replaced current version of the plastic that was used in the present study. This is because when the rotor is lighter, it can further reduce the starting torque for the rotor.

Furthermore, the three-phase wye connection on the coil of the stator of the ironless coreless electricity generator should be changed to three-phase delta connection to see if there will be an increase in the output power of the generator. In terms of the coil on the stator of the generator, using smaller diameter of enamel coated wire in future works seems to be an option as it will increase the coil turns per phase because there will be plenty of space to be wound compared to current version of coil's diameter.

Finally, it would be an interesting research if an increase in the number of rotors and stators of the ironless coreless electricity generator can be made without changing its original design as this might be the way to further increase the output power of the ironless coreless electricity generator.

The logo for UMP (Universiti Malaysia Perlis) is a large, stylized letter 'U' composed of several overlapping geometric shapes in shades of teal, light blue, and yellow. The letters 'UMP' are printed in a bold, white, sans-serif font across the bottom portion of the 'U' shape.

UMP

REFERENCES

- Abdullah, M. A., Yatim, A. H. M., Tan, C. W. and Saidur, R. (2012). A review of maximum power point tracking algorithms for wind energy systems. *Renewable and sustainable energy reviews*, **16**(5), 3220-3227.
- Ahmed D. and Ahmad A. (2013). *An optimal design of coreless direct-drive axial flux permanent magnet generator for wind turbine*. **Journal of Physics: Conference Series** **439** (2013) 012039
- Bianchi, N. and Bolognani, S. (2002). Design techniques for reducing the cogging torque in surface-mounted PM motors. *Industry Applications, IEEE Transactions on*, **38**(5), 1259-1265.
- Breton, C., Bartolome, J., Benito, J. A., Tassinario, G., Flotats, I., Lu, C. W. and Chalmers, B. J. (2000). Influence of machine symmetry on reduction of cogging torque in permanent-magnet brushless motors. *Magnetics, IEEE Transactions on*, **36**(5), 3819-3823.
- Bumby, J. R. and Martin, R. (2005). Axial-flux permanent-magnet air-cored generator for small-scale wind turbines. *IEE Proceedings-Electric Power Applications*, **152**(5), 1065-1075.
- Caricchi, F., Crescimbeni, F. and Santini, E. (1995). Basic principle and design criteria of axial-flux PM machines having counterrotating rotors. *Industry Applications, IEEE Transactions on*, **31**(5), 1062-1068.
- Chalmers, B. J. and Spooner, E. (1999). An axial-flux permanent-magnet generator for a gearless wind energy system. *Energy Conversion, IEEE Transactions on*, **14**(2), 251-257.
- Chan, T. F. and Lai, L. L. (2007). *An axial-flux permanent-magnet synchronous generator for a direct-coupled wind-turbine system*. **Energy Conversion, IEEE Transactions on**, **22**(1), 86-94.
- Chen, J. L. and Liu, T. H. (2012). Implementation of a predictive controller for a sensorless interior permanent-magnet synchronous motor drive system. *Electric Power Applications, IET*, **6**(8), 513-525.
- Chen, Y., Pillay, P. and Khan, A. (2005). *PM Wind Generator Topologies*. **IEEE Transactions on Industry Application**, **Vol. 41**, No. 6, November/December 2005
- Chung, D. W. and You, Y. M. (2014). Design and Performance Analysis of Coreless Axial-Flux Permanent-Magnet Generator for Small Wind Turbines. *Journal of Magnetics*, **19**(3), 273-281.
- Del Ferraro, L., Giulii Capponi, F., Terrigi, R., Caricchi, F. and Honorati, O. (2006, October). Ironless axial flux PM machine with active mechanical flux weakening for automotive applications. *Industry Applications Conference, 2006. 41st IAS Annual Meeting. Conference Record of the 2006 IEEE* (Vol. 1, pp. 1-7). IEEE.

Di Napoli, A., Caricchi, F., Crescimbeni, F. and Noia, G. (1991, August). Design criteria of a low-speed axial-flux PM synchronous machine. *International Conference on the Evolution and Modern Aspects of Synchronous Machines* (pp. 1119-1123).

Doebbelin, R., Benecke, M. and Lindemann, A. *Calculation of Leakage of Core-Type Transformer for Power Electronic Circuits*. **13th International Power Electronics and Motion Control Conference (EPE-PEMC)**, 2008

Drazikowski, L. and Koczara, W. (2011). Permanent magnet disk generator with coreless windings. *COMPEL: The International Journal for Computation and Mathematics in Electrical and Electronic Engineering*, **31**(1), 108-118.

Eastham, J. F., Profumo, F., Tenconi, A., Hill-Cottingham, R., Coles, P. and Gianolio, G. (2002). Novel axial flux machine for aircraft drive: Design and modeling. *Magnetics, IEEE Transactions on*, **38**(5), 3003-3005.

Electrical Engineering, Online Electrical Engineering Study Site. *Principle of DC Generator*. Retrieved from <http://www.electrical4u.com/principle-of-dc-generator/>

Fei, W., Luk, P. C. K. and Jinupun, K. (2010). *Design and analysis of high-speed coreless axial flux permanent magnet generator with circular magnets and coils*. **IET electric power applications**, **4**(9), 739-747.

Fitzgerald, A. E. and Kingsley, C. (1961). *Electric machinery: the dynamics and statics of electromechanical energy conversion*. McGraw-Hill.

Gieras, J. F., Wang, R. J. and Kamper, M. J. (2008). *Axial flux permanent magnet brushless machines (Vol. 1)*. New York, NY: Springer.

Gör, H. and Kurt, E. (2016). Preliminary studies of a new permanent magnet generator (PMG) with the axial and radial flux morphology. *International Journal of Hydrogen Energy*

Gor, H. and Kurt, E. (2016). Waveform characteristics and losses of a new double sided axial and radial flux generator. *International Journal of Hydrogen Energy*.

GreenGear. (2015). Choosing Between A Conventional, Silenced or An Inverter Generator. Retrieved from <http://www.greengearglobal.com/choosing-conventional-silenced-inverter-generator/>

Hosseini, S. M., Agha-Mirsalim, M. and Mirzaei, M. (2008). *Design, Prototyping, and Analysis of a Low Cost Axial-Flux Coreless Permanent-Magnet Generator*. **IEEE Transaction on Magnetics**, **Vol. 44**, No. 1, January 2008

Huang, S., Luo, J., Leonardi, F. and Lipo, T. A. (1999). A comparison of power density for axial flux machines based on general purpose sizing equations. *Energy Conversion, IEEE Transactions on*, **14**(2), 185-192.

Hwang, C. C., Li, P. L., Chuang, F. C., Liu, C. T. and Huang, K. H. (2009). Optimization for reduction of torque ripple in an axial flux permanent magnet machine. *Magnetics, IEEE Transactions on*, **45**(3), 1760-1763.

Javadi, S. and Mirsalim, M. (2010). Design and analysis of 42-V coreless axial-flux permanent-magnet generators for automotive applications. *Magnetics, IEEE Transactions on*, **46**(4), 1015-1023.

Jenal, M., Sulaiman, E., Ahmad, M. Z., Zakaria, S. N. U., Utomo, W. M., Zulkifli, S. A. and Bakar, A. A. (2013, November). Design study of single and three-phase synchronous generator using J-MAG designer. *Clean Energy and Technology (CEAT), 2013 IEEE Conference on* (pp. 226-231). IEEE.

JMAG, Simulation Technologies for Electromechanical Design. Retrieved from <https://jmag-international.com/>

K&J Magnetics, Inc. *Temperature and Neodymium Magnet*. Retrieved from <http://www.kjmagnetics.com/blog.asp?p=temperature-and-neodymium-magnets>

Kobayashi, H., Doi, Y., Miyata, K. and Minowa, T. *Design of axial-flux permanent magnet coreless generator for the multi-megawatts wind turbines. EWEC2009*.

Krishnan, R. (2009). Permanent magnet synchronous and brushless DC motor drives. *CRC press*.

Kurt, E., Gör, H. and Demirtaş, M. (2014). Theoretical and experimental analyses of a single phase permanent magnet generator (PMG) with multiple cores having axial and radial directed fluxes. *Energy Conversion and Management*, **77**, 163-172

Li, H. and Chen, Z. (2008). *Overview of different wind generator systems and their comparisons. IET Renewable Power Generation*, **2**(2), 123-138.

Li, S., Haskew, T. A. and Xu, L. (2010). Conventional and novel control designs for direct driven PMSG wind turbines. *Electric Power Systems Research*, **80**(3), 328-338.

Liang, T. J., Yang, L. S. and Chen, J. F. (2007). Analysis and design of a single-phase AC/DC step-down converter for universal input voltage. *Electric Power Applications, IET*, **1**(5), 778-784.

Lombard, N. F. and Kamper, M. J. (1999). Analysis and performance of an ironless stator axial flux PM machine. *Energy Conversion, IEEE Transactions on*, **14**(4), 1051-1056.

Lopez, H. E. M. (2007). *Maximum Power Tracking Control Scheme for Wind Generator Systems*. Doctoral dissertation, Texas A&M University.

Madawala, U. K. and Boys, J. T. (2005). Magnetic field analysis of an ironless brushless dc machine. *Magnetics, IEEE Transactions on*, **41**(8), 2384-2390.

Mahmoudi, A., Kahourzade, S., Rahim, N. A., Ping, H. W. and Uddin, M. N. (2013). Design and prototyping of an optimised axial-flux permanent-magnet synchronous machine. *Electric Power Applications, IET*, 7(5), 338-349.

Mahmoudi, A., Rahim, N. A. and Hew, W. P. (2011). Axial-flux permanent-magnet machine modeling, design, simulation, and analysis. *Scientific Research and Essays*, 6(12), 2525-2549.

Mirzaei, M., Mirsalim, M. and Abdollahi, S. E. (2007). Analytical modeling of axial air gap solid rotor induction machines using a quasi-three-dimensional method. *Magnetics, IEEE Transactions on*, 43(7), 3237-3242.

Mo, W., Zhang, L., Shan, A., Cao, L., Wu, J. and Komuro, M. (2008). Improvement of magnetic properties and corrosion resistance of NdFeB magnets by intergranular addition of MgO. *Journal of Alloys and Compounds* 461(1), 351-354.

Molina, M. G., dos Santos, E. C. and Pacas, M. (2010, September). Advanced power conditioning system for grid integration of direct-driven PMSG wind turbines. *Energy Conversion Congress and Exposition (ECCE), 2010 IEEE* (pp. 3366-3373). IEEE.

Mosincat, I., Lu, K. and Pedersen, K. (2011). Hysteresis losses influence on the cogging torque of high-efficiency Surface Mounted PM Machines.

Muljadi, E., Butterfield, C. P. and Wan, Y. H. (1999). Axial-flux modular permanent-magnet generator with a toroidal winding for wind-turbine applications. *Industry Applications, IEEE Transactions on*, 35(4), 831-836.

Muyeen, S. M., Takahashi, R., Murata, T. and Tamura, J. (2010). A variable speed wind turbine control strategy to meet wind farm grid code requirements. *Power Systems, IEEE Transactions on*, 25(1), 331-340.

NDT Resource Center. The Hysteresis Loop and Magnetic Properties. Retrieved from <https://www.nde-ed.org/EducationResources/CommunityCollege/MagParticle/Physics/HysteresisLoop.htm>

NEETS Module 1, Chapter 5. (2013). *Direct Current Generators*. Retrieved from http://www.navymars.org/national/training/nmo_courses/NMO2/module5/14177_ch1.pdf

NEETS Module 5. (2013). *Introduction to Generator and Motors*. Retrieved from http://electriciantraining.tpub.com/14177/css/14177_24.htm

Nidec Corporation. (2014). *2-1-3 Rotating Speed Of DC Motor And Counter-electromotive Force*. Retrieved from <http://www.nidec.com/en-Global/technology/motor/basic/00013/>

Nishimura, K., Hirachi, K., Komiyama, S. and Nakaoka, M. (2008, February). Two buck choppers built-in single phase one stage pfc converter with reduced DC voltage

ripple and its specific control scheme. *Applied Power Electronics Conference and Exposition, 2008. APEC 2008. Twenty-Third Annual IEEE* (pp. 1378-1383). IEEE.

Oh, S. C. and Emadi, A. (2004). Test and simulation of axial flux-motor characteristics for hybrid electric vehicles. *Vehicular Technology, IEEE Transactions on*, 53(3), 912-919.

Omron. Omron MX5 Datasheet. Retrieved from mikrokontrol.rs/proizvodi/pdf/I113E-EN-02+MX2+Datasheet.pdf

Parviainen, A., Niemelä, M. and Pyrhönen, J. (2004). Modeling of axial flux permanent-magnet machines. *Industry Applications, IEEE Transactions on*, 40(5), 1333-1340.

Polinder, H., Van der Pijl, F. F., Vilder, D., & Tavner, P. J. (2006). Comparison of direct-drive and geared generator concepts for wind turbines. *Energy conversion, IEEE transactions on*, 21(3), 725-733.

Pop, A. A., Jurca, F., Oprea, C., Chirca, M., Breban, S. and Radulescu, M. M. (2013, September). Axial-flux vs. radial-flux permanent-magnet synchronous generators for micro-wind turbine application. *Power Electronics and Applications (EPE), 2013 15th European Conference on* (pp. 1-10). IEEE.

Portable Generator Review. (2014). Conventional Generator Review. Retrieved from http://www.topportablegeneratorsreview.com/conventional_generators_review.html

Portela, P., Sepúlveda, J. and Esteves, J. S. (2008). *Alternating Current and Direct Current Generator. International Journal on Hands-on Science, Vol.1, No.1, September 2008*

Qiu, Z., Zhou, K. and Li, Y. (2011, July). Modeling and control of diode rectifier fed PMSG based wind turbine. *Electric Utility Deregulation and Restructuring and Power Technologies (DRPT), 2011 4th International Conference on* (pp. 1384-1388). IEEE.

Rizzoni, G. (2007). *Principle and Applications of Electrical Engineering 5th edition*. McGraw-Hill Higher Education.

Saidur, R., Islam, M. R., Rahim, N. A. and Solangi, K. H. (2010). A review on global wind energy policy. *Renewable and Sustainable Energy Reviews*, 14(7), 1744-1762.

Samarins.com. Alternator, How It Works, Symptoms, Testing, Problems, Replacement. Retrieved from <http://www.samarins.com/glossary/alternator.html>

Spooner, E. and Chalmers, B. J. (1992). TORUS': a slotless, toroidal-stator, permanent-magnet generator. *Electric Power Applications, IEE Proceedings B*, 139(6), 497-506.
Stampfi, H. (2003). Linear motor applications: Ironcore versus Ironless Solution. Retrieved from http://www.controldesign.com/assets/Media/MediaManager/wp_035_etel_thompson.pdf

Storr W. (2013). *Transformer Construction*. Electronics-Tutorials.ws. Retrieved from <http://www.electronics-tutorials.ws/transformer/transformer-construction.html>

Tamura, J. (2012). Calculation method of losses and efficiency of wind generators. *Wind Energy Conversion Systems* (pp. 25-51). Springer London.

Teco Electric & Machiner (Pte) Ltd. AEEB. AEVB Low Voltage Series. Retrieved from www.teco.com.sg/admin2/images/e-catalog/Catalogue%20AEEB.pdf

Ting, C. C. and Yeh, L. Y. (2014). Developing the full-field wind electric generator. *International Journal of Electrical Power & Energy Systems*, **55**, 420-428.

Vijayaraghavan, G., Brown, M. and Barnes, M. (2008). Electrical noise and mitigation-Part 1: Noise definition, categories and measurement.

Virtic, P. and Avsec, J. (2011). Analysis of coreless stator axial flux permanent magnet synchronous generator characteristics by using equivalent circuit. *Przegląd Elektrotechniczny*, **87**(3), 208-211.

Virtic, P., Pisek, P., Marcic, T., Hadziselimovic, M. and Stumberger, B. (2008). Analytical analysis of magnetic field and back electromotive force calculation of an axial-flux permanent magnet synchronous generator with coreless stator. *Magnetics, IEEE Transactions on*, **44**(11), 4333-4336.

Vodovozov, V. and Jansikene, R. (2006). *Power Electronic Converters*. Tallinn University of Technology Department of Electrical Drives and Power Electronics.

Wang, R. J., Kamper, M. J., Van der Westhuizen, K. and Gieras, J. F. (2005). Optimal design of a coreless stator axial flux permanent-magnet generator. *Magnetics, IEEE Transactions on*, **41**(1), 55-64.

Z. Zhang, A. Chen, A. Matveev, R. Nilssen, and A. Nysveen, 'High-power generators for offshore wind turbines', *Energy Procedia* **35** (2013) 52 – 61.

Zhang, S., Tseng, K. J., Vilathgamuwa, D. M., Nguyen, T. D. and Wang, X. Y. (2011). Design of a robust grid interface system for PMSG-based wind turbine generators. *Industrial Electronics, IEEE Transactions on*, **58**(1), 316-328.